# IEC TR 63170

Edition 1.0 2018-08

# TECHNICAL REPORT

colour inside

## Measurement procedure for the evaluation of power density related to human exposure to radio frequency fields from wireless communication devices operating between 6 GHz and 100 GHz

IEC Central Office
3, rue de Varembé
CH-1211 Geneva 20
Switzerland

Tel.: +41 22 919 02 11
info@iec.ch
www.iec.ch

**About the IEC**
The International Electrotechnical Commission (IEC) is the leading global organization that prepares and publishes International Standards for all electrical, electronic and related technologies.

**About IEC publications**
The technical content of IEC publications is kept under constant review by the IEC. Please make sure that you have the latest edition, a corrigenda or an amendment might have been published.

**IEC Catalogue - webstore.iec.ch/catalogue**
The stand-alone application for consulting the entire bibliographical information on IEC International Standards, Technical Specifications, Technical Reports and other documents. Available for PC, Mac OS, Android Tablets and iPad.

**IEC publications search - webstore.iec.ch/advsearchform**
The advanced search enables to find IEC publications by a variety of criteria (reference number, text, technical committee,…). It also gives information on projects, replaced and withdrawn publications.

**IEC Just Published - webstore.iec.ch/justpublished**
Stay up to date on all new IEC publications. Just Published details all new publications released. Available online and also once a month by email.

**Electropedia - www.electropedia.org**
The world's leading online dictionary of electronic and electrical terms containing 21 000 terms and definitions in English and French, with equivalent terms in 16 additional languages. Also known as the International Electrotechnical Vocabulary (IEV) online.

**IEC Glossary - std.iec.ch/glossary**
67 000 electrotechnical terminology entries in English and French extracted from the Terms and Definitions clause of IEC publications issued since 2002. Some entries have been collected from earlier publications of IEC TC 37, 77, 86 and CISPR.

**IEC Customer Service Centre - webstore.iec.ch/csc**
If you wish to give us your feedback on this publication or need further assistance, please contact the Customer Service Centre: sales@iec.ch.

# IEC TR 63170

Edition 1.0 2018-08

# TECHNICAL REPORT

colour inside

## Measurement procedure for the evaluation of power density related to human exposure to radio frequency fields from wireless communication devices operating between 6 GHz and 100 GHz

INTERNATIONAL
ELECTROTECHNICAL
COMMISSION

ICS 17.220.20

ISBN 978-2-8322-5878-1

**Warning! Make sure that you obtained this publication from an authorized distributor.**

# CONTENTS

INTERNATIONAL ELECTROTECHNICAL COMMISSION

_____

# MEASUREMENT PROCEDURE FOR THE EVALUATION OF POWER DENSITY RELATED TO HUMAN EXPOSURE TO RADIO FREQUENCY FIELDS FROM WIRELESS COMMUNICATION DEVICES OPERATING BETWEEN 6 GHz AND 100 GHz

## FOREWORD

1) The International Electrotechnical Commission (IEC) is a worldwide organization for standardization comprising all national electrotechnical committees (IEC National Committees). The object of IEC is to promote international co-operation on all questions concerning standardization in the electrical and electronic fields. To this end and in addition to other activities, IEC publishes International Standards, Technical Specifications, Technical Reports, Publicly Available Specifications (PAS) and Guides (hereafter referred to as “IEC Publication(s)”). Their preparation is entrusted to technical committees; any IEC National Committee interested in the subject dealt with may participate in this preparatory work. International, governmental and non-governmental organizations liaising with the IEC also participate in this preparation. IEC collaborates closely with the International Organization for Standardization (ISO) in accordance with conditions determined by agreement between the two organizations.
2) The formal decisions or agreements of IEC on technical matters express, as nearly as possible, an international consensus of opinion on the relevant subjects since each technical committee has representation from all interested IEC National Committees.
3) IEC Publications have the form of recommendations for international use and are accepted by IEC National Committees in that sense. While all reasonable efforts are made to ensure that the technical content of IEC Publications is accurate, IEC cannot be held responsible for the way in which they are used or for any misinterpretation by any end user.
4) In order to promote international uniformity, IEC National Committees undertake to apply IEC Publications transparently to the maximum extent possible in their national and regional publications. Any divergence between any IEC Publication and the corresponding national or regional publication shall be clearly indicated in the latter.
5) IEC itself does not provide any attestation of conformity. Independent certification bodies provide conformity assessment services and, in some areas, access to IEC marks of conformity. IEC is not responsible for any services carried out by independent certification bodies.
6) All users should ensure that they have the latest edition of this publication.
7) No liability shall attach to IEC or its directors, employees, servants or agents including individual experts and members of its technical committees and IEC National Committees for any personal injury, property damage or other damage of any nature whatsoever, whether direct or indirect, or for costs (including legal fees) and expenses arising out of the publication, use of, or reliance upon, this IEC Publication or any other IEC Publications.
8) Attention is drawn to the Normative references cited in this publication. Use of the referenced publications is indispensable for the correct application of this publication.
9) Attention is drawn to the possibility that some of the elements of this IEC Publication may be the subject of patent rights. IEC shall not be held responsible for identifying any or all such patent rights.

The main task of IEC technical committees is to prepare International Standards. However, a technical committee may propose the publication of a Technical Report when it has collected data of a different kind from that which is normally published as an International Standard, for example "state of the art".

IEC TR 63170, which is a Technical Report, has been prepared by IEC technical committee 106: Methods for the assessment of electric, magnetic and electromagnetic fields associated with human exposure.

The text of this Technical Report is based on the following documents:

| Enquiry draft | Report on voting |
|---|---|
| 106/426/DTR | 106/437/RVDTR |

Full information on the voting for the approval of this Technical Report can be found in the report on voting indicated in the above table.

This document has been drafted in accordance with the ISO/IEC Directives, Part 2.

The committee has decided that the contents of this document will remain unchanged until the stability date indicated on the IEC website under "http://webstore.iec.ch" in the data related to the specific document. At this date, the document will be

- reconfirmed,
- withdrawn,
- replaced by a revised edition, or
- amended.

A bilingual version of this publication may be issued at a later date.

**IMPORTANT – The 'colour inside' logo on the cover page of this publication indicates that it contains colours which are considered to be useful for the correct understanding of its contents. Users should therefore print this document using a colour printer.**

# INTRODUCTION

This Technical Report describes methods and measurement techniques for the evaluation of power density related to human exposures due to electromagnetic field (EMF) transmitting devices operating in close proximity to the user at frequencies between 6 GHz and 100 GHz where basic restrictions can be expressed in terms of power density. The types of devices include but are not limited to mobile telephones, tablets, and laptops.

With the rapid development of new wireless technologies in the frequency range 6 GHz to 100 GHz for the fifth generation mobile technology (5G), there is a need to establish assessment procedures to ensure compliance of wireless devices with electromagnetic exposure limits.

For portable devices, the IEC 62209 series of SAR assessment standards for wireless devices used in close proximity to the users are valid up to 6 GHz. For base stations, IEC 62232 defines the methods to assess the compliance boundaries based on reference levels and basic restrictions. SAR tests are applicable when the compliance distance is in close proximity to the radiating sources in the frequency range 300 MHz to 6 GHz. Power density measurements above 6 GHz are also applicable in close proximity to the equipment, but no detailed protocol is available at this stage.

SAR is not considered as the relevant exposure metric above 10 GHz in the International Commission on Non-Ionizing Radiation Protection (ICNIRP) guidelines which specify basic restrictions in terms of free-space incident power density. Similarly, IEEE C95.1-2005 [1][1] requires the assessment of incident power density above 6 GHz.

IEC TC 106 has previously noted the necessity to extend compliance assessment standards for portable devices beyond 6 GHz. However, with the 5G trials scheduled to commence in 2018, IEC TC 106 has decided on a two-step strategy to ensure that the fundamental assessment approaches are available by 2018.

1) IEC TC 106 (AHG10) focused in 2017 on the development of a Technical Report, specifying the state of the art of measurement techniques and test approaches for evaluating portable devices based on power density measurements from 6 GHz to 100 GHz.
2) IEC TC 106 submitted a new work item proposal in early 2018 to develop a new International Standard (IS) on the detailed measurement procedures to continue the work established in the Technical Report.

This informative document serves as the starting point for an International Standard. The methodologies and approaches described in this document can be useful for the assessment of early 5G products introduced for consumer trials. It also contains recommendations for future standardization work and highlights areas that may require additional investigation or consideration.

A few examples for measurements of a mock-up device characterized by an antenna array operating at about 28 GHz are given in Annex H.

[1] Numbers in square brackets refer to the Bibliography.

# MEASUREMENT PROCEDURE FOR THE EVALUATION OF POWER DENSITY RELATED TO HUMAN EXPOSURE TO RADIO FREQUENCY FIELDS FROM WIRELESS COMMUNICATION DEVICES OPERATING BETWEEN 6 GHz AND 100 GHz

## 1 Scope

This document describes the state of the art measurement techniques and test approaches for evaluating the local and spatial-average incident power density of wireless devices operating in close proximity to the users between 6 GHz and 100 GHz.

In particular, this document provides guidance for testing portable devices in applicable operating position(s) near the human body, such as mobile phones, tablets, wearable devices, etc. The methods described in this document may also apply to exposures in close proximity to base stations.

This document also gives guidance on how to assess exposure from multiple simultaneous transmitters operating below and above 6 GHz (including combined exposure of SAR and power density).

NOTE Compliance of devices with sufficiently low radiated power that is incapable of exceeding basic restrictions is addressed by IEC 62479 [2] and therefore not described in this document.

## 2 Normative references

There are no normative references in this document.

## 3 Terms and definitions

For the purposes of this document, the following terms and definitions apply.

ISO and IEC maintain terminological databases for use in standardization at the following addresses:

- IEC Electropedia: available at http://www.electropedia.org/
- ISO Online browsing platform: available at http://www.iso.org/obp

**3.1**
**averaging area**
rectangular or circular area on the evaluation surface (3.9) over which the assessed power density is averaged

Note 1 to entry: Because of rotational symmetry a circular area might be preferable since the result of averaging will not depend on the rotation.

**3.2**
**basic restriction**
restriction on exposure to time-varying electric, magnetic and electromagnetic fields that is based on established biological effects

**3.3**
**RF channel**
specific sub-division of the available frequency range according to the operating parameters of a wireless technology

**3.4**
**conducted power**
power delivered by the power amplifier to a matched load

**3.5**
**correlated signals**
<in time> electromagnetic fields, associated to distinct signal waveforms, yielding non-zero time-domain correlation integral at some time instant

Note 1 to entry: For two power-limited field distributions $\mathbf{F}_1(\mathbf{r},t)$ and $\mathbf{F}_2(\mathbf{r},t)$, the time-domain correlation integral is defined as

$$(\mathbf{F}_1 \otimes \mathbf{F}_2)(\mathbf{r},t) = \lim_{T\to\infty} \frac{1}{2T} \int_{-T}^{T} \mathbf{F}_1(\mathbf{r},\tau)^* \cdot \mathbf{F}_2(\mathbf{r},t+\tau)\,\mathrm{d}\tau \quad (1)$$

where $\mathbf{r}$ is the location vector, the superscript * represents the complex conjugate operation and the symbol · represents the inner product operation

Note 2 to entry: Observe that two fields are uncorrelated at locations where they are geometrically orthogonal. This property does not generally hold at nearby points unless the respective waveforms are uncorrelated.

In case of scalar signals, correlated signal waveforms yield a non-zero time-domain correlation integral at some time instant. For two power-limited signals $s_1(t)$, $s_2(t)$, said integral is defined as:

$$(s_1 \otimes s_2)(t) = \lim_{T\to\infty} \frac{1}{2T} \int_{-T}^{T} s_1(\tau)^* \cdot s_2(t+\tau)\,\mathrm{d}\tau \quad (2)$$

where the superscript * represents the complex conjugate operation.

Note 3 to entry: Two uncorrelated signals would feature a vanishing correlation integral, i.e. the above integral is equal to zero.

Note 4 to entry: Formulas (1) and (2) are originally specified in IEC TR 62630.

**3.6**
**device holder**
fixture constructed of low-loss dielectric material that is used to hold the DUT in the required test position during measurement

**3.7**
**device under test**
**DUT**
device that is tested according to the approaches described in this document to determine the power density

**3.8**
**duty factor**
ratio of the pulse duration to the pulse repetition period of a periodic pulse train

**3.9**
**evaluation surface**
surface, of a prescribed finite dimension, at a prescribed distance and orientation from the DUT where power density is assessed

Note 1 to entry: This is not necessarily the same as the measurement surface. Power density in the evaluation surface can be obtained, for instance, from measurement data in a different surface using reconstruction algorithms.

**3.10**
**exposure ratio**
**ER**
ratio of exposure metric and relevant exposure limit at a given operating frequency and location

EXAMPLE ER = $S/S_{\text{limit}}$

Note 1 to entry: Exposure ratio can also be expressed as a percentage, i.e. ER % = ER (dimensionless) × 100 %.

**3.11**
**far-field region**
region far from a source or aperture where the radiation pattern does not vary with distance from the source

**3.12**
**frequency band**
transmitting frequency range associated with a specific wireless operating mode

**3.13**
**measurement surface**
area, of a prescribed dimension, at a prescribed distance and orientation over which the electric and/or magnetic fields are measured using a probe sensitive to these quantities

Note 1 to entry: If the measurement surface and the evaluation surface are different, the data at the evaluation surface will then be derived from data taken at the measurement surface (measurements) by means of reconstruction algorithms.

Note 2 to entry: The dimension of the measurement surface is determined by the test equipment manufacturer based on the measurement methodology and test setup conditions necessary for evaluating the device under test.

**3.14**
**near-field region**
part of space between the antenna and the far-field region

**3.15**
**operating mode**
wireless protocol or standard used by a device to communicate in the wireless network

Note 1 to entry: Operating mode includes parameters such as modulation, source coding, channel bandwidth, etc.

**3.16**
**plane wave equivalent power density**
<of an electromagnetic wave> power density equal in magnitude to the power density of a plane wave

**3.17**
**power density**
**local power density**
$S$
energy per unit time and unit area crossing the infinitesimal surface d$A$ characterized by the normal unit vector $\hat{\mathbf{n}}$

$$S = \frac{1}{T}\int \left(\mathbf{E}\times\mathbf{H}\right)\cdot\hat{\mathbf{n}}\,\mathrm{d}T$$

where $\mathbf{E}$ and $\mathbf{H}$ are the electric and magnetic fields as function of time, respectively, and $T$ is the period of the waveform.

Note 1 to entry: For time harmonic fields, $\mathbf{E} = \Re\left(\mathbf{E}e^{i\omega t}\right)$, $\mathbf{H} = \Re\left(\mathbf{H}e^{i\omega t}\right)$

$$S = \frac{1}{2}\Re\left(\mathbf{E}\times\mathbf{H}^{*}\right)\cdot\hat{\mathbf{n}}$$

where $\omega$ is the (radian) frequency of the sinusoidal wave being considered and the superscript * represents the complex conjugate operation.

Note 2 to entry: In this document this quantity is also referred to as local power density to distinguish from spatial-average power density.

Note 3 to entry: Power density is expressed in W/m$^2$.

**3.18**
**spatial-average power density**
$S_{\text{av}}$
energy per unit time and unit area crossing a surface of area $A$ characterized by the normal unit vector $\hat{\mathbf{n}}$

$$S_{\text{av}} = \frac{1}{AT}\int\int\left(\mathbf{E}\times\mathbf{H}\right)\cdot\hat{\boldsymbol{n}}\,\mathrm{d}A\,\mathrm{d}T$$

Note 1 to entry: For time-harmonic fields

$$S_{\text{av}} = \frac{1}{2A}\Re\left(\int\mathbf{E}\times\mathbf{H}^{*}\cdot\hat{\mathbf{n}}\,\mathrm{d}A\right)$$

Note 2 to entry: For the purpose of this document, the surface on which power density or spatial-average power density are assessed corresponds to the evaluation surface (3.9).

**3.19**
**probe isotropy**
measure of the degree to which the response of an electric field or magnetic field probe is independent of the polarization and direction of propagation of the incident wave

**3.20**
**readout electronics**
measurement system component that connects to the electric or magnetic field probe and provides an analog to digital conversion of the measured values to the post processor of the measurement system

**3.21**
**reconstruction algorithm**
algorithms, mathematical techniques and procedures that are applied to the measured fields to propagate, transform, project or reconstruct the power density distribution at the evaluation surface to determine spatial-average and/or local power density

**3.22**
**response time**
time required by the measuring equipment to reach 90 % of its final measurement value after a step variation of the input signal

**3.23**
**scanning system**
automatic positioning system capable of placing the measurement probe at specified positions with known accuracy

**3.24**
**small probe**
E- or H-field sensor that has sufficient resolution and is sufficiently non-perturbing so that the measurements can be made to the required accuracy

**3.25**
**uncertainty**

**3.25.1**
**standard uncertainty**
estimated standard deviation of a measurement result, equal to the positive square root of the estimated variance

**3.25.2**
**combined uncertainty**
estimated standard deviation of the measurement result obtained by combining the individual standard uncertainties of both Type A and Type B evaluations using the usual “root-sum-squares” method for combining standard uncertainties

**3.25.3**
**expanded uncertainty**
quantity defining an interval about the result of a measurement that is expected to encompass a distribution of values within a defined confidence interval that could reasonably be attributed to the measured quantity

**3.26**
**uncertainty evaluation**
<Type A> evaluation of uncertainty by the statistical analysis of series of observations (measurements)

**3.27**
**uncertainty evaluation**
<Type B> evaluation of uncertainty by means other than the statistical analysis of series of observations (measurements)

## 4 Symbols and abbreviated terms

### 4.1 Symbols

#### 4.1.1 Physical quantities

The internationally accepted SI units are used throughout this document.

| Symbol | Quantity | Unit | Dimensions |
|---|---|---|---|
| $E$ | Electric field | volt per metre | V/m |
| $f$ | Frequency | hertz | Hz |
| $H$ | Magnetic field | ampere per metre | A/m |
| $\lambda$ | Wavelength | metre | m |
| $S$ | Local power density | watt per square metre | W/m$^2$ |
| $S_{av}$ | Spatial-average power density | watt per square metre | W/m$^2$ |

#### 4.1.2 Constants

| Symbol | Physical constant | Magnitude |
|---|---|---|
| $\eta$ | Intrinsic impedance of free space | 120 $\pi$ $\Omega$ or 377 $\Omega$ |

### 4.2 Abbreviated terms

BS base station
CW continuous wave
DUT device under test
EMF electromagnetic field
ER exposure ratio
NR new radio
PD power density
RF radio frequency
TER total exposure ratio

## 5 Description of the measurement system

### 5.1 General

The measurement system for evaluating power density of portable devices typically consists of the electronic measurement instrumentation, the field probe(s), a scanning system, a DUT holder and the necessary post-processing software. Different measurement methods generally require different test setup, measurement configurations and field reconstruction techniques to determine power density in the evaluation surface. The measurement protocol in this document is based on mechanically positioning the probe in a structured grid relative to the DUT to scan the electric and/or magnetic fields. While some methods require the phase of the fields to be determined, others are based on field amplitude only. The measurement system is validated according to Annex A.

The tests should be performed in a laboratory environment conforming to the following conditions.

1) The test site should be evaluated to minimize the level of RF perturbation due to reflections and ambient noise. In particular, the effect of reflections from cables, test equipment, or other scattering objects should be determined and characterized in the uncertainty budget.

   NOTE International Standards such as CISPR 16-1-4 [3] can provide guidance on minimizing radio frequency disturbances when performing radiated measurements.

2) Ambient temperature should be within the operating range specified for the measurement equipment and DUT.

When possible and allowed by national requirements, an RF source, e.g. a signal generator or a synthesizer and amplifier, may replace the transmitter that supplies power to the antenna input, provided that this does not change DUT performance, including transmit power and power density distributions, or that the impact of power density assessment uncertainty is properly evaluated and remains acceptable. Under such circumstance, the power chain should be carefully evaluated to accurately determine the input power fed to the antenna. Otherwise a base station simulator, a communication test set or acceptable internal test software should be used to set up the device.

### 5.2 Scanning system

Scanning systems typically position the probe to perform measurements on a spherical, cylindrical or planar configuration. For each of these coordinate systems, different physical, mechanical, or electrical solutions may be required for the scanning system. For instance, some implementations might require both translation and rotation of the probe; others, although not addressed in this document, have a fixed probe and the DUT is positioned accordingly. Descriptions of specific scanning methodologies are provided for instance in [4].

Precise probe positioning is critical because the measured field accuracy can have significant impact on the evaluation of power density. The scanning system should ensure that probes are positioned at each measurement point with high accuracy. The measurement resolution is chosen to satisfy both spatial and, if applicable, spectral sampling rate as well as the resolution required by the measurement methodology to maintain conversion accuracy. When sensors at the probe tip are spatially offset or fields are averaged across the probe aperture or volume (e.g. waveguide probes), validation of the probe calibration and measurement point(s) accuracy are necessary to maintain measurement accuracy. Depending on the frequency, small spatial offsets in sensor locations or shifts in measurement point locations can have a large impact on the measured results, especially in steep field gradients or complex field conditions close to the antenna. If sensor offsets are not compensated or accounted for, both the measured results and the output of the field conversion algorithms that are sensitive to such positioning can be influenced substantially.

### 5.3 Device holder

The device holder or an equivalent setup is used to position the DUT during the measurement. The DUT is positioned into a holder with negligible effect on measured fields. To avoid perturbation, a holder made of low loss and low permittivity material(s), with loss tangent $\leq 0{,}005$ and relative permittivity $\leq 1{,}2$ is recommended.

### 5.4 Reconstruction algorithms

Reconstruction algorithms are used to project or transform the measured fields from the measurement surface to the evaluation surface (Figure 1) in order to determine power density or to compute spatial-average and/or local power density with known uncertainty. The term reconstruction algorithms identifies also techniques to resolve the H-field from the E-field (or vice versa) and/or methodologies to retrieve field information from the measured data (e.g. the phase from the amplitude).

The field reconstruction algorithms are validated and documented by the equipment manufacturer. In particular, it should be described in detail how the measured field components at the measurement points are used to determine power density at the evaluation surface. Some examples are provided in Annex G.

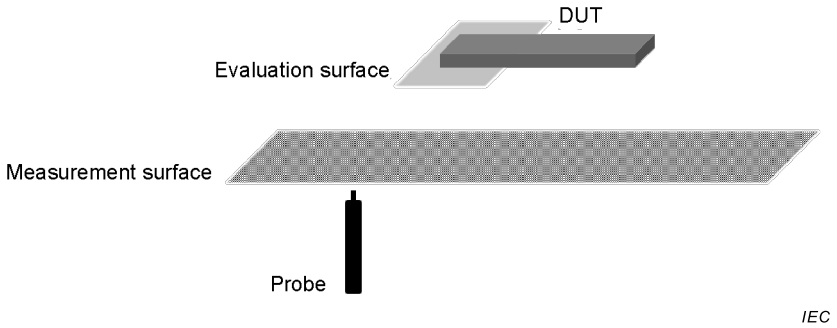


NOTE The measurement and evaluation surface dimensions, their orientations and positions have been simplified for illustration purposes (see Clause 6 for additional information).

**Figure 1 – Simplified view of a generic measurement setup involving the use of reconstruction algorithms**

## 6 Power density assessment

### 6.1 General

The measurements are carried out with good laboratory practice, e.g. in accordance with [5], and other local and national compliance requirements. The evaluations should generally follow a sequence of steps. A high-level flow-chart of the evaluation process is shown in

Figure 2. Beginning with an evaluation plan and measurement approach, the process converges to the full power density evaluation and uncertainty analysis. Proper documentation and reporting completes the evaluation process.

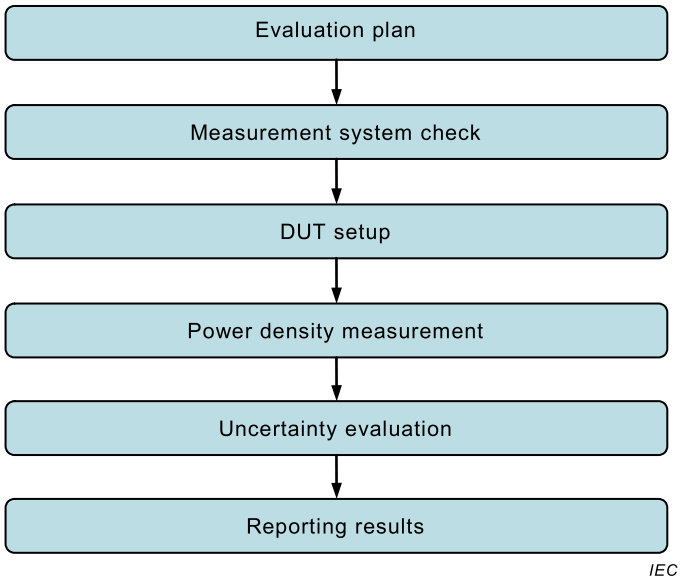


**Figure 2 – Evaluation process overview**

Figure 3 provides an overview of the power density measurement methodology described in this document. The measurement systems and techniques which conform to this general flowchart might vary. A description of each step is provided in 6.2 to 6.5 together with the applicability constraints for each step, the information required to implement the method and generic guidelines on how to characterize the uncertainty of the evaluation.

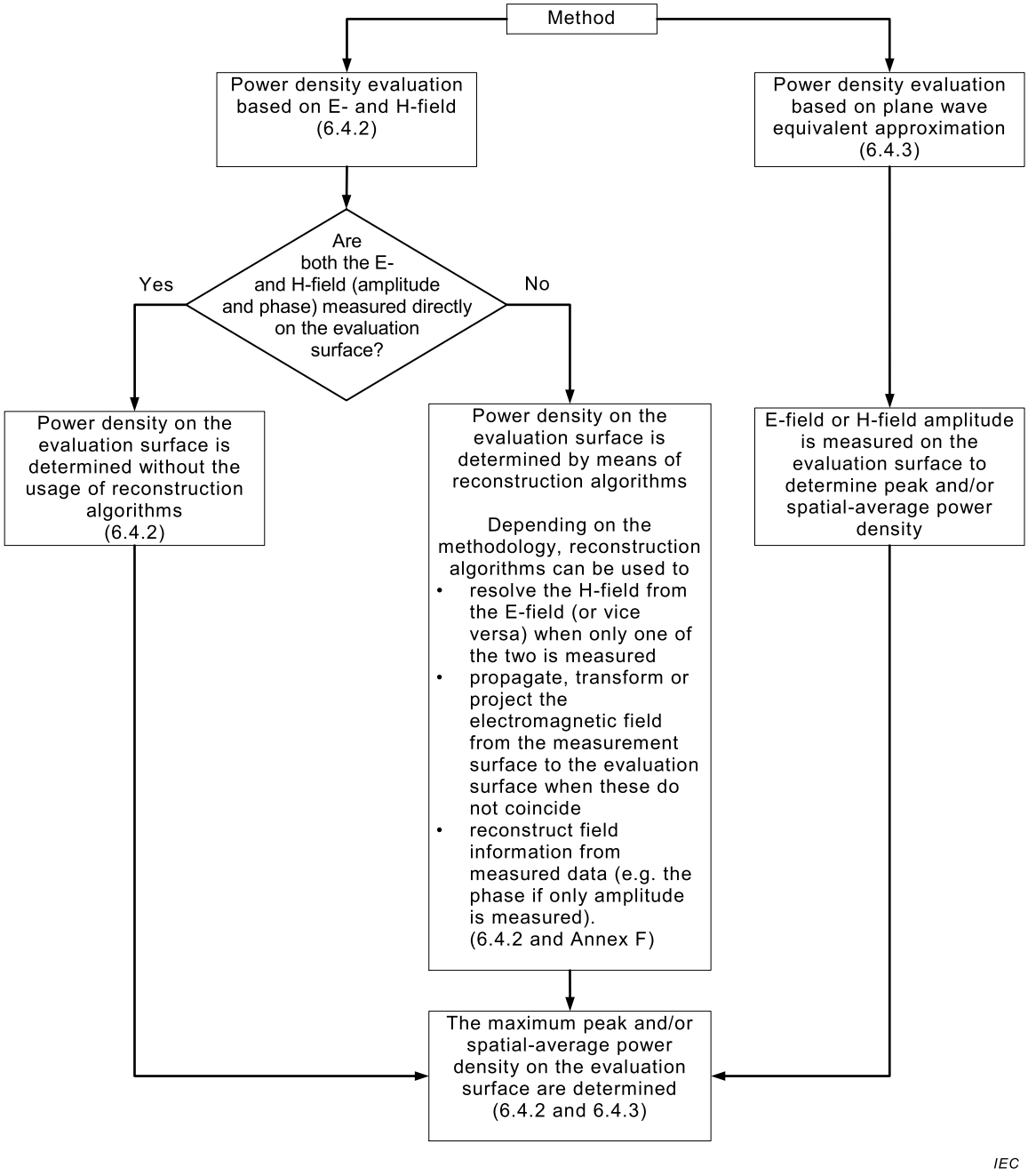


**Figure 3 – Overview of power density measurement methods**

## 6.2 Measurement preparation

### 6.2.1 System check

A system check according to the procedures of Annex A should be completed to verify that the system operates within specifications before conducting measurements to assess the power density of a DUT. The system check confirms the measurement repeatability and post-processing algorithm accuracy with a calibrated source or other known reference source(s) to ensure that the system works correctly and is acceptable for compliance testing. The system check can also detect possible measurement drifts over time and other unexpected problems in the system, such as

- component failures,
- component drift,

- operator errors in the set-up or the software parameters,
- adverse conditions in the system, e.g. RF interference.

### 6.2.2 Preparation of the device under test

The RF output power and frequency (channel) are controlled by a wireless link to a base station, network simulator or test mode software. Alternatively, an external generator or a synthesiser and amplifier may be used to replace the transmitter, provided both measured fields and power density assessment of the DUT are unaffected and it is acceptable by the applicable national regulation, or the impact on power density assessment uncertainty is properly evaluated and remains acceptable. The power chains to all transmitting elements of the antenna array(s) are evaluated to accurately determine the input power fed to the antenna.

The measurements are performed at the maximum power level consistent with product specifications and production variations. The measured power density is scaled to the highest time-averaged maximum output power allowed for production units, including output tolerances. The maximum time-averaged power of the DUT can be verified, for example, if applicable, by conducted power measurements with a fully charged battery or, as appropriate, according to radiated power measurements and other operating parameters to support the scaling.

### 6.2.3 Operating modes

DUTs can transmit in operating modes and frequency bands using different signal characteristics (e.g. modulation, source coding, channel bandwidth, etc.) that require power density tests. The appropriate operating modes should be selected for testing taking into consideration differences in maximum output power and production variations, to ensure maximum power density is assessed.

Guidance for selecting frequency channels within a frequency band for testing is provided in 6.2.4. The frequency channels in each wireless technology (e.g. 5G New Radio and WiGig®[2]) supported by the DUT should be tested in the operating mode corresponding to the maximum RF output power conditions. RF conducted power should be measured and, as necessary, radiated or other methods should be applied, to verify these are the highest output configuration(s). If the DUT is tested in a lower power configuration, evidence of scaling linearity is necessary to scale power density to the highest time-averaged output power level. The scaling factor should be assessed and documented in the test report.

When the DUT is operated in test mode (e.g. using proprietary test software), the maximum output power and transmission characteristics are set to be consistent with actual use conditions.

For devices operating simultaneously with multiple antennas or multiple transmitters (with single or multiple antennas), maximum output power is established for each transmitter and antenna as described above to ensure the aggregate transmit power from all antennas is also at the maximum. The contribution of power density from each antenna is combined as described in 6.5.

NOTE IEC 62209-1 and IEC 62209-2 provide further guidance on operating modes.

### 6.2.4 Test frequencies for DUT

Since power density can vary over the DUT operating bandwidth, the purpose of this subclause is to define the frequency channel or a practical subset of channels where power

---

2 WiGig is a registered trademark of Wi-Fi Alliance. This information is given for the convenience of users of this document and does not constitute an endorsement by IEC.

density measurements are performed. This channel or subset of channels is chosen to characterize the power density of a DUT according to applicable exposure limits.

NOTE For wide band systems the maximum output power of a channel may vary across the frequency band. The required test channels may not include the channel with the highest RF transmit power. Therefore, before performing testing using the specific channels required by this document, it is important to verify the maximum output power of the channels to determine that the chosen channels are indeed producing the highest rated output of the device. It is important that the process used to establish the channels for testing purposes is documented in the test report.

For each wireless technology and frequency band used by the DUT, tests should be performed at the channel closest to the centre of each transmit frequency band. If the width of the transmit frequency band ($\Delta f = f_{high} - f_{low}$) exceeds 1 % of its centre frequency $f_c$, then the channels at the lowest and highest frequencies of the transmit band are also tested. Furthermore, if the width of the transmit band exceeds 10 % of its centre frequency, the following formula is used to determine the number of channels, $N_c$, to be tested:

$$N_c = \min(2 \times \text{roundup}\,[10 \times (f_{high} - f_{low})/f_c] + 1, N)$$

where

$f_c$ is the centre frequency channel of the transmission band in Hz;

$f_{high}$ is the highest frequency channel of the transmission band in Hz;

$f_{low}$ is the lowest frequency channel of the transmission band in Hz;

$N_c$ is the number of channels to be tested;

$N$ is the total number of channels.

NOTE 1 The function $\text{roundup}(x)$ rounds its argument $x$ to the next highest integer. Thus, the number of channels, $N_c$, will always be an odd number. The channels tested are equally spaced apart in frequency (as much as possible) and include the channels at the lowest and highest frequencies. Depending on the field-probe and equipment used, substantially large transmission bands may require multiple probe calibration points to cover the entire frequency band.

NOTE 2 Regulatory agencies may have different requirements on the number of channels to be tested per transmission band, according to frequency allocations and other wireless technology requirements.

NOTE 3 If the test frequency yielding the highest output power does not correspond to the middle channel, the test requirements may vary among different national regulatory authorities.

### 6.2.5 Evaluation surface and DUT test position

For purpose of this document, two evaluation surface and DUT test positioning alternatives are given. A sufficiently large evaluation surface is required for both alternatives to ensure maximum spatial-average and/or the local power density is determined accurately as required by the measurement methodology. Details of the evaluation surfaces and DUT test positions are required in the test report to support the results.

Alternative 1: Assessment of user exposure

Power density is assessed on surface(s) corresponding to local representations of the user's head and/or body surfaces. Evaluation surfaces corresponding to the shape of the SAM phantom or flat phantom inner shell defined in IEC 62209, respectively for head (Figure 4) and body (Figure 5) exposure conditions are used for this alternative. The DUT test positions described in IEC 62209 to assess next to the ear, near body and extremity exposures are used to position portable devices for power density evaluation.

All use conditions described in IEC 62209 for exposures to the user's head, body and extremity, are assessed, unless a technical rationale for considerably reduced exposure potential in some of the use conditions can be justified and demonstrated (see 9.1.5.1).

An evaluation surface conformal to the SAM phantom shape can complicate the power density measurement and evaluation process. As an alternative, measurement or evaluation plane(s)

tangential to the inner shell surface of the SAM phantom shape may be considered when it can be demonstrated to yield conservative power density results (see Figure 4).

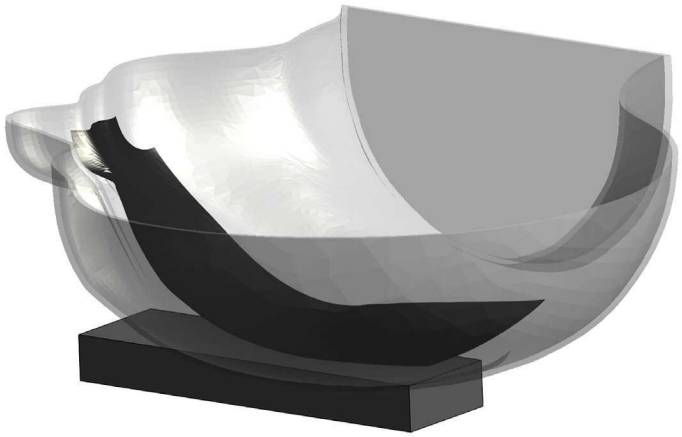


**(a) Evaluation surface corresponding to the SAM phantom surface shape**

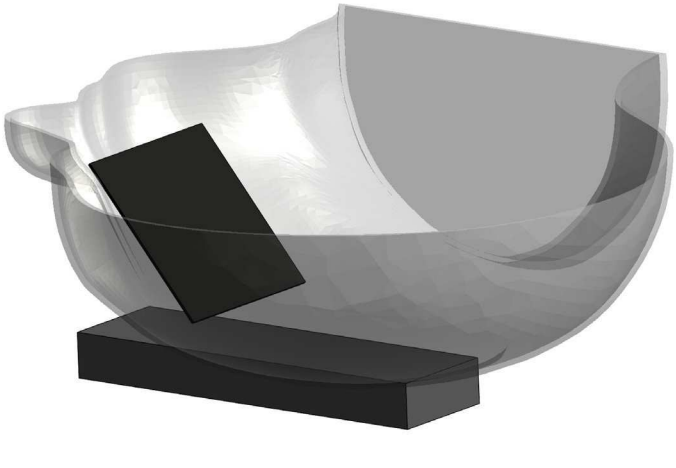


**(b) Evaluation surface tangential to the SAM phantom surface shape**

NOTE The SAM profile identifies only the geometrical shape; power density is evaluated in free-space without the presence of a phantom. The dimension of the evaluation surface for a) and b) is for illustration purposes only.

**Figure 4 – Illustration of evaluation surface (in black)**

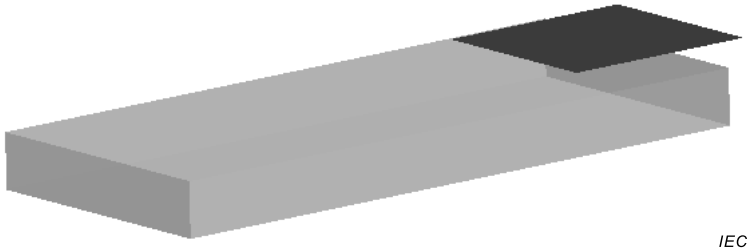


NOTE The dimension of the evaluation is for illustration purposes only.

**Figure 5 – Illustration of evaluation surface corresponding to the flat phantom surface shape**

Alternative 2: Assessment of maximum user exposure potential

Power density is assessed in the evaluation surface(s) corresponding to the maximum available local or spatial-average power density. The separation distance can be measured from the geometrical centre point of the antenna or antenna array on the surface of the device to the evaluation surface (Figure 6).

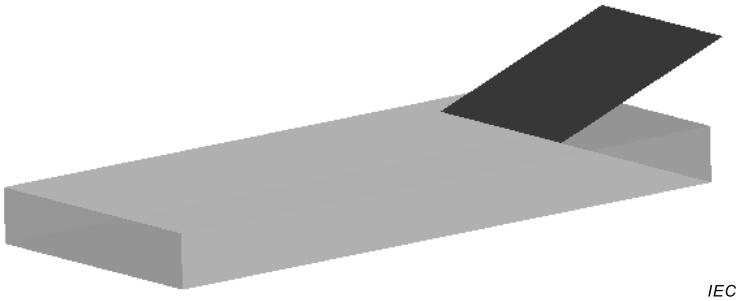


NOTE The dimension of the evaluation surface is for illustration purposes only.

**Figure 6 – Illustration of evaluation surface corresponding to the maximum available local or spatial-average power density**

Additional information for both alternatives is available in Clause 9.

### 6.3 Tests to be performed

The highest spatial-average and/or local power density among all use conditions is determined according to the maximum power density for the device positions, configurations and operational modes tested in each frequency band.

### 6.4 General measurement procedure

#### 6.4.1 General

A flow-chart describing the overall measurement procedure is provided in Figure 3. In order to determine near-field power density, the E- and H-field are necessary. The time averaged power density $S_{\text{av}}$ over a surface of area $A$ characterized by the normal vector $\hat{\mathbf{n}}$ is given by (see 3.17)

$$S_{\text{av}} = \frac{1}{T \cdot A} \int\int \mathbf{E} \times \mathbf{H} \cdot \hat{\mathbf{n}} \mathrm{d}T \mathrm{d}A, \tag{1}$$

where $T$ is the averaging time and **E** and **H** are the electric and magnetic fields as function of time respectively. For time harmonic fields, $\mathbf{E} = \Re\left(\mathbf{E}e^{i\omega t}\right)$, $\mathbf{H} = \Re\left(\mathbf{H}e^{i\omega t}\right)$ and

$$S_{\text{av}} = \frac{1}{2A} \Re\left(\int \mathbf{E} \times \mathbf{H}^{*} \cdot \hat{\mathbf{n}} \mathrm{d}A\right) \quad , \tag{2}$$

where $\mathbf{H}^{*}$ represents the complex conjugate of the H-field phasor.

In the far-field of the source, the E-field and H-field at every point in space are orthogonal to each other, they are in phase, and they are related through a scalar constant: $\mathbf{H} = \frac{\hat{\mathbf{r}} \times \mathbf{E}}{\eta}$. Therefore, the power density can be simplified to:

$$S_{\text{av}} = \frac{1}{2\eta A}\left(\int |\mathbf{E}|^2 \hat{\mathbf{r}} \cdot \hat{\mathbf{n}} \mathrm{d}A\right) \quad \text{or} \quad S_{\text{av}} = \frac{\eta}{2A}\left(\int |\mathbf{H}|^2 \hat{\mathbf{r}} \cdot \hat{\mathbf{n}} \mathrm{d}A\right), \tag{3}$$

where $\hat{\mathbf{r}}$ is the vector corresponding to the radial direction and $\eta$ is the free-space wave impedance. This enables power density in the far field to be determined by assessing only the amplitude of either the electric or magnetic field.

At short distances from the source there is no simple relationship between E-field and H-field. Therefore, both E-field and H-field need to be assessed to determine the correct power density. The plane wave equivalent approximation may underestimate or overestimate power density when the evaluation plane is in the near-field. Preliminary criteria to establish at which distance this approximation is valid are provided in 6.4.3.

When the national regulation or the applicable exposure standard provides a different expression or interpretation for the incident power density, those expressions or interpretations are used to evaluate $S_{\text{av}}$.

### 6.4.2 Power density assessment based on E- and H-field

Within a short distance from the transmitting source, power density is determined based on both electric and magnetic fields. Generally, the magnitude and phase of two components of either the E-field or H-field are needed on a sufficiently large surface to fully characterize the total E-field and H-field distributions. Nevertheless, solutions based on direct measurement of E-field and H-field can be used to compute power density (see, for example, Clause H.4). The measurement points are chosen according to the requirements of the methodology used. Together, these points form the measurement surface. When the measurement surface does not correspond to the evaluation surface, reconstruction algorithms are necessary to project or transform the fields from the measurement surface to the evaluation surface. The general measurement approach is summarized in a) to g).

a) Measure the E- or H-field on the measurement surface at a reference location where the field is well above the noise level. This reference level will be used at the end of this procedure to assess output power drift of the DUT during the measurement.

b) Scan the electric and/or magnetic field on the measurement surface. The requirements of measurement surface dimensions (as, for instance, the ratio between the field strength measured at the edges of the scan area with respect to the peak) and spatial resolution are dependent on the measurement system and assessment methodology applied. Measurements are therefore conducted according to the instructions provided by the measurement system manufacturer.

   The distance from the measurement surface to the DUT is chosen carefully to avoid field perturbation by the probe(s). A part of the signal incident on the probe can be scattered and reflected back and forth between the DUT and the probe. These multiple DUT-probe reflections can alter the field distribution surrounding the device. The reflection errors generally decrease with increasing measurement distance. For miniature rectangular or circular waveguide probes, a few wavelengths are typically necessary to avoid unacceptable field perturbation. For low-directivity DUT antennas, the distance may be reduced. The field perturbation of probes consisting of small dipole or small loop sensors to the measured field can be sufficiently small for distances down to a $\lambda$ or even fractions of a $\lambda$. In any case, probe perturbation and the uncertainty due to multiple reflections need to be characterized.

c) Measurement spatial resolution can depend on the measured field characteristic and measurement methodology used by the system. Planar scanners typically require a step

size of less than $\lambda/2$. When measurements are acquired in regions where evanescent modes are not negligible, smaller spatial resolution may be required [4]. Similar criteria also apply to cylindrical scanning systems where the spatial resolution in the vertical direction should be less than $\lambda/2$. In the azimuth direction, the angular step size $\Delta\phi$ should be less than $\lambda/(2\rho_{\text{meas}})$ in radians, where $\rho_{\text{meas}}$ denotes the radial distance at the measurement locations. For spherical systems, the maximum angular step sizes in elevation and azimuth can be defined analogously as $\Delta\theta = \Delta\phi = \lambda/(2R_{\text{meas}})$ where $R_{\text{meas}}$ denotes the radial distance at the measurement locations. The positioning uncertainty of the probe sensors at the measurement points should be analysed and documented.

d) If only one field (E-field or H-field) is measured, the other field is calculated from the measured field using a reconstruction algorithm. As Formula (2) requires knowledge of both amplitude and phase, reconstruction algorithms can also be used to obtain field information from the measured data (e.g. the phase from the amplitude if only the amplitude is measured). In addition, when the measurement surface does not correspond to the evaluation surface, reconstruction algorithms are employed to project or transform the fields from the measurement surface to the evaluation surface. In substance, reconstruction algorithms are the set of algorithms, mathematical techniques and procedures that are applied to the measured field on the measurement surface to determine E- and H-field (amplitude and phase) on the evaluation surface. An overview and description of applicable algorithms and techniques is provided in Annex F.

   The validation of reconstruction algorithms should be demonstrated and documented in detail, including the minimum measurement plane dimensions and separation distance from the source to which the algorithm is applicable to the particular measurement probe or methodology.

   If both E-field and H-field are directly measured (amplitude and phase) on the evaluation surface, a reconstruction algorithm is not needed to assess power density.

e) Use Formula (2) to determine the spatial-average power density distribution on the evaluation surface. The spatial averaging area, $A$, is specified by the applicable exposure limits or regulatory requirements. If the shape of the area is not provided by the relevant regulatory requirements, a circular shape is recommended (see Annex E).

f) The maximum spatial-average and/or local power density on the evaluation surface is the final quantity to determine compliance against applicable limits.

g) Measure the E-field or H-field on the measurement surface position at the reference location chosen in step a). The power drift of the DUT is estimated as the difference between the squared amplitude of the field values taken in steps a) and g). When the drift is smaller than ± 5 %, this term should be considered in the uncertainty budget. Drifts larger than 5 % due to the design and operating characteristics of the device should be accounted for or addressed according to regulatory requirements to determine compliance

### 6.4.3 Power density measurement based on the evaluation of E-field or H-field amplitude only

If the evaluation surface is in the far-field of the DUT, power density is given by Formula (3) and only the amplitude of the electric or magnetic fields need to be measured on the evaluation surface to correctly derive power density. If, for the tested configuration, the separation distance between the DUT transmitting antennas and the evaluation surface fulfils the far-field criteria in Table 1 [6], the following procedure can be used as an alternative to that provided in 6.4.2. As shown in Annex D, Formula (3) might be accurate also at shorter distances than those specified in Table 1 and can be used if justified.

a) Measure the local E-field or H-field on the evaluation surface at a reference location where the field is well above the noise level. This reference level will be used at the end of this procedure to assess output power drift of the DUT during the measurement.

b) Measure the electric or magnetic field amplitude on the evaluation surface. A spatial resolution of at most $\lambda/2$ is recommended. A coarser sampling resolution can be adopted provided that the impact on the measurement uncertainty is characterized and documented.

c) Use Formula (3) to determine the spatial-average power density on the evaluation surface. The averaging area, $A$, is specified by the applicable exposure limits or regulatory requirements. If the shape of the area is not provided by the relevant regulatory requirements, a circular shape is recommended. In Formula (3) the radial vector is considered to be determined from the geometrical centre of the transmitting antenna[3]. If no information about the DUT antenna is available, power density can be conservatively assessed by Formula (4):

$$S_{\text{av}} = \frac{1}{2\eta A}\int |\mathbf{E}|^2 \, \mathrm{d}A \tag{4}$$

Formula (4) is more conservative than Formula (3) if the evaluation surface is not orthogonal to the Poynting vector.

d) Calculate the maximum spatial-average and/or local power density over the evaluation surface.

e) Measure the E-field or H-field on the evaluation surface position at the reference location chosen in step a). The power drift of the DUT is estimated as the difference between the squared amplitude of the field values taken in steps a) and e). When the drift is smaller than ± 5 %, this term should be included in the uncertainty budget. Drifts larger than 5 % due to the design and operating characteristics of the device should be accounted for or addressed according to regulatory requirements to determine compliance.

**Table 1 – Minimum separation distance between the DUT's antenna and the evaluation surface for which Formula (3) applies**

| Antenna dimension | Minimum distance |
|---|---|
| $D < \frac{1}{3}\lambda$ | $1{,}6\,\lambda$ |
| $\frac{1}{3}\lambda < D < 2{,}5\,\lambda$ | $5D$ |
| $D > 2{,}5\lambda$ | $\frac{2D^2}{\lambda}$ |
| $D$ is the maximum linear dimension of the antenna operating in the selected configuration. | |

## 6.5 Measurements of devices with multiple antennas or multiple transmitters

### 6.5.1 General

Subclause 6.5 describes how to determine the combined exposure from multiple antennas operating simultaneously such as those of an array or of individual sources operating within different frequency bands.

The fields generated by the antennas can be correlated or uncorrelated. At different frequencies, fields are always uncorrelated, and the aggregate power density contributions can be summed according to spatially averaged values of corresponding sources at any point in space, $\mathbf{r}$, to determine the total exposure ratio (TER). Assuming $I$ sources, the TER at each point in space is equal to

[3] In theory, Formula (3) is exact at infinite distance where the antenna appears as a point source and the definition of $\hat{\mathbf{r}}$ is unambiguous. Since the minimum separation between the observation point and the DUT antenna should fulfil the requirements in Table 1 and it is therefore much larger than the maximum antenna size, the error introduced by considering the origin over any other point of the DUT antenna is expected to be small.

$$\mathrm{TER}^{\mathrm{uncorr}}(\mathbf{r}) = \sum_{i=1}^{I} \mathrm{ER}_i = \sum_{i=1}^{I} \frac{S_{\mathrm{av},i}(\mathbf{r}, f_i)}{S_{\mathrm{lim}}(f_i)} \tag{5}$$

where $S_{\mathrm{av},i}$ is the power density (as defined in 6.4) for the source $i$ operating at a frequency $f_i$ and $S_{\mathrm{lim}}$ is the power density limit as specified by the relevant standard.

Exposure from transmitters operating above and below $f_{\mathrm{tr}}$, where $f_{\mathrm{tr}}$ denotes the transition frequency where the basic restrictions change from being defined in terms of SAR to being defined in terms of power density, are therefore uncorrelated and the TER is determined as

$$\mathrm{TER}^{\mathrm{uncorr}}(\mathbf{r}) = \mathrm{TER}(\mathbf{r})_{f \le f_{\mathrm{tr}}} + \mathrm{TER}(\mathbf{r})_{f > f_{\mathrm{tr}}} \tag{6}$$

NOTE For frequencies below the transition frequency, the exposure ratio is assessed using the procedures in IEC 62209-1 and IEC 62209-2 by dividing the resulting spatial-peak SAR value with the corresponding limit.

Figure 7 illustrates how SAR and power density at a point $\mathbf{r}$ can be combined assuming power density on a plane surface and SAR at the surface of a flat phantom (e.g. for body exposure). Before summing the TERs [see Formula (6)], the corresponding SAR and power density values are to be spatially averaged, around $\mathbf{r}$, according to the applicable standard (e.g. 1 g or 10 g for SAR, 4 $\mathrm{cm}^2$ for power density in the example of Figure 7). For locations inside the phantom, the peak spatial-average SAR of individual points are not centred on the surface of the 1 g or 10 g cube.

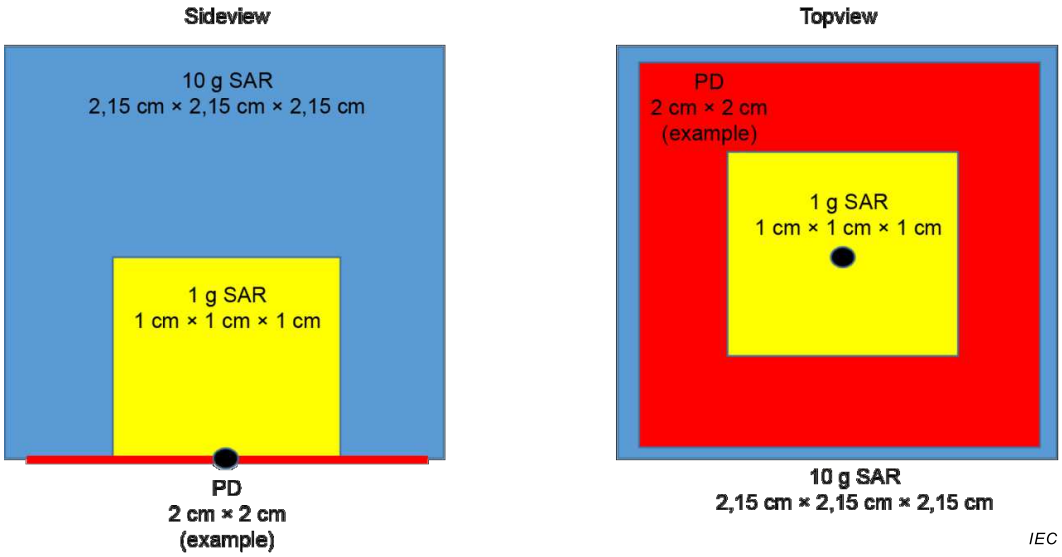


**Figure 7 – SAR and power density evaluation at a point $\mathbf{r}$**

For correlated fields, the determination of the combined exposure from $I$ simultaneously transmitting sources requires the true vector summations according to

$$\mathbf{E}^{\mathrm{corr}}(\mathbf{r}) = \sum_{i=1}^{I} \mathbf{E}_i(\mathbf{r}, f) \tag{7}$$

$$\mathbf{H}^{\mathrm{corr}}(\mathbf{r}) = \sum_{i=1}^{I} \mathbf{H}_i(\mathbf{r}, f) \tag{8}$$

From Formulas (7) and (8), the average power density is determined according to Formulas (2), (3) or (4) from which $TER^{corr}$ is obtained by normalizing with the appropriate exposure limit.

### 6.5.2 Examples

#### 6.5.2.1 General

The generic expressions in Formulas (5) to (8) can be used to obtain the total exposure once the contribution from each antenna or antenna element in an array is assessed. Further guidance on how to measure exposure for multiple transmitters is provided in 6.5.2.2 and 6.5.2.3 for two possible DUT configurations.

#### 6.5.2.2 DUT with one array antenna operating at $f > f_{tr}$

The fields transmitted by the elements of the array can be correlated or uncorrelated depending on the transmission technique adopted by the DUT. For instance:

– for transmission modes making use of beamforming the fields can be correlated as each antenna port is fed by the same signal scaled in phase and, eventually, in amplitude.

– for spatial multiplexing the fields are uncorrelated as the input to the antenna ports corresponds to independent linear combination of one or more ‘data layers’.

In case of correlated fields, the electric and magnetic field on the evaluation surface(s) are determined, as described in 6.4, for each antenna element operating separately. $\mathbf{E}^{corr}$ and $\mathbf{H}^{corr}$ are obtained according to Formulas (7) and (8) for all possible linear combinations corresponding to different phase and amplitude weights (codebook). The combined averaged power density is therefore assessed according to Formula (2) and the maximum value for all combinations is selected. The combining of the electric and magnetic fields requires knowledge of both amplitude and phase for each component.

If the codebook is unknown, an overestimate of the combined power density distribution on the evaluation surface is given by

$$\frac{1}{2}\sum_{i=1,l=1}^{I,L}\left|\left(\mathbf{E}_i(\mathbf{r})\times\mathbf{H}^*_l(\mathbf{r})\right)\cdot\hat{\mathbf{n}}\right|, \tag{9}$$

where $\mathbf{E}_i$ and $\mathbf{H}_l$ are the electric and magnetic field for the antenna $i$ and $l$, respectively. The power density obtained in this fashion is then spatially averaged according to the applicable limits. Formula (9) might largely overestimate power density. More accurate but more complex methodologies, providing the upper bound of power density for array antennas are described in [7]. Formula (9) requires knowledge of both amplitude and phase of the electric and magnetic field components. A simpler expression, based on the amplitude only is provided in Formula (10):

$$\frac{1}{2}\sum_{j=1,i=1}^{J,I}\left|\mathbf{E}_i(\mathbf{r})\right|\cdot\left|\mathbf{H}_l(\mathbf{r})\right|. \tag{10}$$

Formula (10) leads to an even larger overestimation of the combined power density compared with Formula (9).

An alternative to combining exposures obtained separately for the different antennas is to conduct repeated measurements corresponding to all phase (and amplitude) combinations between the transmitters. This evaluation is time consuming and may not be practical.

When the fields from the different antennas are uncorrelated, power density is determined according to 6.4 for all antennas operating simultaneously. Otherwise, if the contribution for each element is known, the power density distribution contributions on the evaluation surface can be determined as

$$\mathbf{S}(\mathbf{r}) = \sum_{i=1}^{I} \mathbf{S}_i(\mathbf{r}) \tag{11}$$

The maximum spatial-average power density on the evaluation surface is calculated from the distribution of the combined power density $\mathbf{S}(\mathbf{r})$.

#### 6.5.2.3 DUT with one array antenna opertating at $f > f_{tr}$ and one antenna operating at $f < f_{tr}$ both transmitting simultaneously

Power density, and therefore the exposure ratio, for the array operating at above $f_{tr}$ is determined according to 6.5.2.2. For the transmitter below $f_{tr}$, exposure is assessed in terms of SAR using the procedures in IEC 62209 series of SAR assessment standards. When these values are known, the following options can be used to obtain the TER for the DUT.

#### 6.5.2.4 Alternative 1: Evaluation by considering spatial exposure distributions

Exposure ratios (for frequencies above and below $f_{tr}$) are summed point-by-point [according to Formula (6)]. The TER is then taken as the maximum value of this summation. This methodology is the most accurate but it requires evaluation of localized SAR and local or spatial-average power density at common locations in space. For instance, this is possible if the power density is determined on evaluation surface(s), corresponding to a representation of the user's head or body surface, consistent with the SAM and/or body phantom definitions in IEC 62209 (see Alternative 1 in 6.2.5), where summing of TER for additional points inside the phantom is not necessary.

If the antennas are located at different positions, it might be necessary to evaluate SAR nearby the antennas operating above $f_{tr}$ and power density nearby the antennas transmitting below $f_{tr}$.

For array antennas above $f_{tr}$ which are used for beamforming (correlated exposure), the power density is assessed for all possible phase and amplitude excitations (unless the antenna precoding weight providing the maximum TER is known) and then combined with the TER for SAR. In general, the ERs for SAR and power density are to be combined for the device positions, configurations and operational modes resulting in the maximum TER.

#### 6.5.2.5 Alternative 2: Evaluation by selection of highest exposure ratio

If the SAR and power density maxima are spatially separated, the aggregate exposure may be evaluated by selecting the highest exposure ratio in terms of peak spatial-average SAR ($f \le f_{tr}$) and maximum spatial-average or local power density ($f > f_{tr}$) in accordance with the applicable exposure limits. This procedure gives an accurate estimate of the TER when the measured exposure distributions have little or no overlapping contributions.

#### 6.5.2.6 Alternative 3: Evaluation by summation of peak exposure ratios

The maximum ER for each source distribution is determined independently according to peak spatial-average SAR or maximum spatial-average / local power density requirements and summed irrespective of where the maximum ER occurs on the phantom or evaluation surface(s). This procedure is the easiest approach to determine the TER. It is also the most conservative procedure since, in many cases, the maximum ER for each source ($f \le f_{tr}$ and $f > f_{tr}$) will be at different spatial locations. The resulting TER is expected to largely

overestimate the exposure. When compliance can be determined according to Alternative 3, Alternative 1 and Alternative 2 may be avoided.

# 7 Uncertainty estimation

## 7.1 General considerations

The concepts of uncertainty estimation in the measurement of the power density (PD) from wireless devices are based on the general rules provided by ISO/IEC Guide 98-3 [8]. Nevertheless, uncertainty estimation for complex measurements remains a difficult task and requires high-level specialized engineering knowledge. Clause 7 provides a general description of the uncertainty terms. Unless identified otherwise, the uncertainty of the power density assessment is determined according to the averaging area specified by the applicable exposure standard or regulatory requirements. For each uncertainty component, the following general approach is applied [8].

- Determine the type of evaluation that will be used to estimate the uncertainty component. Type A evaluation is a statistical analysis of a series of observations. Type B evaluation is estimation by any other means than Type A.
- Determine the statistical distribution of the uncertainty component. If a large number of observations are available from a Type A evaluation, the statistical distribution is known by plotting the results. Otherwise, the statistical distribution is determined from knowledge of the physics of the uncertainty component.
- Calculate the standard uncertainty. For Type A evaluation, the standard uncertainty is the estimated standard deviation of the data. For Type B evaluation, the standard uncertainty is estimated by dividing the maximum deviation by the coverage factor. The coverage factors for different statistical distributions are available in [8].

## 7.2 Uncertainty model

The combined standard uncertainty of the measured power density is the root sum squared of uncertainty contributions from the following influences:

1) uncertainty terms dependent on the measurement system (7.3);
2) uncertainty terms dependent on the device under test (DUT) and environmental factors (7.4).

Combining of uncertainty terms to determine the total expanded uncertainty is described in 7.5.

## 7.3 Uncertainty components dependent on the measurement system

### 7.3.1 Calibration of the measurement equipment

Calibration uncertainty is assessed and documented by the system manufacturer. Depending on the system implementation, the probe is directly calibrated together with its readout electronics or, if applicable, the readout electronics is calibrated separately. In the latter case, additional uncertainties resulting from the connection of the two parts after calibration are taken into account, e.g. mismatch uncertainty for a RF probe and RF readout having different impedances.

### 7.3.2 Probe correction

Probe correction is the difference between the receiving properties of the physical probe compared to an ideal probe that measures the field at a point in space. This term is especially important in close proximity to a source where fields may vary significantly over the volume of the probe. More information is available in [4] about probe correction for specific near field implementations (planar, cylindrical and spherical). The uncertainty in the receiving properties of the probe affecting probe correction is included.

### 7.3.3 Isotropy

Probe isotropy is a measure of the deviation in probe response to arbitrary field polarization. In general, fields emitted by small portable wireless devices are of arbitrary polarization.

### 7.3.4 Multiple reflections

The field scattered by a probe is partly scattered back to the DUT to be retransmitted again. This effect depends on the frequency, the structure of the probe and the probe distance to the DUT. Since this effect is a characteristic of a specific probe, it is determined by the manufacturer during the probe calibration. If algorithms are applied to compensate for the multiple reflections, then the PD uncertainty can be determined with the same evaluation hardware and software used for performing the measurements.

### 7.3.5 System linearity

The evaluation of system linearity is performed such that all components of the system introducing potential non-linearities are assessed. For instance, if a vector-probe contains no non-linear element but its readout electronic does, then the tests to evaluate this uncertainty contribution should include the readout electronics. This evaluation is performed by measuring the PD over the dynamic range of the measurement system and determining the maximum deviation from the best-fit straight line that goes through the origin.

### 7.3.6 Probe positioning

The mechanical restrictions of the field probe positioner can introduce deviations in the accuracy and repeatability of probe positioning. The uncertainty is due to the accuracy of the mechanical movement of the probe.

### 7.3.7 Sensor location

The uncertainty is due to mechanical uncertainties in the sensor location during manufacturing. The actual distance of the sensor from the DUT is different from the assumed (nominal) distance, and each sensor location varies in a certain tolerance range.

### 7.3.8 Amplitude and phase drift

This term describes the influence of short-term and long-term drift of the measurement equipment on the measured PD. It is not related to the drift of the power of the DUT. Short-term drifts (e.g. over a period of minutes or hours) are caused by influences such as equipment heating, electromagnetic interference and changes in ambient conditions. Long-term drifts (e.g. over a period of days to months) are caused by component drift, amplifier stability and long-term fluctuations in dielectric parameters of materials of probe and related measurement equipment.

Uncertainty due to amplitude and phase drifts is evaluated from trend analysis of PD measurements taken at different times. The uncertainties of short-term and long-term drifts are evaluated separately and combined assuming that they are statistically independent.

### 7.3.9 Amplitude and phase noise

This term is the component noise of the measurement system. Amplitude and phase noise is random fluctuations in the measurement due to short-term changes such as component noise. This uncertainty is evaluated from the data taken to estimate the uncertainty due to short-term amplitude and phase drifts. This uncertainty can be evaluated from measurement data taken at several frequencies across the applicable range and for all system states if relevant. For example, if a system includes amplifiers with several gain states, the uncertainty analysis can be performed on data obtained for all possible gain states.

#### 7.3.10 Data point spacing

This component is determined based on the spatial resolution specified by the measurement equipment manufacturers.

#### 7.3.11 Measurement area truncation

The uncertainty for measurement surface truncation is determined according to implementation of the measurement methodology for capturing the field distributions required to maintain power density assessment accuracy. The criteria to minimize truncation errors are typically specified by the measurement system manufacturer.

#### 7.3.12 Reconstruction algorithms

The numerical techniques that are applied to the measured fields to propagate, transform, project or reconstruct the power density distribution at the evaluation surface introduce errors and their uncertainty should be estimated. This is especially important considering that some systems might make use of very complex reconstruction algorithms, e.g. phase retrieval algorithms making use of amplitude only data. This is typically specified according to implementations of the algorithms by the system manufacturer.

### 7.4 Uncertainty terms dependent on the DUT and environmental factors

#### 7.4.1 Probe coupling with DUT

The probe partly scatters the impinging power radiated by the DUT. In addition to causing multiple reflections (see 7.3.4), the modification of the DUT loading causes a reaction of the power amplifier that may adjust its output power. This uncertainty term is evaluated as the difference between the transmission coefficient of the DUT, $T = [1 - S_{11}{}^2]$, with and without the presence of the probe, where $S_{11}$ is the magnitude of the reflection coefficient of the antenna.

#### 7.4.2 Modulation response

This uncertainty term might be relevant only for certain types of systems (e.g. system that is making use of diode-loaded probes). It can be assessed by using any source with a setup the same as or equivalent to a setup used for system verification. The signal generation setup simulates the modulation for which the uncertainty is determined according to the specification of the communication system standard. The PD is measured with the modulated signal and with CW at the same RMS power (verification that the power meter is a true RMS detector and that the amplifier is sufficiently linear for the entire dynamic range of the signal is required).

#### 7.4.3 Integration time

Measurement integration-time uncertainties may arise when test devices do not emit a continuous signal. When the integration time and discrete sampling intervals used in the probe electronics are not synchronized with the pulsed characteristics of the measured signal, the RF energy at each measurement location may not be fully or correctly captured. This uncertainty should be evaluated according to the signal characteristics of the test device prior to the PD measurement. Measurements at a single point should be made consecutively using the chosen integration time and progressively larger integration times.

#### 7.4.4 DUT alignment

This uncertainty term is determined by evaluating the PD for different mechanical errors in the DUT position, related to the mechanical tolerances of the device holder or similar hardware used to secure the DUT and position it in the required orientations for measurement.

### 7.4.5 RF ambient conditions

The ambient RF level is evaluated by performing PD measurements using the same equipment setup used for testing the DUT, however with the RF power switched off.

### 7.4.6 Measurement system immunity/secondary reception

During measurements, the fields radiated by the DUT may be picked up by parts of the measurement system other than the field sensors. This may result in undesirable effects susceptible to increase the measurement uncertainty. For example, the uncertainty assessment can be carried out by using the validation sources in specified test positions and blocking the direct field reception from the probe supposed to perform the measurement. PD measurements should be performed in these conditions at frequencies specified for the validation.

### 7.4.7 Drift of DUT

The measurement drift of the DUT is accounted for by the first and last step of the measurement process defined in 6.4.2 or 6.4.3. The drift is recorded as the percentage difference of the secondary reference measurement, $\mathrm{Ref}_{\mathrm{secondary}}$ from the primary reference measurement, $\mathrm{Ref}_{\mathrm{primary}}$:

$$\mathrm{drift} = 100\% \times \left(\mathrm{Ref}_{\mathrm{secondary}} - \mathrm{Ref}_{\mathrm{primary}}\right) / \mathrm{Ref}_{\mathrm{primary}} \tag{12}$$

## 7.5 Combined and expanded uncertainty

The contributions of each component of uncertainty should be recorded with description, probability distribution, sensitivity coefficient, $c_i$, and uncertainty value, $u(x_i)$ of the uncertainty component, $x_i$. A recommended tabular form is shown in Table 2.

If all uncertainty components, $x_i$, are statistically independent, the combined standard uncertainty $u_c$ for spatial-average PD measurement is estimated according to Formula (13):

$$u_c = \sqrt{\sum_{i=1}^{m} c_i^2 \cdot u^2(x_i)} \tag{13}$$

If some uncertainty components are statistically dependent on others, Formula (14) can be applied to calculate the combined standard uncertainty:

$$u_c = \sqrt{\sum_{i=1}^{m} c_i^2 \cdot u^2(x_i) + 2\sum_{i=1}^{m-1} \sum_{j=i+1}^{m} c_i c_j u(x_i) u(x_j) r(x_i, x_j)} \tag{14}$$

In Formula (14), $r(x_i, x_j)$ is the correlation coefficient which is calculated from the estimated covariance $u(x_i,x_j)$ associated with the two components $x_i$ and $x_j$:

$$r(x_i, x_j) = \frac{u(x_i, x_j)}{u(x_i) u(x_j)} \tag{15}$$

In the special case where all uncertainty terms are completely correlated (i.e. $r(x_i, x_j) = 1$), the uncertainty is a linear sum of the individual components:

$$u_c(y) = \sum_{i=1}^{m} c_i \cdot u(x_i) \quad (16)$$

Further description and examples of evaluating uncertainty are provided in ISO/IEC Guide 98-3 [8].

The expanded uncertainty $U$ is estimated by multiplying the standard uncertainty by a coverage factor of $k$ representing a confidence interval of 95 %. The coverage factor is $k$ = 2 if the combined uncertainty has a Gaussian distribution. Otherwise, see [8] for more information.

The evaluation of several uncertainty components can be combined and assessed directly by Monte-Carlo-method or other methods. In such cases the calculation of the correlation coefficient may not be needed.

**Table 2 – Example of measurement uncertainty evaluation template for power density measurements**

| Source of uncertainty | Description | Unc. ± % | Prob. Dist. | Div. | $c_i$ | Standard uncertainty ± % | $\nu_i$ or $\nu_{eff}$ |
|---|---|---|---|---|---|---|---|
| ***Uncertainty terms dependent on the measurement system*** | | | | | | | |
| Calibration | | | | | | | |
| Probe correction | | | | | | | |
| Isotropy | | | | | | | |
| Multiple reflections | | | | | | | |
| System linearity | | | | | | | |
| Probe positioning | | | | | | | |
| Sensor location | | | | | | | |
| Amplitude and phase drift | | | | | | | |
| Amplitude and phase noise | | | | | | | |
| Data point spacing | | | | | | | |
| Measurement area truncation | | | | | | | |
| Reconstruction algorithms | | | | | | | |
| ***Uncertainty terms dependent on the DUT and environmental factors*** | | | | | | | |
| Probe coupling with DUT | | | | | | | |
| Modulation response | | | | | | | |
| Integration time | | | | | | | |
| DUT alignment | | | | | | | |
| RF ambient conditions | | | | | | | |
| Immunity / secondary reception | | | | | | | |
| Drift of the DUT | | | | | | | |
| | | | | | | | |
| Combined standard uncertainty | | | | | | | |
| Expanded uncertainty (95 % confidence interval) | | | | | | | |

# 8 Measurement report

## 8.1 General

### 8.1.1 General

The test report includes all test results, the necessary information related to the configurations tested, the methods and instrumentation used for the assessment of the DUT.

If SAR measurements were also required to assess the full compliance of the DUT, the reporting includes the items set forth in other applicable IEC standard(s), including any additional reporting requirements identified by national regulatory agencies.

### 8.1.2 Items to be recorded in the measurement report

All information required to perform repeatable tests, calculations, and/or measurements is recorded to obtain results within the acceptable calibration and uncertainty range. Furthermore, the measurement report should include the following specific information:

1) General information
   a) identification of the test laboratory;
   b) identification of the DUT including hardware and software revision numbers, serial number, e.g. International Mobile Equipment Identity (IMEI);
   c) compliance requirements, e.g. test standards, guidelines, recommendations, etc.;
   d) applicable exposure limits, e.g. ICNIRP, IEEE/ICES, etc.;
   e) a list of accreditations provided by national or international bodies to perform testing to applicable standards, procedures, etc. with the expiry date of the accreditation.
2) Report summary (for all power density related data)
   a) frequency bands and configurations:
      i) list of all frequency bands and modulations tested;
      ii) list of all test configurations assessed;
   b) tabulated average power density values over the testing positions, bands, operating modes and device configurations including all applicable tune-up specifications;
   c) tabular and graphical results for the highest maximum average power density measurement for each frequency band and modulation;
   d) reference to exposure limits and a statement of compliance. The statement of compliance takes into account the combined exposure from multiple antennas operating simultaneously.
3) Detailed description of the DUT and test details
   a) description of the form factor of the DUT and a brief description of its intended function(s);
   b) description of the positions and orientations to be tested, including photos;
   c) description of the available and tested antenna(s) and accessories, including batteries;
   d) description of the available and tested operating modes, power levels and frequency bands;
   e) detailed description and rationale for any test reductions used during the evaluations;
   f) detailed description of the applicable test mode software used along with the specific configurations used for each operating mode tested (i.e. power level, antenna, frequency and modulation settings);
   g) testing environmental condition, e.g. temperature;
   h) type of power density measurement performed (i.e. evaluation of both E-field and H-field vs. evaluation of E-field or H-field field only);

i) results of all tests performed (i.e. maximum spatial-average power density and/or local power density for each test);

j) graphical representation of the evaluation surface with respect to the DUT for the maximum average power density value of each operating mode);

k) information on the measured drift for each test including the maximum drift measured;

l) details on scaling of the results (i.e. tune-up tolerance scaling and power drift scaling as applicable).

4) Uncertainty estimation

   a) uncertainty for measurement of the DUT (Table 2);

   b) uncertainty budget of the system check;

   c) uncertainty budget of the system validation.

5) Measurement system

   a) measurement system main component description including:

      i) probe(s), including information on dimensions, isotropy, spatial resolutions, dynamic range and linearity;

      ii) readout electronics;

      iii) device holder;

      iv) scanning systems;

      v) other relevant components.

   b) calibration data for relevant components (e.g. probe calibration certificates) might be provided in the measurement report.

   c) results of system check:

      i) measurement results for each frequency band;

      ii) deviation from the power density target value(s);

      iii) detailed description of the reference radiating source.

6) Validation of the power density measurement method

   a) reconstruction algorithm, including the validation data, and detailed description on how power density is determined using the measured field components;

   b) results of the computations, measurements and/or other assessments performed by the measurement system developer in order to validate the power density measurement method;

   c) a description of any additional analyses or conditions imposed by the system developer used to validate the power density measurement methodology;

   d) reference radiating source description and power density distribution for each frequency band;

   e) range of operating frequencies and modulations;

   f) power density method uncertainty.

# 9 Recommendation for future work

## 9.1 Measurement standard for EMF compliance assessment of devices operating at frequencies above 6 GHz

### 9.1.1 General

This document describes possible methods and measurement techniques for the evaluation of power density from transmitting devices operating close to the user at frequencies between 6 GHz and 100 GHz. While this document is informative and details the current state of knowledge, IEC TC 106 submitted a new work item proposal in early 2018 for an International Standard (IS) addressing the same frequency range. This document provides extensive

material for the development of such an IS. Nevertheless, some items requiring additional considerations have been identified and are discussed in Clause 9.

In general, the complexity of devices has increased dramatically over the years. Additional effort should be made in specifying methods, procedures and in identifying equipment which allow for an increased efficiency of EMF compliance testing; thus limiting the amount of redundant compliance testing required without jeopardizing the conservativeness of the testing regime.

### 9.1.2 Test frequencies

Subclause 6.2.4 defines the channel or a practical subset of channels where power density measurements are performed. The procedure comes from the SAR standards where testing is performed close to the phantom and likely to affect the tuning of the antennas differently at different frequencies. Since power density measurements are conducted in free-space and there are no frequency-varying tissue simulant parameters, the possibility to reduce the number of channels to be assessed should be investigated.

### 9.1.3 Evaluation surfaces

Subclause 6.2.5 provides two alternatives which can be used to define the surface(s) and orientations with respect to the DUT where power density is to be evaluated. For both alternatives, further investigations to simplify the procedure of identifying the surface orientation are needed. Some aspects related to these two options need further investigation.

– In Alternative 1, the evaluation surface corresponding to the shape of the inner surface of the SAM phantom and flat phantom defined by IEC 62209 series of SAR assessment standards are used. For some measurement techniques based on near-field reconstruction algorithms, the fields are therefore to be projected on a complex surface (corresponding to the SAM). Although possible in theory, the implications on the accuracy and feasibility of such solution in individual implementations need to be further investigated. According to Alternative 1, evaluation surfaces in the shape of a plane tangential to the SAM can also be used. This will lead to flat (and therefore less complex) surfaces. Nevertheless, each point of the SAM surface would correspond to a plane with a different orientation. As a result, such solution might require reconstruction of the power density on several planes.
– For Alternative 2, power density is assessed in the evaluation plane(s) corresponding to the maximum available local or spatial-average power density. As these are not known a priori, methods and optimization techniques to find such plane(s) are to be examined. A brute force approach could be applied where power density is evaluated (e.g. by means of a reconstruction algorithm) on different planes. However, this approach might result in a very time-consuming process. Furthermore, it might be difficult to make use of Alternative 2 when evaluating exposure for multiple transmitters and combining SAR and power density distributions (6.5.2.4) since the evaluation plane is defined independently from what is specified by IEC 62209 (to notice that the more conservative combining methods described in 6.5.2.5 and 6.5.2.6 would still apply). Another factor to be considered when using Alternative 2 for DUT with multiple transmitters (e.g. antenna arrays making use of beamforming) is that the plane providing the largest power density might vary with the applied antenna weight.

For multiple exposure conditions, both alternatives may be applied to evaluate combined total exposure ratio (TER). Alternative 1 may be used in conjunction with Alternative 2 to reduce the complexity of the test procedures. Some test positions or exposure scenarios (e.g. head exposure) can be assessed according to Alternative 1. The remaining test positions or exposure scenarios (e.g. body exposure) may be optimized by using Alternative 2, ensuring that the assessment fully takes into account all necessary test positions and exposure scenarios.

Exploratory and investigative work should continue while more devices operating in the targeted frequency range (6 GHz to 100 GHz) are made available. Other alternatives than the

ones specified in 6.2.5 might provide better solutions. For instance, the possibility to use only planar evaluation surfaces parallel to the faces or edges of a device should be considered as it would greatly simplify the overall measurement procedure. Evaluation surfaces conformal to the DUT shape should be also investigated as they could be used to maintain a fixed separation distance for devices characterized by curved surfaces.

### 9.1.4 Evaluation of exposure from multiple transmitters

In this document, 6.5 describes how to determine the total combined exposure from multiple antennas operating simultaneously. The following items are to be considered for further study.

– As the number of antennas simultaneously transmitting is increased, simplified procedures to reduce the complexity of the tests need to be specified in the future IS. In principle, the fields for each antenna element operating separately are to be assessed for correlated sources. Otherwise, repeated measurements for all possible excitations should be conducted which might not be practical. The measurement time could be reduced by synchronizing the measurement system with the software control of the DUT to cycle through the antenna ports in a single scan. Alternatively, if the signal is processed so that the contribution from each port can be separately detected when demodulated, measurements could be conducted for a single scan with all transmitters operating simultaneously. The possibility of adopting such solutions should be investigated in the IS.

– For uncorrelated sources, a large number of combinations corresponding to different device positions and operational modes may be required in order to evaluate the maximum TER (see 6.5). Moreover, when the TER is determined by spatial summation of the ER distributions, the contribution of each source at common locations in space is needed. This might imply that the volume or area where exposure is assessed should be enlarged resulting in an increased measurement time. Procedures and equipment to speed up this process should be addressed in a future IS. For instance, well defined and effective criteria to identify antenna elements characterized by exposure distributions with little or no overlap (see 6.5.2.5), and for which exposure can be assessed independently, should be defined.

– Since portable devices are expected to operate simultaneously above and below the transition frequency where the basic restrictions change from SAR to power density, a future IS should provide further guidance on how to combine exposure from different metrics. In this document, some guidance is given in 6.5.2.3.

### 9.1.5 Other future work items

#### 9.1.5.1 Energy steering methods

Some devices might make use of beamforming techniques or alternative antennas to steer the transmitted energy away from the user when operated in close proximity to the head or body. The future IS should provide clear procedures describing how this can be factored into applicable test conditions.

#### 9.1.5.2 Reconstruction algorithms

In this document, the term reconstruction algorithm is used in a broad sense to identify algorithms, mathematical techniques and procedures that are applied to the measured fields to propagate, transform, project or reconstruct the power density distribution at the evaluation surface in order to determine spatial-average and/or local power density. It includes algorithms to (back-)project the field from the measurement to the evaluation surface, to retrieve the phase of the field from amplitude only measurements, to calculate the H-field from the measured E-field (or vice versa), etc. (see Annex G). During the development of the IS, the requirement for separate terms to identify different techniques should be taken into consideration in order to avoid misinterpretations.

#### 9.1.5.3 Uncertainty evaluation

Clause 7 provides a general description of the uncertainty components related to power density measurements. More detailed guidance and recommendations on how to evaluate the contribution of each component should be provided in the IS.

### 9.2 Numerical standard for EMF compliance assessment of devices operating at frequencies above 6 GHz

IEC TC 106 and IEEE/ICES TC 34/SC 2 are developing the IEC/IEEE 62704 series of standards for the application of numerical methods for compliance testing of wireless devices in the frequency range from 30 MHz to 6 GHz. The main objective of these standards is to quantify human exposure in terms of the basic restrictions using verified simulation software and algorithms (e.g. calculation of the maximum spatial-average SAR), including defined protocols for the development, validation and uncertainty assessment of the numerical models of the DUT and the exposed phantom(s). The IEC/IEEE 62704 series comprises general standards on the requirements and application of the Finite Difference Time-Domain (FDTD) and Finite Element (FE) methods as well as application oriented standards for the assessment of the EMF exposure to vehicle mounted antennas and mobile phones.

For the compliance testing of certain 5G devices transmitting above 6 GHz, the methods set forth in the first edition of IEC/IEEE 62704-1 [9] cannot be applied directly. Enhanced transmission technologies, such as phased array systems common to these devices, and the quantification of the exposure in terms of the incident power density, pose additional requirements on the simulation software. For example, it includes particular interpolation and superposition techniques for incident fields and averaging algorithms for the calculation of the incident power density in terms of the basic restrictions [ICNIRP 1998]. For the development of standardized numerical techniques, ICES TC 34 recently approved the development of a new numerical standard within the Project P1528.6 which addresses these issues with the objective of providing a conservative estimate of the power density of the exposure of the head or body of the users of wireless devices. As in the previous series of numerical standards, the new standard will focus on the particular requirements and verification techniques for the FDTD and FE methods. Furthermore the standard will give general guidance for model validation and numerical uncertainty assessment. The activity will be carried out in parallel with the development of the measurement standard for compliance assessment of 5G devices. The role of numerical methods in finding the worst case conditions for measurement testing should be carefully considered. Annex G gives an example of compliance assessment where numerical techniques are used in combination with measurements.

### 9.3 Updates to IEC 62232

For base stations with transmit frequencies in the range 110 MHz to 100 GHz, IEC 62232 [10] defines the methods to assess the compliance boundaries based on reference levels and basic restrictions. SAR tests are recommended when the compliance distance is in the close proximity of the transmitters operating in the 300 MHz to 6 GHz frequency range. It is recommended to leverage the ongoing IEC 62232 maintenance period to include the testing methods described in this document, in particular for equipment with a transmit frequency above 6 GHz having zero compliance boundary dimensions (E0 installation class, see IEC 62232) or with small compliance boundaries. In the same way as IEC 62232 makes reference to IEC 62209-2 [11] for the detailed specification of SAR tests below 6 GHz, IEC 62232 should be able to leverage on a dedicated measurement standard for power density at frequencies above 6 GHz. In this way, IEC 62232 updates would mainly focus on the specific requirements for base stations.

# Annex A
(informative)

# Measurement system check and validation

## A.1 Background

### A.1.1 General

The goal of Annex A is to define possible system check and system validation procedures that enable users and third parties to verify the performance of the measurement system and procedure by applying consistent protocols:

1) System check: procedure that uses specific reference sources to verify that the system is operational and repeatable for the intended measurements.
2) System validation: procedure that uses specific reference sources to validate that a system meets the accuracy, performance and uncertainty specifications required before it is deployed and also after hardware or relevant software changes have been performed.

NOTE System validation is normally performed by the system manufacturer.

Examples of reference sources for validation are defined in Annex B and for system check in Annex C.

### A.1.2 Objectives of system check

System check provides a fast and reliable method to routinely verify that the measurement system is operational with no system component failures, including probe defects, drifts or deviation from target performance requirements. A system check also verifies the repeatability of the measurement system before compliance testing.

The system check is a complete measurement using simple well-defined reference sources (see for instance Annex C). The system check is successful if the measured results are within the tolerances described in A.3.2. The instrumentation and procedures used for system check should ensure the system is ready for performing compliance tests.

### A.1.3 Objectives of system validation

System validation provides a means to independently evaluate the system against its specifications and its specified uncertainties, i.e. if the measurement uncertainty is conservative. The outcome of the system validation is an assurance that the system provides accurate results.

Although the validation tests can be performed independently, they or a subset thereof are usually performed and documented by the measurement system manufacturer on an annual basis or whenever modifications are made to the system, such as software or hardware changes. The selection of the subset should be justified.

The validation tests should cover the frequencies, power levels, and signal modulations an individual system supports or the subset should cover the range of usage. The set of measurement configurations should be evaluated and reported. The set of reference sources defined in Annex B have been determined to be sufficient to validate any assessment techniques.

## A.2 Measurement setup and procedure for system check and system validation

### A.2.1 General

Clause A.2 describes the required power measurement setup for system check and system validation.

### A.2.2 Power measurement setups

Both system check and system validation procedures require accurately measured and stable forward power at the RF input of the reference sources.

A recommended test setup for using off-the-shelf instrumentation with a reference source is shown in Figure A.1. The system includes a signal generator, an optional frequency multiplier, 10 dB to 20 dB attenuators, a power meter including power sensor, the reference antenna, cables, connectors and adapters.

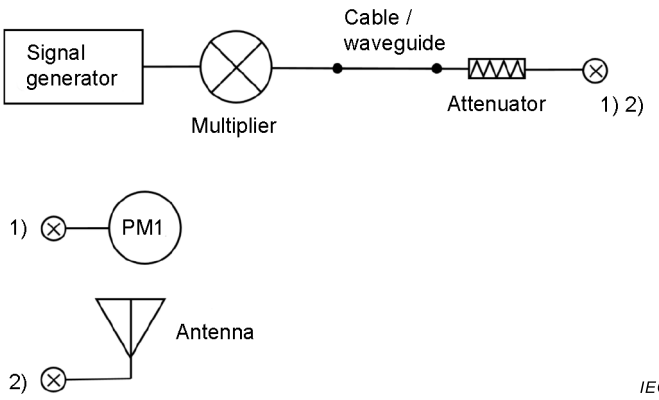


Either 1) the power meter PM1 or 2) the reference antenna is connected at the output of the attenuator (⊗).

**Figure A.1 – A recommended power measurement setup for system check and system validation**

The requirements of the components used in the setup shown in Figure A.1 are described in a) to e).

a) The signal generator should be stable (after warm-up). The forward power to the reference antenna should be high enough to avoid the influence of measurement noise.

b) A frequency multiplier (optional) is used to convert the frequency to the reference frequency.

c) An attenuator (≥ 10 dB) should be placed before the power meter and antenna to provide good matching and to improve the accuracy of the power sensor (some higher power heads come with a built-in calibrated attenuator). The exact attenuation at each test frequency should be verified and used in the calculations.

d) The influence of the cable or waveguide between the multiplier and the reference antenna should be evaluated as part of the uncertainty assessment.

e) The power meter PM1 should be of high quality. If the power meter and reference antenna require different connector systems, a calibration grade, high-quality adapter should be used.

To avoid unacceptable power drifts during system validation and system check, the equipment should be allowed to warm-up for the duration recommended by the manufacturer(s) before any measurement.

### A.2.3 Procedure to normalize the measured power density

The power density measurement results should be normalized to the delivered input power to an input power level of 0 dBm and compared to the appropriate target values of the calibrated reference sources.

The test procedure is described in steps a) to i).

a) Connect the equipment as shown in Figure A.1, with the power meter PM1 connected at location ⊗.

b) Adjust the power output from the signal generator until the forward power $P_f$ at PM1 is at the desired power level.

c) Ensure that the power output is stable over time within ± 0,05 dB.

d) Connect the equipment as shown in Figure A.1 with the reference antenna connected at location ⊗ instead of the power meter PM1.

e) Measure the power density as specified in this document.

f) Connect the equipment as in step a) and remeasure the forward power $P_f$.

g) Verify that the output power has not changed by more than 0,1 dB from step b).

h) Normalize the measured power density by the ratio $R$ = 1 mW / $P_f$.

i) Compare the measured values with the appropriate target values.

## A.3 System check

### A.3.1 System check sources and test conditions

The sources used for system check can be different than those required for the system validation. Example reference sources for system check are provided in Annex C. System check sources should have good positioning repeatability, mechanical stability, and impedance matching for the measurement conditions. In Annex C, a pyramidal horn antenna is used as an example to illustrate system check source usage.

### A.3.2 Test procedure

The system check is a local power density measurement. The measured fields are used to determine the power density at the reference distance. Results are normalized to 0 dBm input power at the system check source, and compared with the numerically validated target values for maximum power density. The RF power measurement setup and power density normalization procedure are described in Clause A.2.

The system check is successful if:

– the difference between the normalized measured local power density and the numerically validated target value is within the reported expanded uncertainty of the measurement system, and

– the difference between the measured local power density and the measured reference value is within ±10 % for system repeatability.

The measured reference value is determined for the individual measurement system after calibration, using the same source.

## A.4 System validation

### A.4.1 Reference sources and test conditions

Validation test conditions should be selected based on system specifications defined by the manufacturer and according to measurement requirements for the system at the testing laboratory. Examples of reference sources that meet these criteria are provided in Annex B.

System validation should cover the range of frequencies applicable to the system. If the measurement system is broadband, it is sufficient to perform the validation at the following frequencies: 10 GHz (6 GHz to 20 GHz), 30 GHz (20 GHz to 45 GHz), 60 GHz (45 GHz to 75 GHz) and 90 GHz (75 GHz to 100 GHz). If the measurement system does not cover the entire frequency range, the validation should be performed at the above frequencies that fall within the frequency range used by the system.

The reference sources should be calibrated in amplitude and phase at the defined reference distances.

### A.4.2 System validation procedure

System validation is characterized by power density measurements.The measured fields are used to determine the maximum spatially averaged power densities at a planar evaluation surface. Results are normalized to 0 dBm input power at the reference source, and compared with the numerically validated target values for maximum local power density and spatial-average over a circular area (e.g. 1 $cm^2$ and 4 $cm^2$). The RF power measurement setup and power density normalization procedure are described in Clause A.2.

# Annex B
(informative)

# Examples of reference sources

## B.1 Background

Annex B describes examples of reference sources that can be used for system check and/or system validation.

Dipole arrays and slot arrays have been chosen in Annex B as reference sources. Arrays of electric dipoles and magnetic dipoles represent the range of sources under test that are relevant to this document. They meet the specifications of A.4.1, and they can easily be specified and calibrated for the frequencies defined in A.4.1. Annex B describes the design and physical characteristics of these reference sources.

To meet the target values described below, the microwave source feeding the antenna should have harmonics better than −20 dBc and spurious emissions less than −40 dBc.

## B.2 Cavity-fed dipole arrays

### B.2.1 Description

This category of validation antennas consists of a cavity-backed array of dipoles arranged in an offset lattice according to the modes generated into the resonant cavity. The dipoles are printed onto one face of a low-loss dielectric substrate and excited by non-resonant rectangular slots located on the opposite face of the substrate as shown in Figure B.1. The excitation modes are generated by the resonant cavity. A probe feed from an SMA connector is used, as shown in Figure B.1(c). For higher frequencies, the feeding may require a waveguide transition instead of a probe feed. The diameter of the iris from the waveguide transition should be tuned to give the best match. The arrays have been optimized to achieve a reflection coefficient better than −25 dB. In order to fine-tune the array, two tuning screws are included in the centres of both cavity walls that are perpendicular to the dipoles and the probe.

Figure B.1 shows the perspective, top and side views of the dipole array. The variable descriptions and main dimensions are shown in Table B.1 for each frequency.

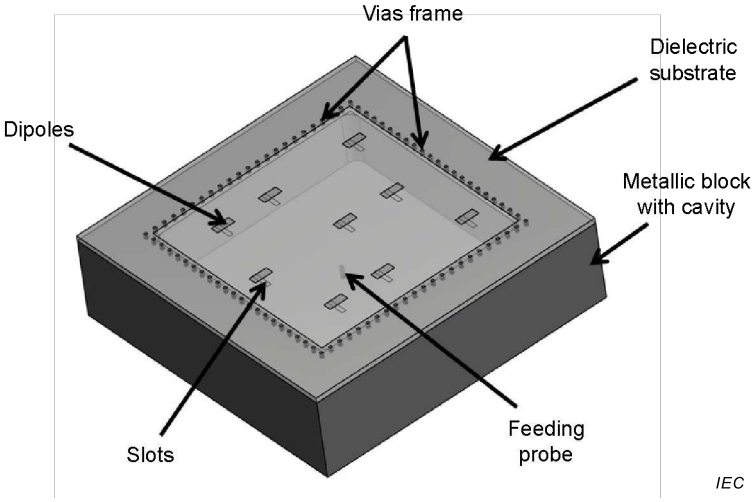


**(a) Perspective view**

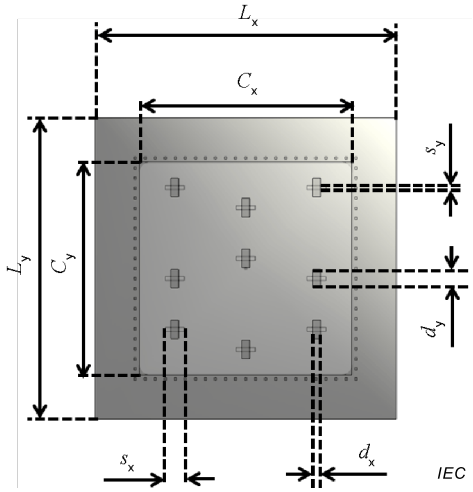


**(b) Top view**

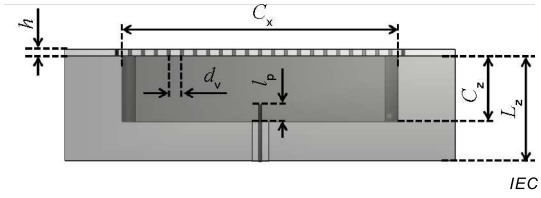


**(c) Lateral view showing the probe feed with length $l_p$**

This diagram corresponds to the 30 GHz design.

**Figure B.1 – Main dimensions for the cavity-backed array of dipoles**

**Table B.1 – Main dimensions for the cavity-backed dipole array at each frequency of interest**

| Frequency [GHz] | Number of dipoles & slots along x | Number of dipoles & slots along y | Dipole width $d_x$ [mm] | Dipole length $d_y$ [mm] | Slot length $s_x$ [mm] | Slot width $s_y$ [mm] |
|---|---|---|---|---|---|---|
| 10 | 3 | 3 | 2,40 ± 0,05 | 5,10 ± 0,05 | 5,70 ± 0,05 | 1,20 ± 0,05 |
| 30 | 3 | 3 | 0,8 ± 0,05 | 1,86 ± 0,05 | 1,90 ± 0,05 | 0,40 ± 0,05 |
| 60 | 3 | 3 | 0,40 ± 0,02 | 0,986 ± 0,02 | 0,95 ± 0,02 | 0,20 ± 0,02 |
| 90 | 3 | 3 | 0,267 ± 0,01 | 0,640 ± 0,01 | 0,633 ± 0,01 | 0,133 ± 0,01 |

| Frequency [GHz] | Relative position in x dimension of each dipole/slot centre with respect to the centre of the cavity [mm] | Relative position in y dimension of each dipole/slot centre with respect to the centre of the cavity [mm] | Distance between vias $d_v$ [mm] | Feeding probe length inside the cavity $l_p$ [mm] | Cavity length $C_x$ [mm] | Cavity width $C_y$ [mm] | Cavity height $C_z$ [mm] |
|---|---|---|---|---|---|---|---|
| 10 | −21,18/0/+21,18<br>−21,18/0/+21,18<br>−21,18/0/+21,18<br>(± 0,05) | +24,18/+18,18/+24,18<br>−3/+3/-3<br>−18,18/−24,18/−18,18<br>(± 0,05) | 1 ± 0,05 | 4,0 ± 0,05 | 63,54 ± 0,05 | 63,54 ± 0,05 | 10 ± 0,05 |
| 30 | −7,06/0/+7,06<br>−7,06/0/+7,06<br>−7,06/0/+7,06<br>(± 0,05) | +8,06/+6,06/+8,06<br>−1/+1/−1<br>−6,08/−8,06/−6,06<br>(± 0,05) | 1 ± 0,05 | 1,3 ± 0,05 | 21,18 ± 0,05 | 21,18 ± 0,05 | 5 ± 0,05 |
| 60 | −3,53/0/+3,53<br>−3,53/0/+3,53<br>−3,53/0/+3,53<br>(± 0,02) | +4,03/+3,03/+4,04<br>−0,5/+0,5/−0,5<br>−3,03/−4,03/−3,03<br>(± 0,02) | 0,5 ± 0,05 | N/A | 10,66 ± 0,025 | 10,66 ± 0,025 | 3,0 ± 0,05 |
| 90 | −2,35/0/+2,35<br>−2,35/0/+2,35<br>−2,35/0/+2,35<br>(± 0,01) | +2,69/+2,02/+2,69<br>−0,33/+0,33/−0,33<br>−2,02/−2,69/−2,02<br>(± 0,01) | 0,5 ± 0,05 | N/A | 7,10 ± 0,02 | 7,10 ± 0,02 | 2,0 ± 0,05 |

| Frequency [GHz] | Substrate thickness $h$ [mm] | Substrate relative permittivity $\varepsilon_r$ | Substrate electric loss tangent tan(δ) | Metallic block length $L_x$ [mm] | Metallic block width $L_y$ [mm] | Metallic block height $L_z$ [mm] |
|---|---|---|---|---|---|---|
| 10 | 0,813 ± 0,05 | 3,63 | 0,0027 | 75 ± 0,05 | 75 ± 0,05 | 12 ± 0,05 |
| 30 | 0,525 ± 0,05 | 3,63 | 0,0027 at 10 GHz | 30 ± 0,05 | 30 ± 0,05 | 8 ± 0,05 |
| 60 | 0,305 ± 0,025 | 3,63 | 0,0027 at 10 GHz | 20 ± 0,05 | 20 ± 0,05 | 6,5 ± 0,5 |
| 90 | 0,203 ± 0,02 | 3,60 | 0,0027 at 10 GHz | 15 ± 0,05 | 15 ± 0,05 | 5,5 ± 0,5 |

### B.2.2 Target values

Table B.2 provides the target values for the E-field, H-field and power density from the cavity-backed dipole arrays defined in B.2.1. All target values are the maximum values in planes at distances of $d$ = 2 mm, 5 mm, 10 mm and 25 mm parallel to the top surface of the dielectric substrate. $E_{max}$ = max(|$E_{total}$|) and $H_{max}$ = max(|$H_{total}$|) are the maximum local E-field and H-field magnitudes. $S_{max}$ is the maximum value of $S$ defined in 3.17, where the normal vector $\hat{\mathbf{n}}$ is the direction of the local power density, not the normal of the plane parallel to the antenna. $S_{av}$ is the maximum spatial-average power density, as defined in Formula (1), for circular surfaces of 1 cm$^2$ and 4 cm$^2$ areas. The accepted power is 0 dBm.

**Table B.2 – Target values for the cavity-backed dipole arrays at different frequencies ($u_s$ ($k$ = 1) = 0,5 dB)**

| $f$ | $d$ | Max. E-field | Max. H-field | Max. local power density | $S_{av}$ 1 cm$^2$ | $S_{av}$ 4 cm$^2$ |
|---|---|---|---|---|---|---|
| | | $E_{max}$ | $H_{max}$ | $S_{max}$ | | |
| [GHz] | [mm] | [V/m] | [A/m] | [W/m$^2$] | [W/m$^2$] | [W/m$^2$] |
| 10 | 2 | 48,50 | 0,20 | 3,19 | 1,05 | 0,57 |
| | 5 | 24,19 | 0,06 | 1,18 | 0,85 | 0,48 |
| | 10 | 14,86 | 0,04 | 0,63 | 0,51 | 0,34 |
| | 20 | 14,07 | 0,03 | 0,47 | 0,43 | 0,33 |
| 30 | 2 | 42,12 | 0,13 | 4,32 | 1,28 | 0,98 |
| | 5 | 33,50 | 0,09 | 2,77 | 1,17 | 0,81 |
| | 10 | 31,76 | 0,08 | 2,64 | 1,43 | 0,64 |
| | 20 | 25,23 | 0,07 | 1,73 | 1,22 | 0,54 |
| 60 | 2 | 79,30 | 0,24 | 17,25 | 6,94 | 3,97 |
| | 5 | 90,27 | 0,24 | 21,44 | 5,00 | 3,17 |
| | 10 | 68,17 | 0,18 | 12,45 | 4,24 | 2,57 |
| | 20 | 41,15 | 0,11 | 4,57 | 2,99 | 1,96 |
| 90 | 2 | 123,99 | 0,33 | 40,75 | 6,77 | 5,49 |
| | 5 | 109,62 | 0,29 | 32,27 | 5,09 | 4,25 |
| | 10 | 75,26 | 0,20 | 15,30 | 4,01 | 3,29 |
| | 20 | 41,62 | 0,11 | 4,69 | 2,88 | 2,37 |

The patterns of |$E_{total}$| and $\Re(S)_{total} = 0.5 \cdot \Re\left(\mathbf{E} \times \mathbf{H}^*\right)$ are shown in Figures B.2, B.3, B.4 and B.5 for the cavity-backed array of dipoles at the operating frequencies of 10 GHz, 30 GHz, 60 GHz and 90 GHz, respectively, each for the distances 2 mm, 5 mm, 10 mm and 20 mm from the antenna surface normalized to an accepted power of 0 dBm.

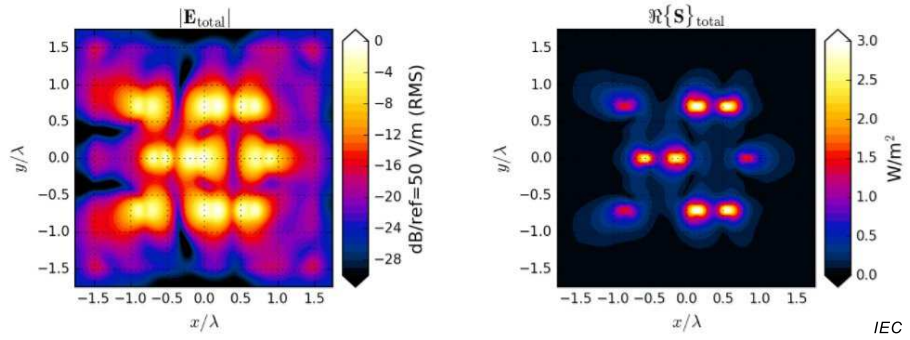


(a) $d$ = 2 mm

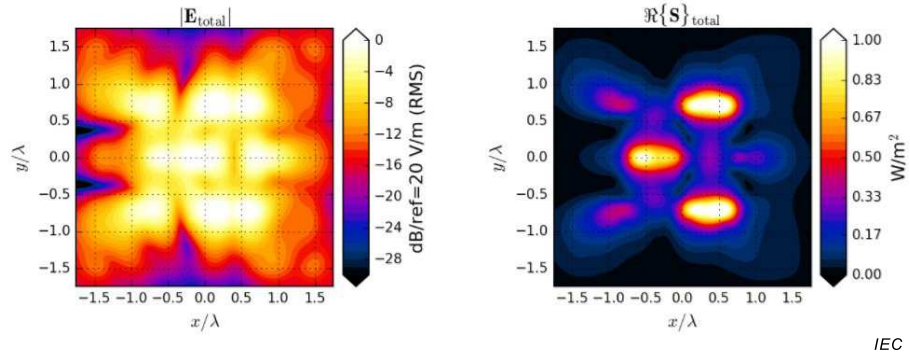


(b) $d$ = 5 mm

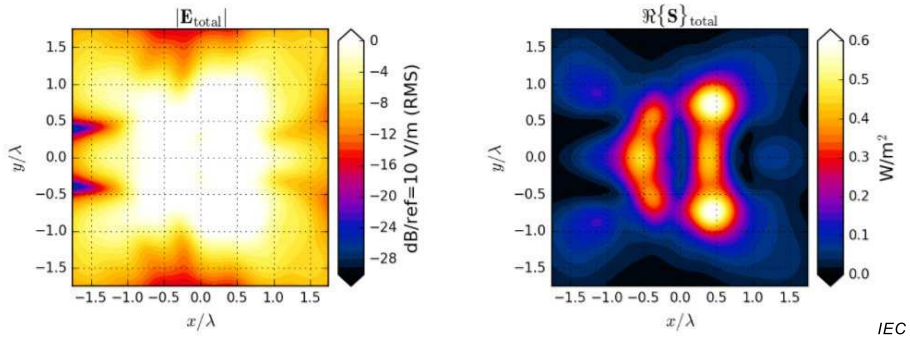


(c) $d$ = 10 mm

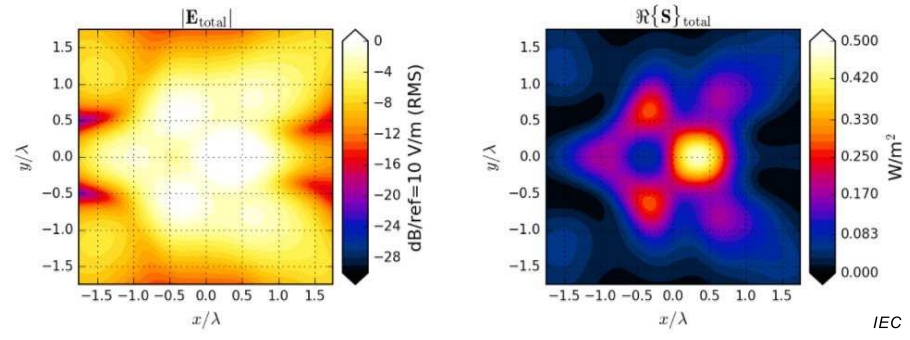


(d) $d$ = 20 mm

**Figure B.2 – 10 GHz patterns for the $|E_{\text{total}}|$ and Re$\{S\}_{\text{total}}$ for the cavity-backed array of dipoles at various distances, $d$, from the upper surface of the dielectric substrate**

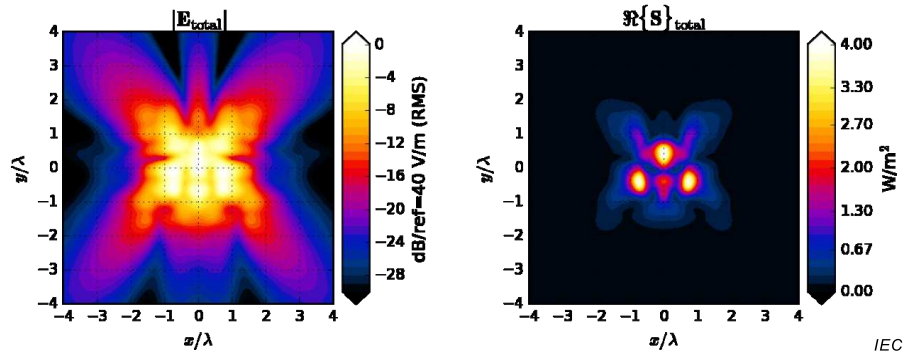


(a) $d$ = 2 mm

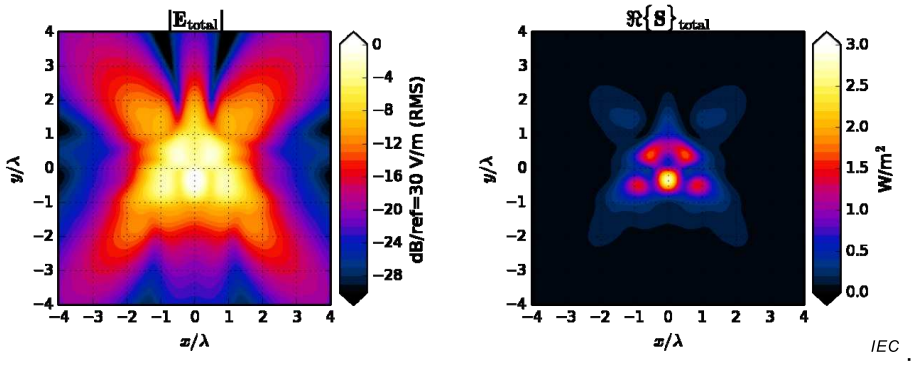


(b) $d$ = 5 mm

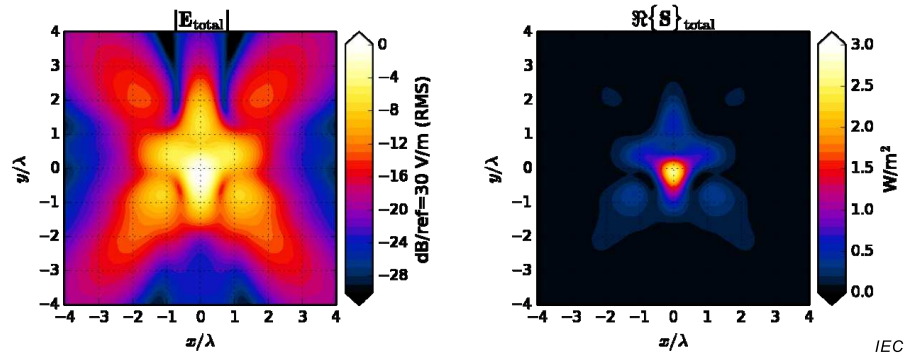


(c) $d$ = 10 mm

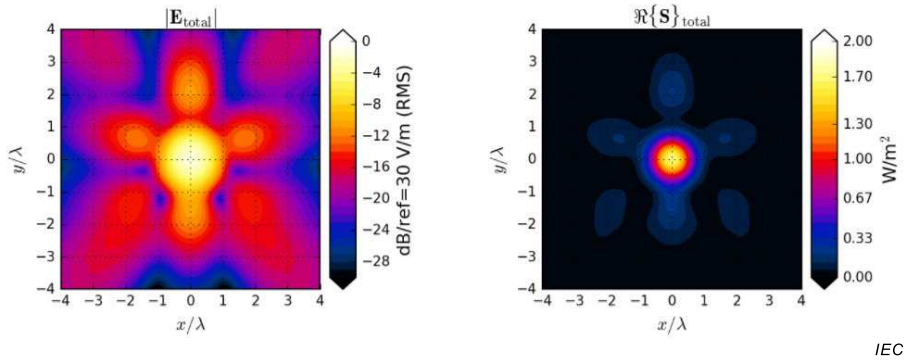


(d) $d$ = 20 mm

**Figure B.3 – 30 GHz patterns for the $|E_{total}|$ and Re$\{S\}_{total}$ for the cavity-backed array of dipoles at various distances, $d$, from the upper surface of the dielectric substrate**

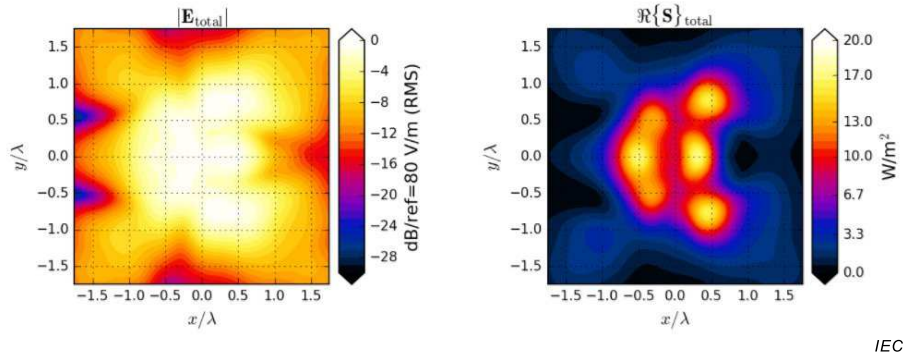


**(a) $d$ = 2 mm**

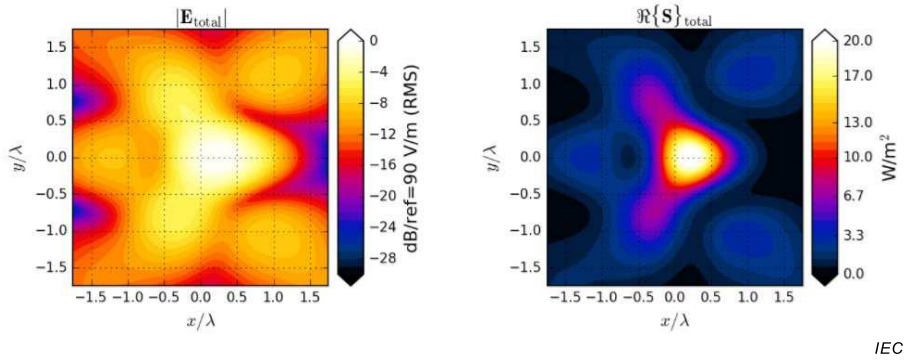


**(b) $d$ = 5 mm**

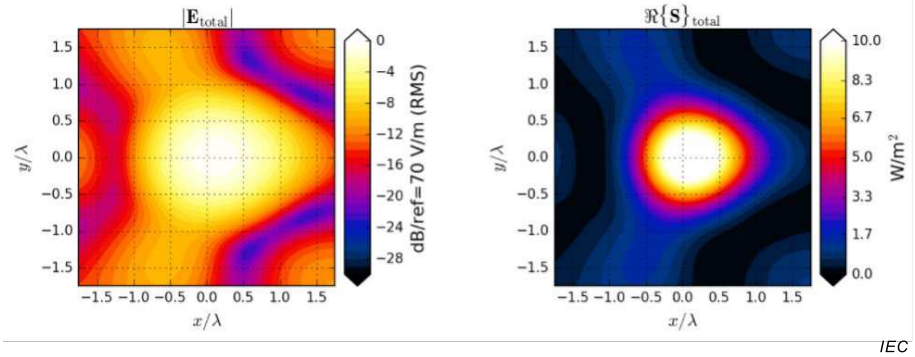


**(c) $d$ = 10 mm**

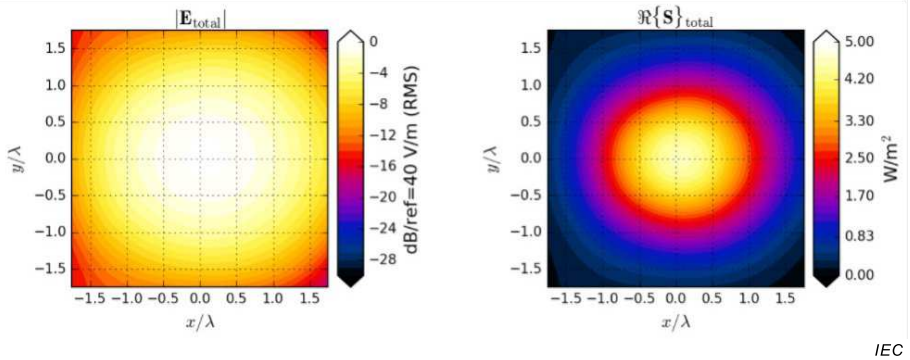


**(d) $d$ = 20 mm**

**Figure B.4 – 60 GHz patterns for the $|E_{\text{total}}|$ and $\text{Re}\{S\}_{\text{total}}$ for the cavity-backed array of dipoles at various distances, $d$, from the upper surface of the dielectric substrate**

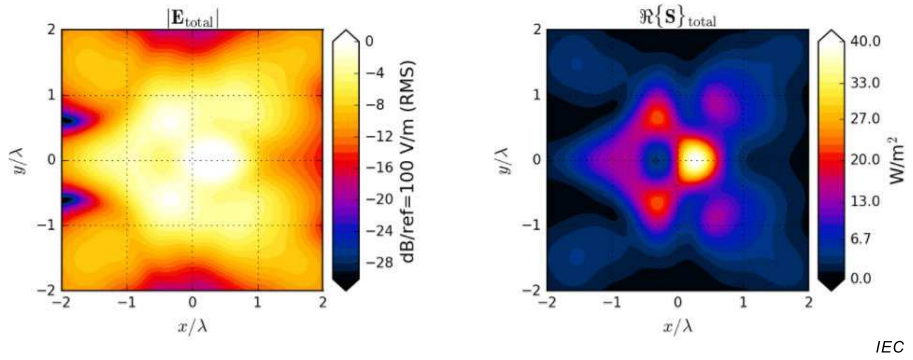


**(a) $d$ = 2 mm**

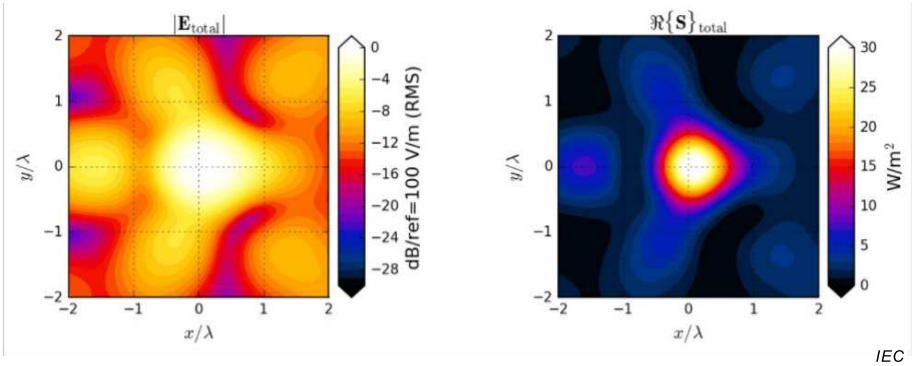


**(b) $d$ = 5 mm**

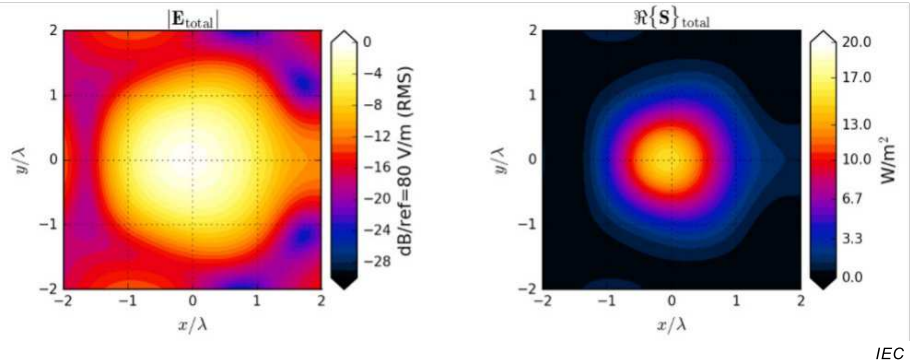


**(c) $d$ = 10 mm**

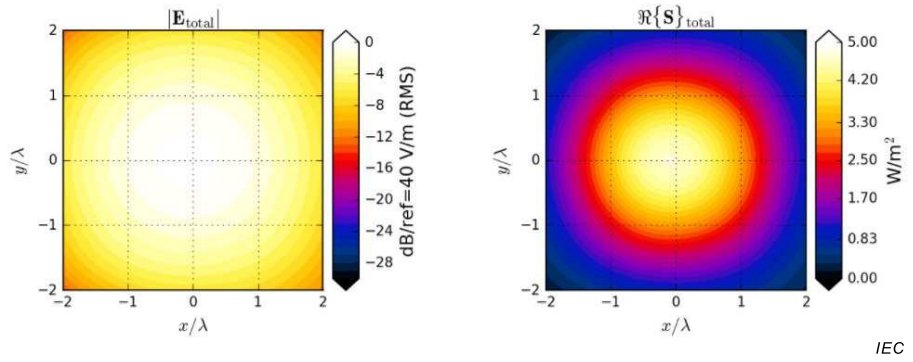


**(d) $d$ = 20 mm**

**Figure B.5 – 90 GHz patterns for the $|E_{\text{total}}|$ and Re$\{S\}_{\text{total}}$ for the cavity-backed array of dipoles at various distances, $d$, from the upper surface of the dielectric substrate**

## B.3 Pyramidal horns loaded with a slot array

### B.3.1 Description

This category of reference antenna consists of a pyramidal horn loaded with an array of rectangular slot antennas on the aperture. Because of the mismatch experienced by the pyramidal horn as a result of the loading with the arrays, the slot arrays have been optimized to guarantee a reflection coefficient better than −20 dB at the design frequency. The slots are symmetrically arranged on the horn aperture. They have been fabricated on a 0,15 mm thick metal sheet. Figure B.6 shows the main dimensions for a generic stainless steel stencil. The details for the dimensions of the stencil are summarized in Table B.3 for each frequency. The main dimensions for the pyramidal horns are shown in Figure B.7 and Table B.4.

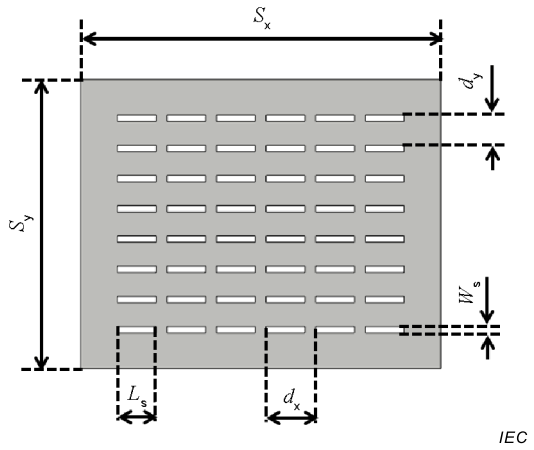


The number of elements shown corresponds to the 90 GHz design.

**Figure B.6 – Main dimensions for the 0,15 mm stainless steel stencil with slot array**

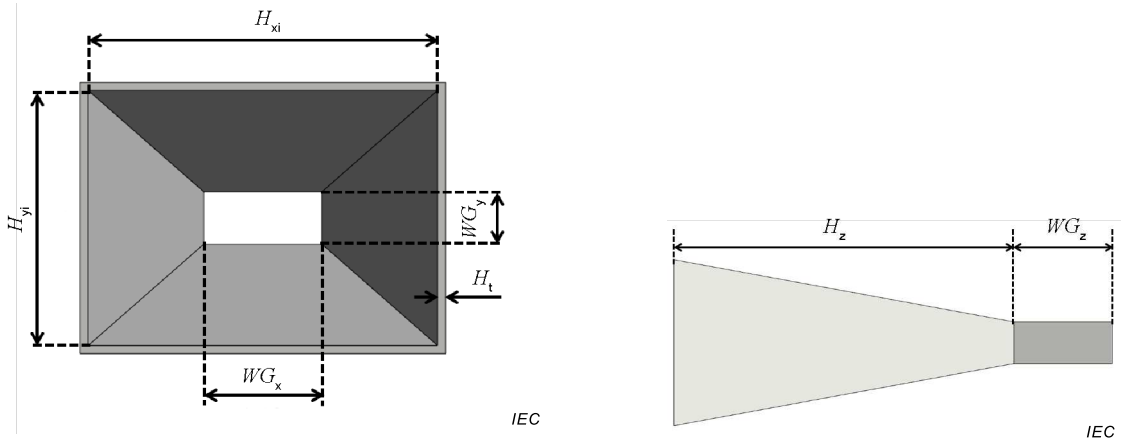


**(a) Front view** **(b) Side view**

**Figure B.7 – Main dimensions for the pyramidal horn antennas**

**Table B.3 – Main dimensions for the stencil with slot array for each frequency**

| Frequency [GHz] | Stencil length $S_x$ [mm] | Stencil width $S_y$ [mm] | Stencil thickness [mm] | Number of slots along x | Number of slots along y | Slot length $L_s$ [mm] | Slot width $W_s$ [mm] | Spacing between slots along x $d_x$ [mm] | Spacing between slots along y $D_y$ [mm] |
|---|---|---|---|---|---|---|---|---|---|
| 10 | 57,0 ± 0,01 | 47,0 ± 0,01 | 0,150 ± 0,01 | 3 | 5 | 17,5 ± 0,01 | 2,4 ± 0,01 | 22,0 ± 0,015 | 10,0 ± 0,015 |
| 30 | 42,50 ± 0,01 | 33,80 ± 0,01 | 0,150 ± 0,01 | 6 | 7 | 5,40 ± 0,01 | 0,80 ± 0,01 | 6,70 ± 0,015 | 4,47 ± 0,015 |
| 60 | 23,40 ± 0,01 | 18,80 ± 0,01 | 0,150 ± 0,01 | 5 | 8 | 2,75 ± 0,01 | 0,42 ± 0,01 | 4,00 ± 0,015 | 2,08 ± 0,015 |
| 90 | 16,70 ± 0,01 | 13,40 ± 0,01 | 0,150 ± 0,01 | 6 | 8 | 1,80 ± 0,01 | 0,30 ± 0,01 | 2,30 ± 0,015 | 1,40 ± 0,015 |

**Table B.4 – Main dimensions for the corresponding pyramidal horn at each frequency**

| Frequency [GHz] | Horn typical gain [dB] | Horn aperture along x (internal) $H_{xi}$ [mm] | Horn aperture along y (internal) $H_{yi}$ [mm] | Horn size along z $H_z$ [mm] | Horn thickness $H_t$ [mm] | Waveguide length $WG_x$ [mm] | Waveguide width $WG_y$ [mm] | Waveguide segment $WG_z$ [mm] |
|---|---|---|---|---|---|---|---|---|
| 10 | 15 | 67,6 ± 0,2 | 49,5 ± 0,2 | 108 ± 0,2 | 1,53 ± 0,1 | 22,86 ± 0,1 | 10,16 ± 0,05 | 30 ± 0,05 |
| 30 | 20 | 40,0 ± 0,1 | 31,3 ± 0,1 | 47,6 ± 0,1 | 1,25 ± 0,1 | 7,112 ± 0,1 | 3,556 ± 0,05 | 11 ± 0,05 |
| 60 | 20 | 21,33 ± 0,1 | 16,65 ± 0,1 | 26,25 ± 0,1 | 1,25 ± 0,1 | 3,7592 ± 0,1 | 1,8796 ± 0,05 | 6,2 ± 0,05 |
| 90 | 20 | 14,2 ± 0,1 | 11 ± 0,1 | 17,35 ± 0,1 | 1,25 ± 0,1 | 2,54 ± 0,1 | 1,27 ± 0,05 | 10,6 ± 0,05 |

### B.3.2 Target values

Table B.5 provides the target values for the E-field, H-field and power density from the pyramidal horn defined in B.3.1. All target values are the maximum values in planes at distances of $d$ = 2 mm, 5 mm, 10 mm and 20 mm parallel to the top surface of the dielectric substrate. $E_{max}$ = max($|E_{total}|$) and $H_{max}$ = max($|H_{total}|$) are the maximum local E-field and H-field magnitudes. $S_{max}$ is the maximum value of $S$ defined in 3.17, where the normal vector $\hat{\mathbf{n}}$ is the direction of the local power density, not the normal of the plane parallel to the antenna. $S_{av}$ is the maximum spatial-average power density, as defined in Formula (1), for circular surfaces of 1 cm$^2$ and 4 cm$^2$ area. The accepted power is 0 dBm.

**Table B.5 – Target values for the pyramidal horns loaded with slot arrays at different frequencies ($u_s$ ($k$ = 1) = 0,5 dB)**

| $f$ [GHz] | $d$ [mm] | Max. E field $E_{max}$ [V/m] | Max. H field $H_{max}$ [A/m] | Max. local power density $S_{pk}$ [W/m$^2$] | $S_{av}$ 1 cm$^2$ [W/m$^2$] | $S_{av}$ 4 cm$^2$ [W/m$^2$] |
|---|---|---|---|---|---|---|
| 10 | 2 | 49,01 | 0,09 | 2,07 | 1,15 | 0,83 |
| | 5 | 25,39 | 0,05 | 1,16 | 0,96 | 0,76 |
| | 10 | 16,41 | 0,05 | 0,76 | 0,73 | 0,66 |
| | 20 | 15,78 | 0,04 | 0,69 | 0,65 | 0,59 |
| 30 | 2 | 35,37 | 0,10 | 2,93 | 1,83 | 1,36 |
| | 5 | 29,66 | 0,09 | 2,60 | 1,64 | 1,27 |
| | 10 | 25,65 | 0,07 | 1,85 | 1,47 | 1,22 |
| | 20 | 22,75 | 0,06 | 1,44 | 1,19 | 0,98 |
| 60 | 2 | 62,18 | 0,15 | 8,24 | 5,43 | 2,90 |
| | 5 | 52,07 | 0,13 | 6,54 | 4,52 | 2,77 |
| | 10 | 48,91 | 0,14 | 6,74 | 3,94 | 2,46 |
| | 20 | 38,23 | 0,10 | 3,99 | 2,98 | 1,94 |
| 90 | 2 | 82,20 | 0,24 | 19,55 | 8,30 | 2,67 |
| | 5 | 71,62 | 0,19 | 13,57 | 7,16 | 2,55 |
| | 10 | 50,67 | 0,14 | 6,70 | 5,37 | 2,26 |
| | 20 | 44,95 | 0,12 | 5,48 | 3,64 | 1,92 |

The patterns of $|E_{total}|$ and $\Re(S)_{total} = 0{,}5 \cdot \Re\left(\boldsymbol{E} \times \boldsymbol{H}^*\right)$ are shown in Figures B.8, B.9, B.10 and B.11 for the horn loaded with the array of slots at the operating frequencies of 10 GHz, 30 GHz, 60 GHz and 90 GHz, respectively, each for the distances 2 mm, 5 mm, 10 mm and 20 mm from the antenna surface normalized to an accepted power of 0 dBm.

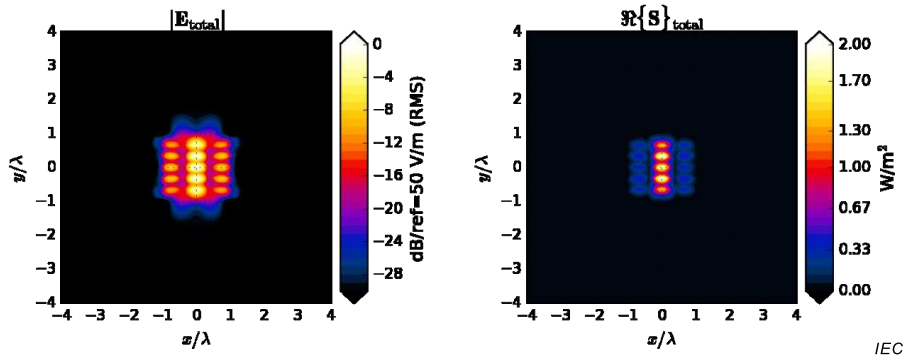


(a) $d$ = 2 mm

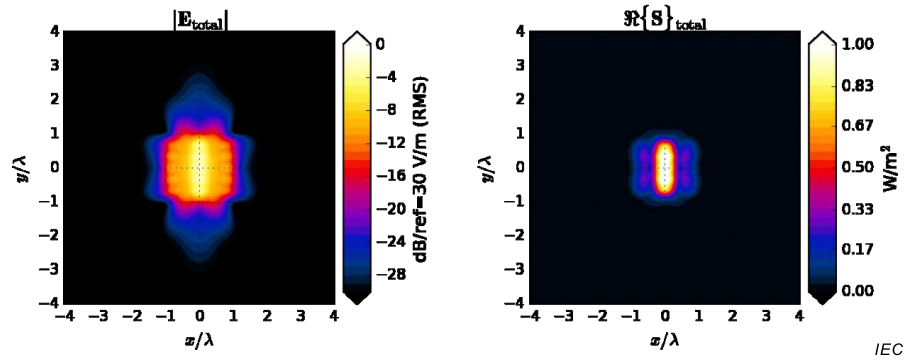


(b) $d$ = 5 mm

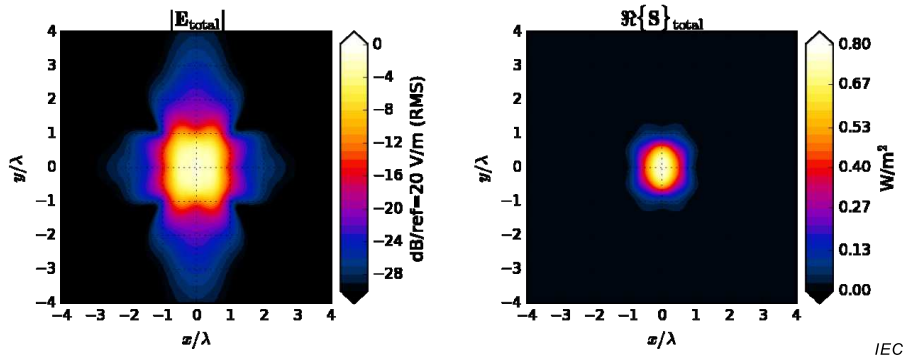


(c) $d$ = 10 mm

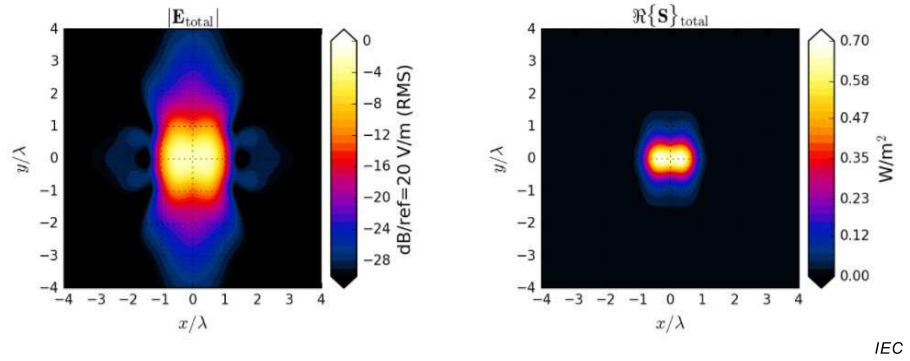


(d) $d$ = 20 mm

**Figure B.8 – 10 GHz patterns for the $|E_{\text{total}}|$ and Re$\{S\}_{\text{total}}$ for the pyramidal horn loaded with an array of slots at various distances, $d$, from the array surface and $P_{\text{in}}$ = 0 dBm**

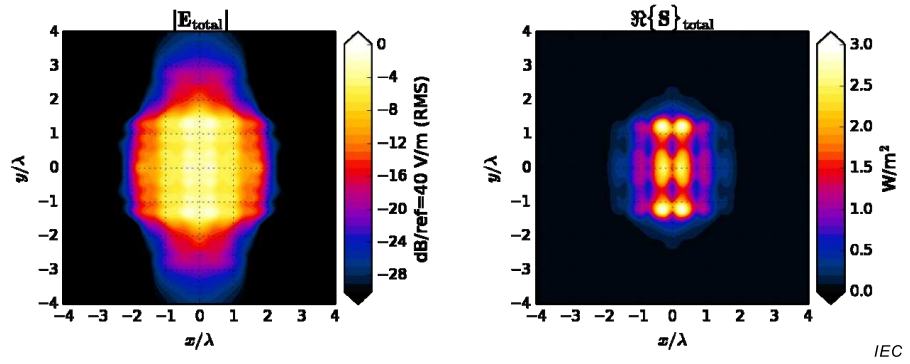


(a) $d$ = 2 mm

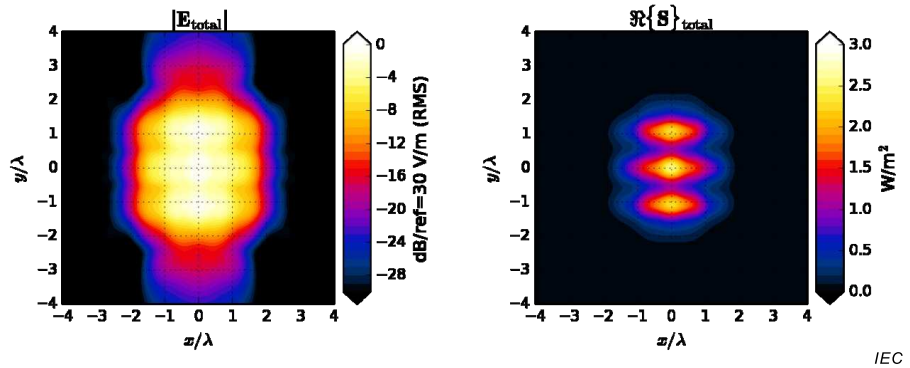


(b) $d$ = 5 mm

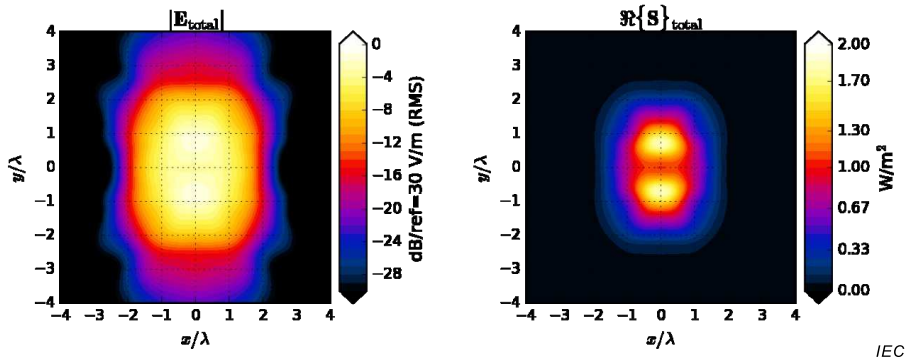


(c) $d$ = 10 mm

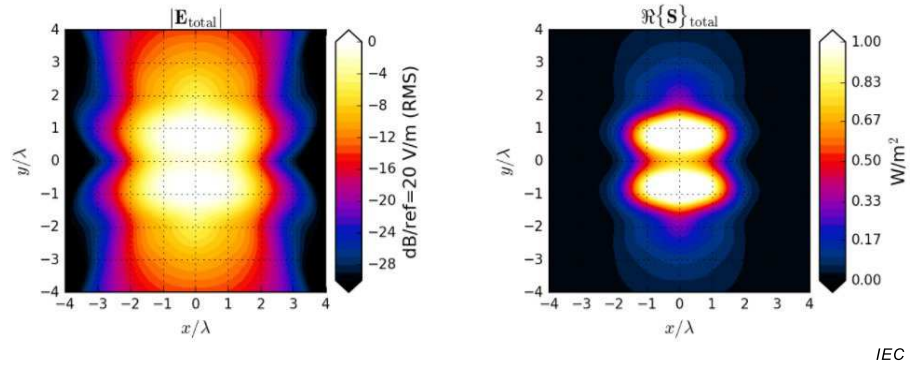


(d) $d$ = 20 mm

**Figure B.9 – 30 GHz patterns for the $|E_{\text{total}}|$ and $\text{Re}\{S\}_{\text{total}}$ for the pyramidal horn loaded with an array of slots at various distances, $d$, from the array surface and $P_{\text{in}}$ = 0 dBm**

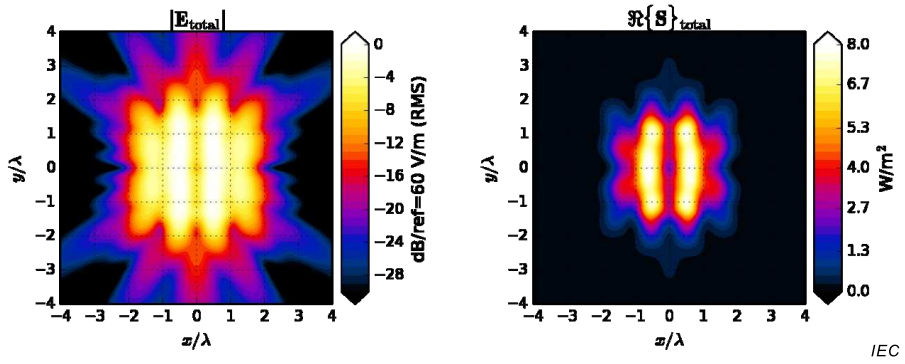


(a) $d$ = 2 mm

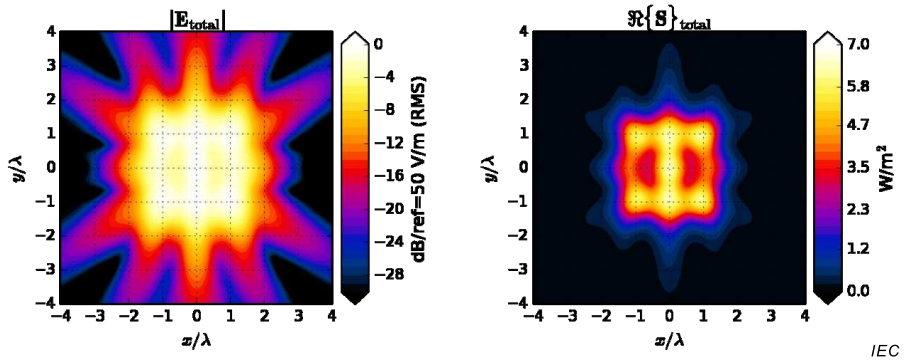


(b) $d$ = 5 mm

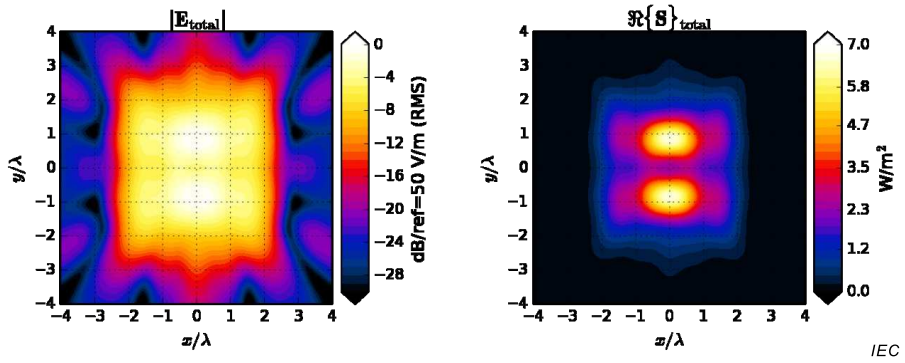


(c) $d$ = 10 mm

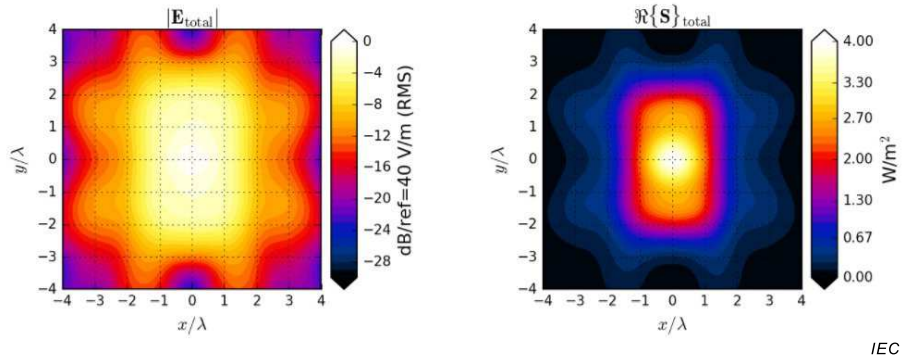


(d) $d$ = 20 mm

**Figure B.10 – 60 GHz patterns for the $|E_{total}|$ and $Re\{S\}_{total}$ for the pyramidal horn loaded with an array of slots at various distances, $d$, from the upper surface of the slot array**

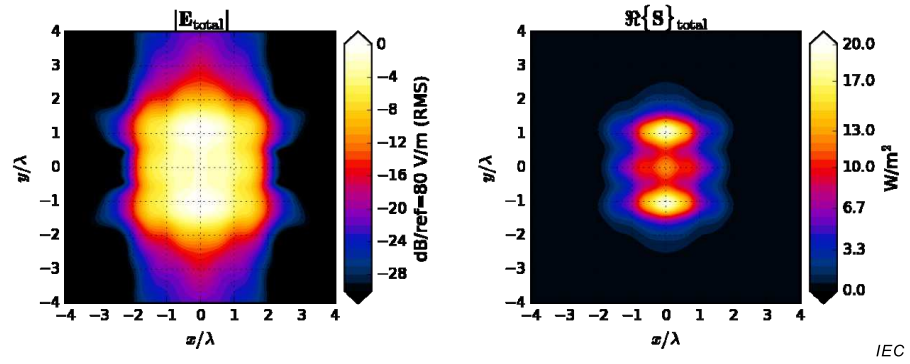


(a) $d$ = 2 mm

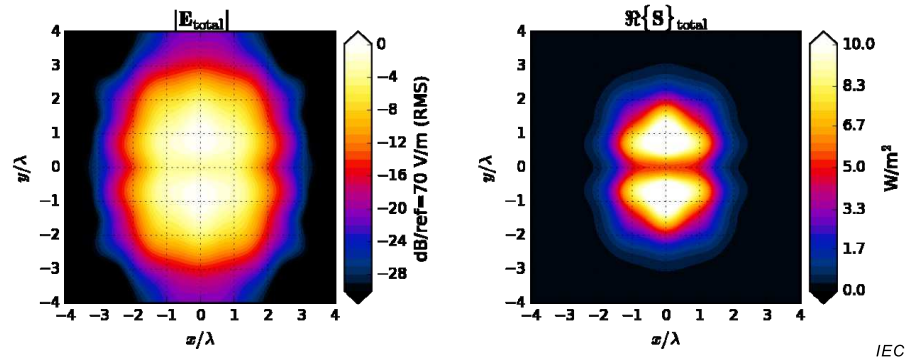


(b) $d$ = 5 mm

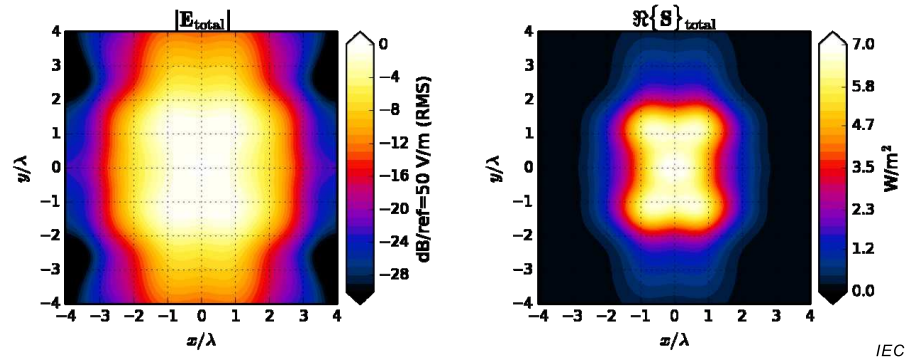


(c) $d$ = 10 mm

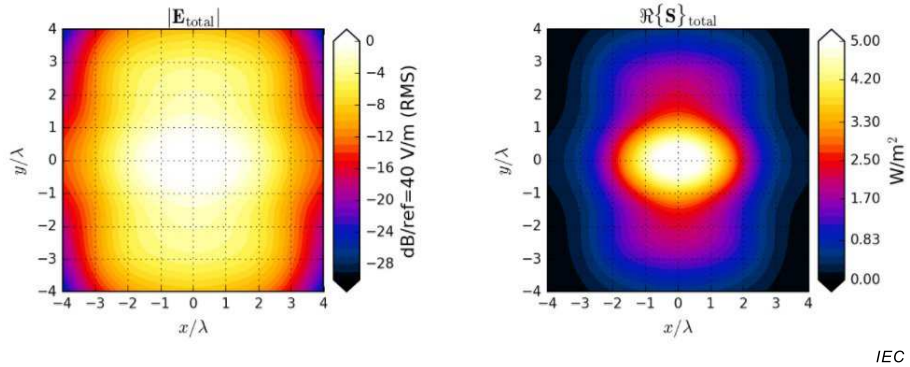


(d) $d$ = 20 mm

**Figure B.11 – 90 GHz patterns for the $|E_{\text{total}}|$ and Re$\{S\}_{\text{total}}$ for the pyramidal horn loaded with an array of slots at various distances, $d$, from the upper surface of the slot array**

# Annex C
(informative)

# Examples of system check sources

## C.1 Background

Annex C defines a selection of system check sources meeting the criteria of A.3.1.

## C.2 Source description

The system check sources are pyramidal horn antennas as shown in Figure B.7. At the centre of the aperture, the horn antennas provide a linearly-polarized electric field in the y direction and a linearly-polarized magnetic field in the x direction. These horn antennas typically have a coaxial feed.

The system check sources are defined at four frequencies: 10 GHz, 30 GHz, 60 GHz and 90 GHz. The dimensions of the pyramidal horn antenna at each of these frequencies are defined in Table B.4. The return loss is typically better than 20 dB. The microwave source feeding the horn antenna should have harmonics less than −20 dBc.

## C.3 Target values

Table C.1 provides the target values for the E-field, H-field and power density from the pyramidal horn antennas. All target values are the maximum values at a distance of $d$ = 150 mm from the horn aperture. $E_{max}$ = max($|E_{total}|$) and $H_{max}$ = max($|H_{total}|$) are the maximum local E-field and H-field magnitudes. $S_{max}$ is the maximum value of the local power density $S$ defined in 3.17.

**Table C.1 – Target values for pyramidal horn antennas at different frequencies**

| Frequency | $d$ | Max. E-field | Max. H-field | Max. local power density |
|---|---|---|---|---|
| | | $E_{max}$ | $H_{max}$ | $S_{max}$ |
| [GHz] | [mm] | [V/m] | [mA/m] | [mW/m$^2$] |
| 10 | 150 | 6,54 | 17,60 | 116,67 |
| 30 | 150 | 8,75 | 23,7 | 215 |
| 60 | 150 | 9,66 | 26,1 | 261,3 |
| 90 | 150 | 12,66 | 33,6 | 425,2 |
| All results are normalized to a forward power of 0 dBm. | | | | |

# Annex D
(informative)

# Information on the applicability of far-field methods

## D.1 Background

Annex D introduces investigated results of evaluation methods based on

- equivalent isotropic radiated power (EIRP) (D.2), and
- plane wave equivalent approximation (D.3).

These two methods are rigorous in the far-field but their applicability at closer distances required investigation [12]. The main difference between them is whether E-field or H-field is measured or not. The evaluation method using EIRP only requires input power and antenna gain while measurement of E- or H-field is necessary for the plane wave equivalent approximation.

## D.2 Evaluation method using EIRP

### D.2.1 General

In the far-field, power density $S_{\text{eirp}}$ (W/m$^2$) is given by Formula (D.1). As this evaluation only requires input power and antenna gain, electromagnetic field measurements close to antennas are not necessary.

$$S_{\text{eirp}} = \frac{\text{EIRP}}{4\pi d^2} = \frac{PG}{4\pi d^2} \quad \text{(W/m}^2\text{)} \tag{D.1}$$

where

$P$ is the input power (W);

$G$ is the antenna gain;

$d$ is the distance between antennas and evaluation point (m).

### D.2.2 Numerical simulated results

In order to investigate the accuracy of Formula (D.1), $S_{\text{eirp}}$ was compared to numerical simulations of $S_{\text{av}}$ using Formula (1) for patch and slot antennas operating at 28,5 GHz as shown in Figure D.1. For the arrays, the individual antenna elements are spaced at a distance of 0,5$\lambda$ and fed in-phase. Figure D.2 shows calculated results of $S_{\text{eirp}}$ by Formula (D.1) and numerical simulated results of $S_{\text{av}}$ averaged over 1 cm$^2$, 4 cm$^2$, and 20 cm$^2$ rectangular areas, respectively. Antenna gains used in these calculations are indicated in parenthesis on each graph. The distance and power density are normalized to the free-space wavelength ($\lambda$) and maximum $S_{\text{eirp}}$, respectively. The results show that $S_{\text{eirp}}$ is larger than the actual spatial-average power density close to the antenna. For instance, $S_{\text{eirp}}$ is approximately 6 dB to 16 dB larger than the power density averaged over 1 cm$^2$ area at distance of 0,5$\lambda$. The results suggest that evaluation based on EIRP provides an overestimate of power density. This approach may be used to show compliance of devices without requiring more complex and accurate near field measurements described in this document.

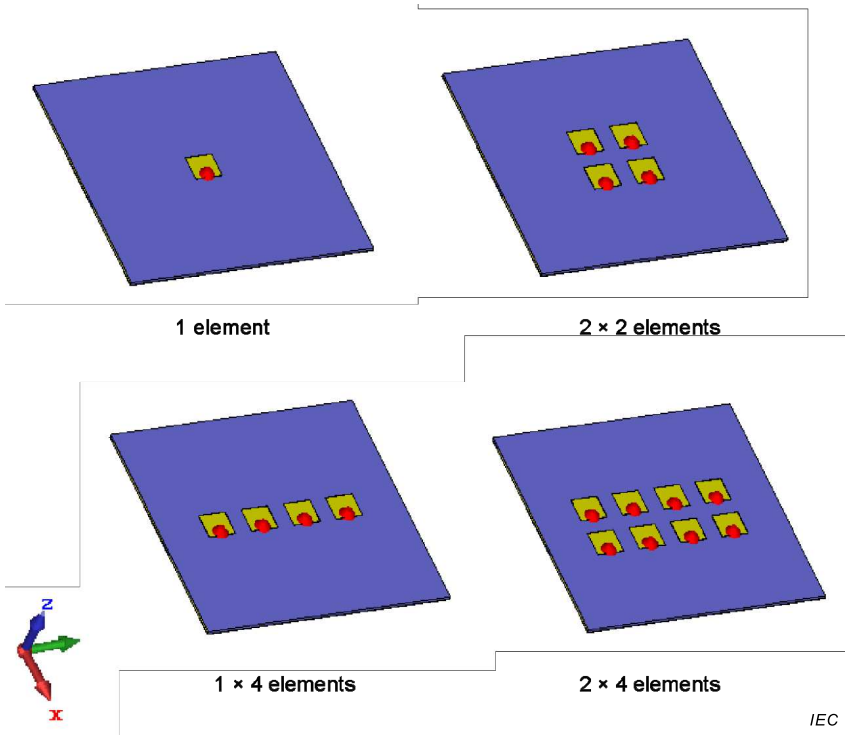


(a) Patch antennas

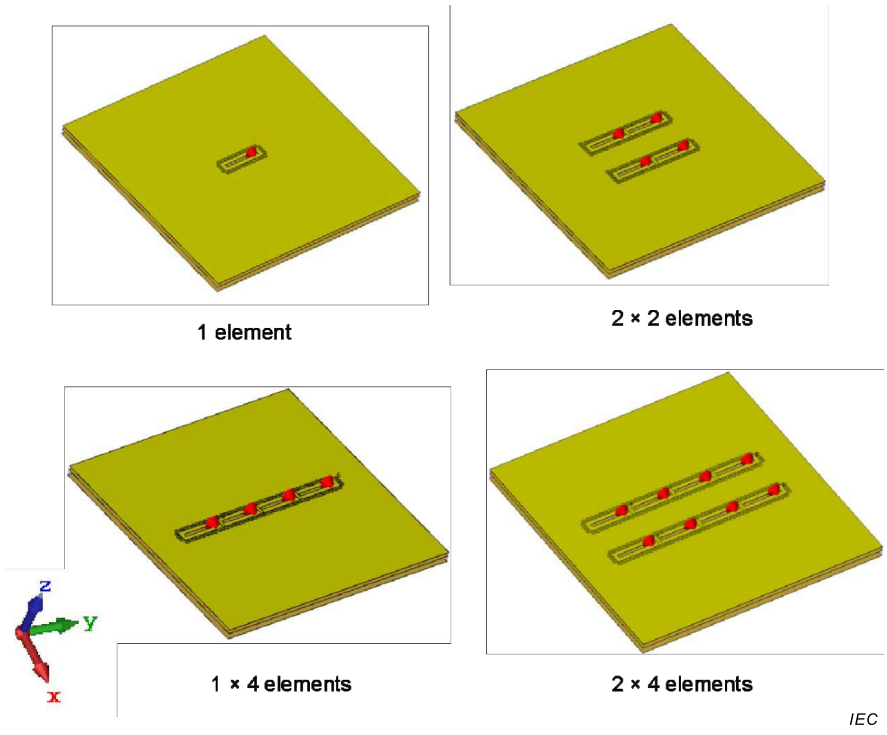


(b) Slot antennas

**Figure D.1 – Antenna models at 28,5 GHz**

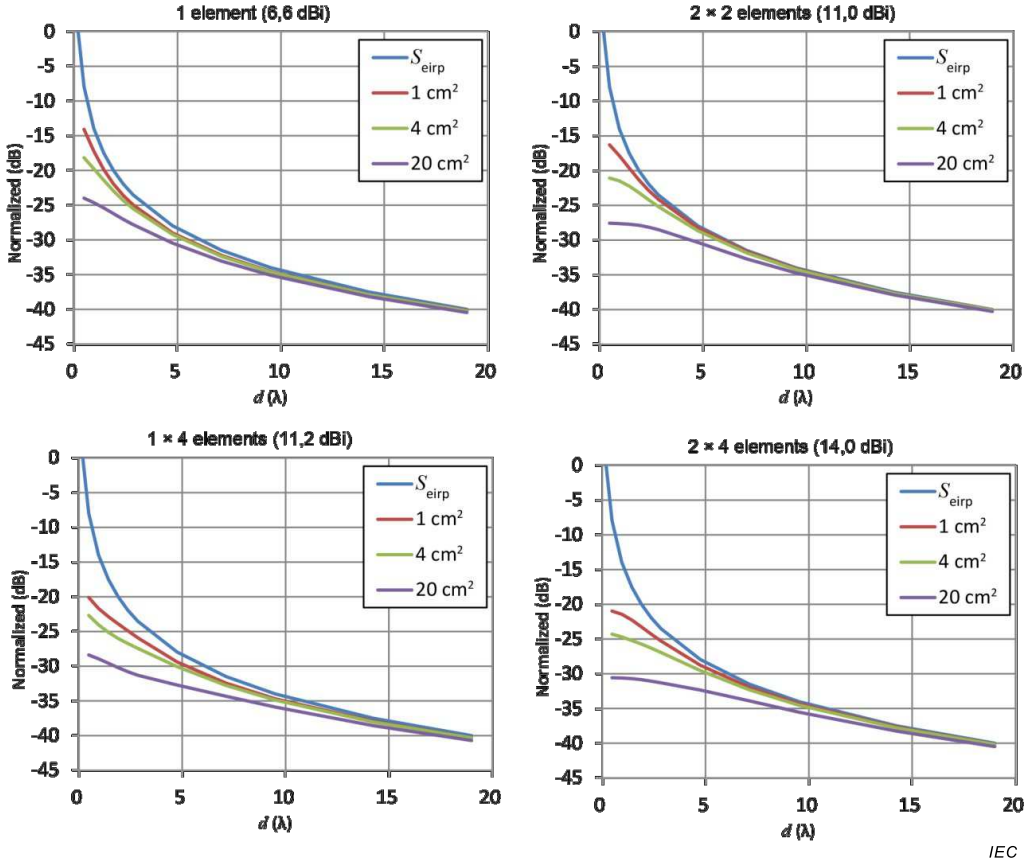


(a) Patch antenna

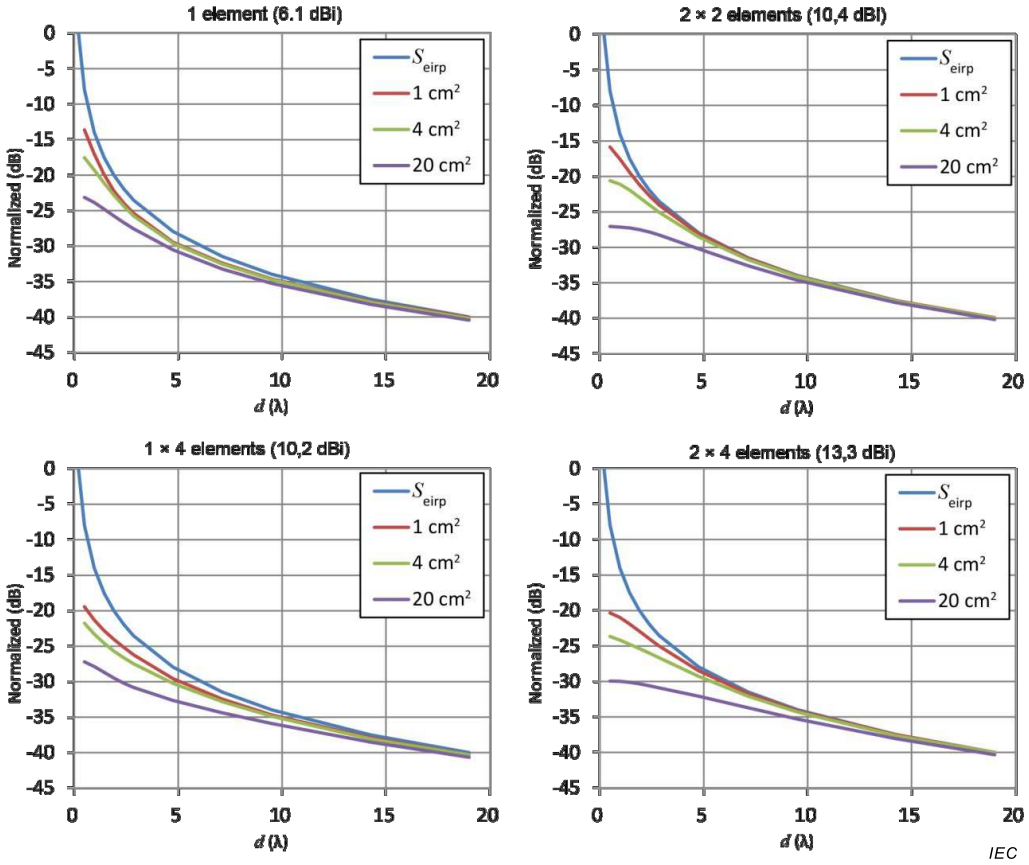


(b) Slot antenna

**Figure D.2 – $S_{eirp}$ compared to $S_{av}$ (normalized to maximum of $S_{eirp}$)**

## D.3 Plane wave equivalent approximation

### D.3.1 General

Based on the plane wave equivalent approximation, the spatial-average power density is determined according to Formula (3). In the direction of propagation, the power density for a plane wave is therefore given by

$$S_{\mathrm{e}} = \frac{|E|^2}{377} \quad \text{or} \quad 377|H|^2 \tag{D.2}$$

where

$E$ is the RMS electric field (V/m);

$H$ is the RMS magnetic field (A/m).

### D.3.2 Numerical simulated results

In this case both $S_{\mathrm{e}}$ and $S_{\mathrm{av}}$ are obtained by numerical simulations for the same configurations described in Clause D.2. Figure D.3 shows the ratio of $S_{\mathrm{e}}$ to $S_{\mathrm{av}}$ versus distance ($\lambda$). Vertical red dotted lines show the minimum separation distance calculated according to Table 1 which is the minimum separation distance between the antenna and the evaluation surface for which Formula (3) applies. $D$ is the maximum linear dimension of the antenna operating in the selected configuration.

Figure D.3 shows that, for the cases investigated, the distance from antennas where the difference between $S_{\mathrm{e}}$ and $S_{\mathrm{av}}$ exceeds 1 % does not depend on the antenna dimension. In addition, the minimum separation distances obtained by Table 1 are much larger compared to the results for 1 cm$^2$ and 4 cm$^2$ especially for antenna arrays. Figure D.4 summarizes the ratios for all antennas. The results indicate that, for the investigated cases, a separation distance of a few $\lambda$ might be sufficient to use the plane wave equivalent approximation by applying a compensation factor of 1, e.g. $S_{\mathrm{e}} \times 1{,}2$.

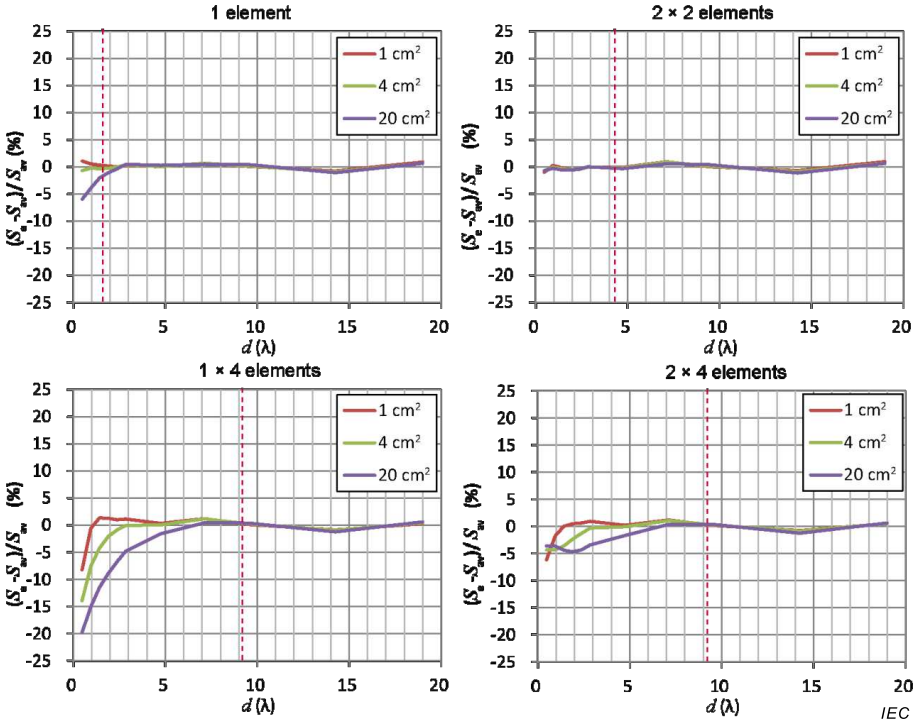


(a) Patch antenna

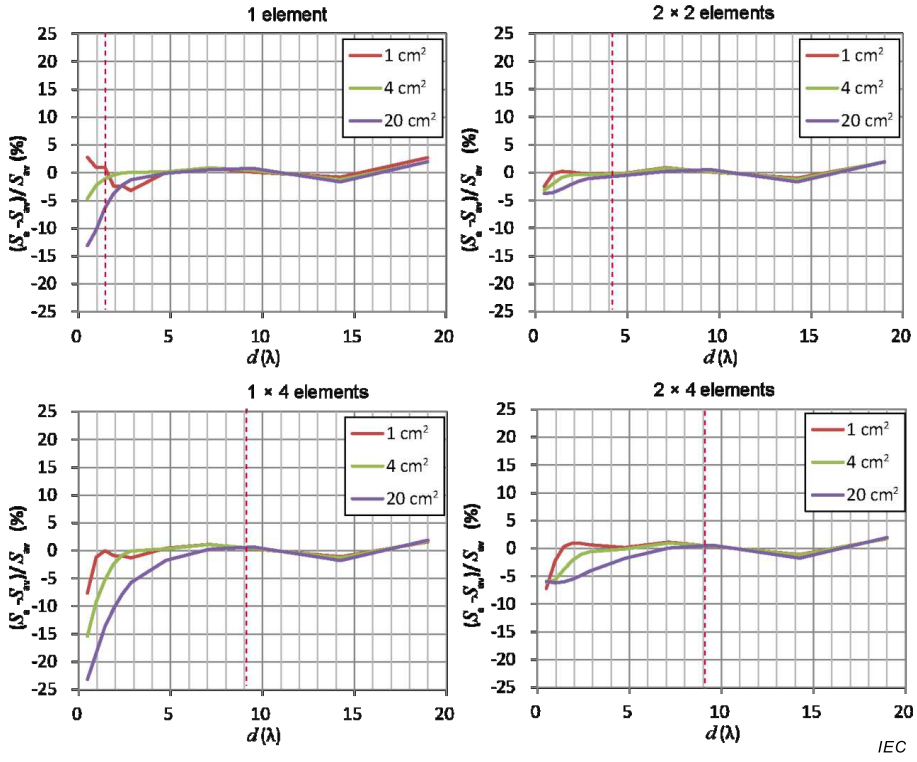


(b) Slot antenna

**Figure D.3 – Plane wave equivalent approximation ($S_e$) and simulation ($S_{av}$) results**

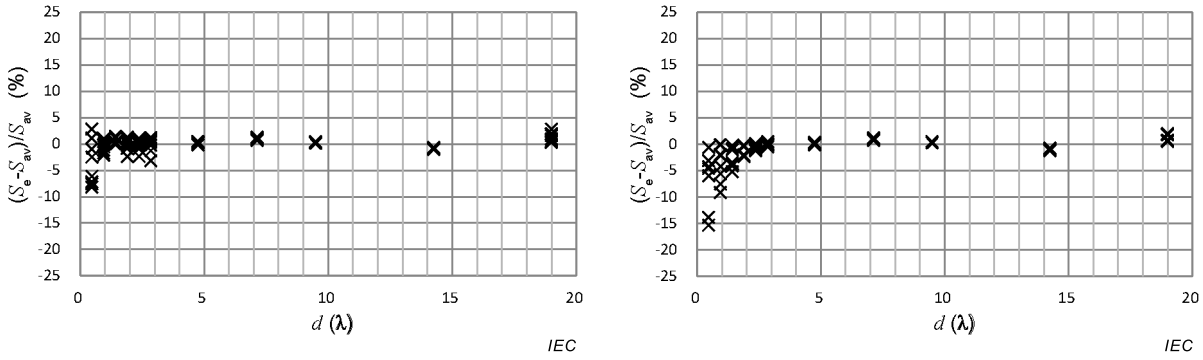


(a) Average area: 1 cm$^2$ (b) Average area: 4 cm$^2$

**Figure D.4 – Difference of $S_e$ to $S_{av}$ for all antennas (%)**

# Annex E
(informative)

# Rationale for the use of square or circular shapes for the averaging area applied to the power density for compliance evaluation

## E.1 General

Annex E discusses the difference in averaging areas with square and circular shapes, which are used to derive the spatial-average of power density over an evaluation surface $S_{av}$. As discussed below the averaging area with a square shape cannot be uniquely determined over an evaluation surface and the derived $S_{av}$ will vary and may adversely impact reproducibility in the compliance assessment of power density.

## E.2 Method using computational analysis

Computational simulations were conducted using the Method of Moment (MoM) at several frequencies from 30 GHz to 100 GHz. Patch array antennas with 2 × 2 and 1 × 4 elements were used as sources. Each element was excited with equal amplitude and phase. The spatial-average power density $S_{av}$ was derived from Formula (2) for averaging area of 1 cm$^2$ and 4 cm$^2$ and separation distances between the antenna and evaluation surface ranging from 1 mm to 10 mm. Spatial resolutions used to derive $S_{av}$ were 1 mm, 0,5 mm, and 0,2 mm at 30 GHz, 60 GHz, 100 GHz, respectively.

The antennas were rotated up to 90 degrees from the initial set position as shown in Figure E.1. The spatial maximum value of $S_{av}$ averaged over the square shape was derived for each antenna positioning.

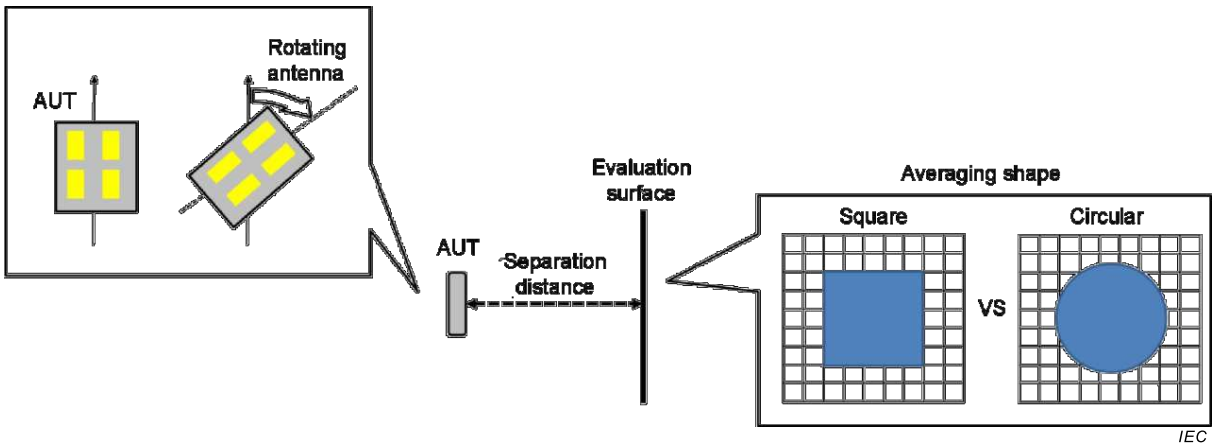


AUT = antenna under test

**Figure E.1 – Schematic view of the assessment of the variation of $S_{av}$ using square shape by rotating AUT**

## E.3 Areas averaged with square and circular shapes

Figure E.2 shows the ratio between $S_{av}$ when averaged over squares compared with the circle as a function of the separation distance from each antenna. The solid lines in the figure are given by the mid-range of $S_{av}$ for square averaging shape while the vertical bars represent the range of the spread values by rotating the antenna.

Because of the spread in $S_{av}$ obtained for different orientations of the square averaging area, it is recommended to use a circular averaging area to ensure better reproducibility.

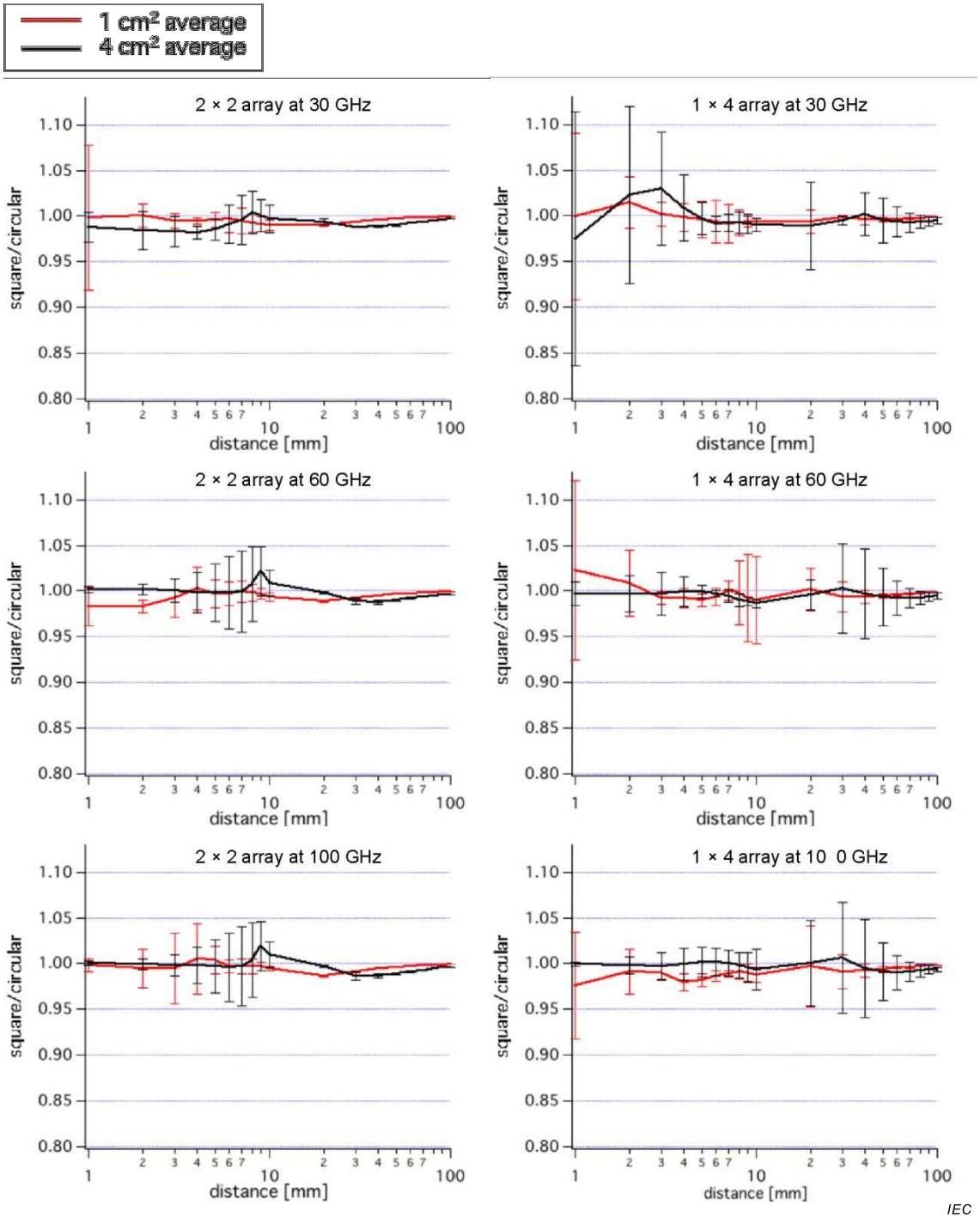


**Figure E.2 – Comparison of maximum values of $S_{av}$ averaged toward square and circular shapes**

# Annex F
(informative)

# Near field reconstruction algorithms

## F.1 General

In electromagnetic (EM) field measurements, from a theoretical point of view, the presence of a measurement instrument, wherever it is, always affects the measurement outcomes since it perturbs the electromagnetic field radiated by the device under test (DUT). The relevance of such bias is highly variable depending on the type of probe in use.

In recent years probe and measurement solutions have been developed which are claimed to have limited or even negligible impact on the DUT, thus making direct near field measurements possible.

On the other hand, for many of the measurement systems currently in use, the impact of probes may become quantitatively severe, to the point of jeopardizing the reliability of the results, when the measurements need to be taken close to the DUT. In these cases post-processing algorithms are therefore necessary.

Conceptually the standard way to tackle this problem is to take field measurements far enough from the DUT, so that perturbations on the latter are negligible, and then reconstruct the quantities of interest in proximity of the DUT by computational methods. However, such type of operation is a mathematically ill-posed problem: a function mapping near field into far field exists, but it is not invertible.

In the literature this class of problems is known as "inverse problems" and it has been for decades an active field of research for both the applied mathematics and engineering communities. As mentioned in the previous paragraph, inverse problems do not admit exact (closed-form) solutions, but only approximated ones; consequently, numerous methods and approaches have been proposed, each one with its own merits and drawbacks depending on the specificities of the problem and on the details of each algorithm.

In the context of this document, it is worth remarking that, being approximated solutions, all these methods bring along a numerical error which must be taken into account in the uncertainty budget, and which is distinct from the random and/or systematic errors of the measurement setup.

The existing approaches to address inverse problems in electromagnetics can be divided in two main groups:

1) field expansion and (back-)projection methods [4][13][14][15][16];
2) source reconstruction (or inverse source) methods [17][18][19].

Clauses F.2 to F.4 provide a general introduction to these approaches.

- Clause F.2 contains an overview of field expansion methods.
- Clause F.3 contains an overview of source reconstruction methods.
- Clause F.4 contains a discussion on possible implementations.

## F.2 Field expansion methods

### F.2.1 General

Here the fields are measured on a scanning surface, which may typically be a plane, a sphere or a cylinder. The measured spatial data are converted into the spectral domain and expanded in terms of modes, i.e. according to a basis of solutions of the wave equation. The basis for the expansion is chosen in order to have basis functions which are orthogonal on the scanning surface; hence we may encounter expansions in planar, spherical or cylindrical waves depending on the scanning surface. On the other hand, the choice of the scanning surface is typically dictated by the DUT characteristics and by the measurement requirements. It is worth mentioning that it is possible to pass from one basis to another, for example from a spherical wave expansion to a plane wave expansion [20].

Among the basis decompositions mentioned above, the plane wave spectrum (PWS) decomposition is at present the most widely used in the domain of human exposure assessment to RF fields.

### F.2.2 The plane wave spectrum expansion

#### F.2.2.1 General

In the framework of assessment of human exposure to radiation from wireless devices, the PWS method consists in measuring the electromagnetic field, in amplitude and phase, on a measurement plane at a large enough distance from the DUT, so that the perturbations caused by the measurement system become negligible. The measured values are then back-projected, by means of a reconstruction algorithm, to the position where the electromagnetic field actually needs to be assessed.

Globally the electromagnetic field counts six complex degrees of freedom: amplitude and phase for each of the three components of the electric (E) and magnetic (H) field. However, it follows from Maxwell equations in a source-free, homogeneous, linear, non-magnetic and isotropic medium that the number of independent complex degrees of freedom of the EM field is only two; therefore, in order to determine the EM field it is sufficient to measure two of its complex components. Usually, the amplitude and phase of the two components of the E-field tangential to the measurement plane are those which are measured directly.

In the harmonic regime, PD can be expressed as the real part of the complex Poynting vector. It is worth recalling that the time-averaged value of the Poynting vector represents the energy flow of the electromagnetic field through a given surface element during the considered period of time.

At short distances (fractions of a wavelength) from a source, the reactive parts of the E- and H-fields might contribute to the time-averaged Poynting vector (although they do not contribute to the total radiated power). The error introduced by back-projection of pure far-field data needs to be characterized.

A typical PWS algorithm may be decomposed into the following steps.

- Let P0 be the measurement plane. The two components of the E-field tangential to P0 are measured, in amplitude and phase. P0 should be chosen parallel to the target plane P1.
- The measured values are converted into spectral domain and back-projected to the target plane P1 using plane wave expansion (e.g. by means of a discrete Fourier transform).
- The normal component of the E-field on plane P1 is calculated using Gauss law, in spectral domain.
- The H-field is calculated from the E-field using the spectral formulation of the Maxwell–Faraday equation.

- The E-field and H-field vector fields are converted into space-time domain by means of an inverse discrete Fourier transform.
- The PD is calculated.

A sample test case of the PWS method and its reconstruction error is sketched in F.2.2.2.

### F.2.2.2 Reconstruction error in PWS: an example

The reconstructing error of the PWS technique was assessed by computational simulation using a patch antenna and one-dimensional array antenna with four elements. Operating frequencies were set as 30 GHz and 60 GHz. Spatial-average of power density $S_{av}$ was derived from Formula (2) and averaging area are set as 1 cm$^2$ and 4 cm$^2$ at separation distance between the antenna and evaluation surface ranging from 1 mm to 20 mm.

Measurement plane for the reconstruction was set at 5λ away from DUT antennas. Resolution of the electric fields used for the reconstruction was set to 0,4λ. Measurement plane was set to cover approximately −30 dB from the peak of amplitude of electric field.

Figures F.1 and F.2 show back projection error (dB) for assessment of maximum values of $S_{av}$: ratio of the value obtained by the back projection to that by the computational simulation. Note that the maximum values of $S_{av}$ are conservatively estimated, if a value of back projection error is positive. The accuracy of the back projection depends on the accuracy of the electric field measurement, the condition for the measurement (e.g. measurement resolution, size of the measurement plane, etc.) and the relative distance from the evaluation surface to the source.

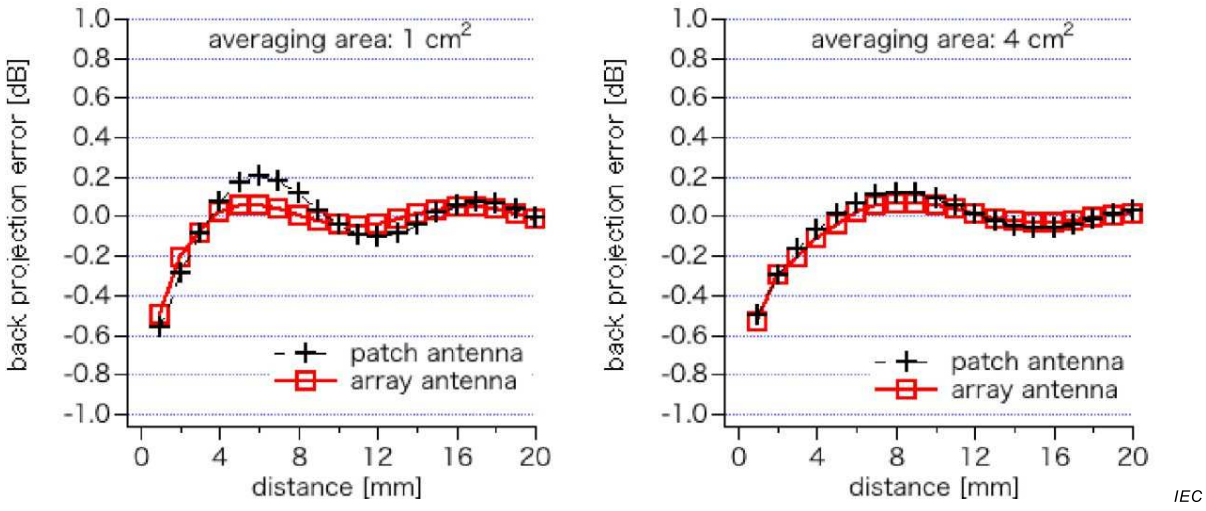


**Figure F.1 – Comparison of maximum values of $S_{av}$ between the computational simulation and back projection at 30 GHz**

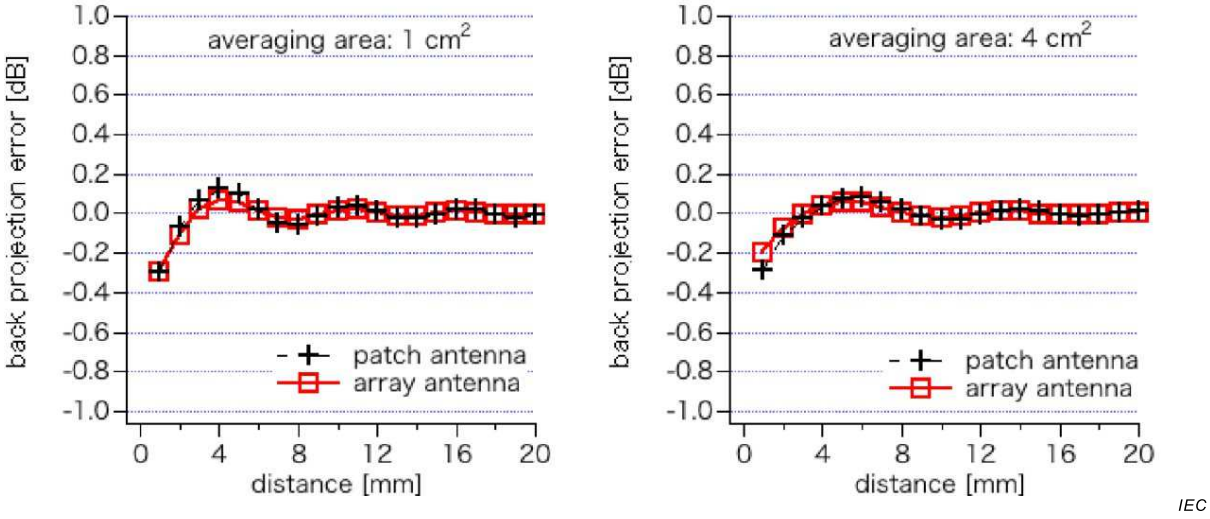


**Figure F.2 – Comparison of maximum values of $S_{av}$ between the computational simulation and back projection at 60 GHz**

## F.3 Inverse source methods

Inverse source problems arise in many scientific and industrial areas besides antenna measurements, such as biomedical imaging, tomography, transport equations, etc. As a consequence, these have been extensively studied and it would be hardly possible to list all the algorithms and variations which have been developed. Therefore, only the main principles for the EM domain will be illustrated.

The input data for the problem are typically the complex values of the electric field, radiated from the DUT, tangent to a given measurement surface. The primary output are equivalent currents on a reconstruction surface which encloses the DUT; these equivalent currents are then used as sources to calculate the EM field radiated from the DUT in the space region of interest.

The main technical difficulty is to obtain the equivalent current distributions from the radiated field data, i.e. to inverse the electric field integral equation (EFIE):

$$\mathbf{E}(\mathbf{r}) = j\omega\mu_0 \int_S \left[ \mathbf{J}(\mathbf{r}') + \frac{1}{k_0^2} \nabla\nabla\bullet\mathbf{J}(\mathbf{r}') \right] G(\mathbf{r},\mathbf{r}')\mathrm{d}S + \int_S \mathbf{M}(\mathbf{r}') \times \nabla G(\mathbf{r},\mathbf{r}')\mathrm{d}S \qquad \text{(F.1)}$$

where $G(\mathbf{r},\mathbf{r}')$ is the free space Green function, $\mathbf{J}$ and $\mathbf{M}$ are the electric and magnetic equivalent currents, respectively, that are positioned at $\mathbf{r}'$, $S$ is the reconstruction surface and $\mathbf{r}$ belongs to the measurement surface.

Again, mathematically this is an ill-posed problem. Several numerical algorithms have been conceived to re-shape Formula (F.1) into a matrix equation of the form $Ax = b$, through expansion of the currents on a set of basis functions. Anyway, the matrix $A$ remains ill-conditioned and therefore a regularization procedure is required. Among the most used mathematical approaches, it is worth mentioning: singular value decomposition (SVD), $L^2 – L^1 – L^0$ minimizations, Tikhonov regularization, Morozov regularization, etc. [21][22]

Another point to be stressed is that in standard EM problems addressed by an inverse source method, the measurement surface is relatively close to the DUT while the regions where one wants to estimate the field values are further away. In other words, inverse source methods are traditionally used to perform a near field to far field transformation. On the other hand, in

the present framework, the measurement surface will most likely lie in the far field region, while the quantity to be evaluated is the PD in the near field or very near field region. This is a further source of inaccuracy that needs to be characterized, since by far field measurements one cannot get information on the reactive part of the EM field.

## F.4 Implementation scenarios

### F.4.1 General

For most of the reconstruction methods, as well as in this document, it is assumed as standard to have the two complex tangential components of the E-field as inputs, i.e. measured directly. However, this is not the only possible scenario, since reconstruction algorithms can be implemented otherwise: in F.4.2 to F.4.4 some other implementation scenarios are summarized.

### F.4.2 Alternative field measurements

Strictly speaking, nothing prohibits to measure directly also the third component of the E-field, which may be useful to overcome problems in its numerical reconstruction. In the same spirit, nothing prohibits to measure two or three components of the H-field and derive the E-field from these, or even measure all the components of the EM field directly.

Actually, all these approaches are theoretically equivalent and the choice of one over the other depends exclusively on the technical solutions available, and on their efficiency.

### F.4.3 Phase-less approaches

In case the phases of the electric and/or magnetic field cannot be measured directly, they can be numerically retrieved from multiple measurements of the field amplitudes, using for instance interferometric or iterative procedures such as the Gerchberg–Saxton algorithm [23]. The reconstructed phases can then be used, together with amplitudes, as input for either field expansions or inverse sources methods. The errors coming from phase reconstruction algorithms should as well be taken into account in the uncertainty budget.

### F.4.4 Direct or quasi-direct near field measurements

As mentioned in Clause F.1, advancement in probe technology, such as miniaturized and/or non-metallic probes, may lower considerably the perturbations on the DUT, thus making the role of reconstruction algorithms less crucial. Therefore, a scenario should not be excluded in which direct near-field measurements on the evaluation surface will be possible, with limited use of post-processing algorithms, or with no use at all. In the latter case, the uncertainty budget will not contain contributions from reconstruction algorithms, but only errors coming from the measurement setup.

# Annex G
(informative)

# Example of a mixed (numerical and experimental) approach to assess EMF compliance for a WiGig device

## G.1 General

Numerical techniques are valuable to assess EMF compliance, and as a minimum, in combination with measurement, to identify the locations where the worst-case maxima occur to reduce measurement time for devices operating above 6 GHz. Additionally, the models can be used from design phase to final compliance, optimizing product performance and assurance of timely compliance. While near-field millimetre-wave probes and measurement techniques are under development, numerical techniques have been successfully applied, with some limitations to assess compliance for certain low power 60 GHz WiGig radios in tablet and notebook devices.

## G.2 Approach used to assess conformance

An approach had been used to assess conformance with respect to human exposure limit. This approach is based on the following steps.

1) Determine the location and orientation of the evaluation surface(s) or plane(s) and configurations based on exposure conditions of the platform to users (and bystanders if applicable).
2) If the transmitting antenna is an array involving beam-steering or beam forming, the phase combination leading to the maximum power density is determined, through numerical simulations, as follows.
    a) Finding the location of maximum power density on the evaluation surface in each evaluation configuration using an upper-bound method. The basic concept behind the upper-bound method is to assume that there could be an “ideal beam forming” mechanism that could align the phases of all the elements for both E-field and H-field. When this ideal mechanism is used, all complex phasors are aligned to the same phase, hence the phasor absolute value can be used instead of the phasor. The E-field (and H-field) for any direction is the sum of the magnitude of the fields. This method identifies the location of the maximum power density on the evaluation plane, independent of the antenna phases. It allows finding the location for an upper bound of power density with this “ideal beam forming” mechanism.
    b) The antenna phases are then adjusted (according to the device codebook) to maximize the power density across the spatial averaging area that was found using the upper-bound method in a). The method that is used to find the required antenna phases is as follows.
        i) Turn on elements one-by-one and calculate for each active element the power density in the spatial averaging window.
        ii) Sort the antenna elements based on their spatial-average power density contribution at the location determined by the upper-bound method. The elements are arranged in descending order of power density from the highest to the lowest, #0 to #$n$−1 (where $n$ is the number of elements in the array).
        iii) Turn on #0 with phase P0 = 0 (reference).
        iv) Turn on #1 and change the phase to maximize the power and find the phase P1.
        v) Keep P0 and P1 on, then turn on #2 and do same.
        vi) Repeat for the rest of the elements.
3) Calculate the power density with the antenna phases that were found in 2) b).

4) Repeat the steps from 1) to 3) for all channels. The channel leading to highest power density is therefore determined as well as the corresponding phase configuration.

5) Validate the simulation by measurement at distances supported by the measurement method. This is achieved by comparing E-field, H-field, local and spatial-average power density values and distributions for the highest exposure conditions (in terms of antenna excitations and frequency channel) found in 4).

Figure G.1 shows an example of the evaluation plane and antenna position for a platform with WiGig technology (step 1).

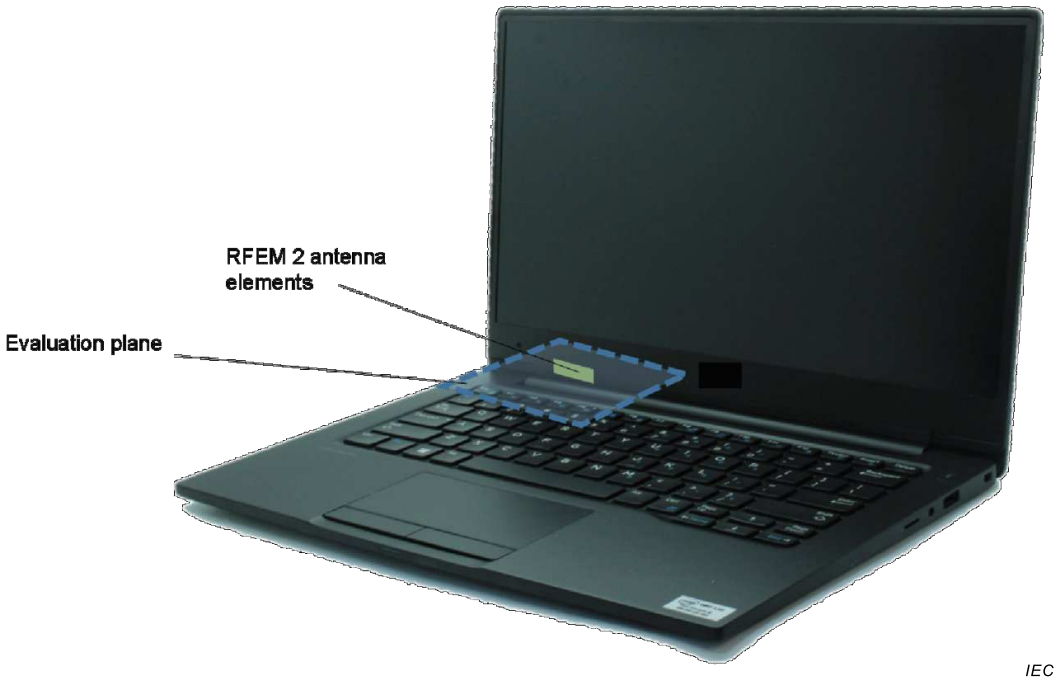


RFEM = Radio Front End Module

**Figure G.1 – Evaluation plane and antenna position**

Table G.1 shows the phase shift (in degrees) between antennas providing maximum power density found for the three WiGig frequency channels (step 2).

**Table G.1 – Phase shifts between antenna elements leading to the maximum power density for each channel**

| Antenna index | Phases [degrees] | | |
|---|---|---|---|
| | Channel 1 | Channel 2 | Channel 3 |
| 0 | **315** | 0 | 45 |
| 1 | **45** | 90 | 90 |
| 2 | **135** | 180 | 180 |
| 3 | **315** | 315 | 315 |
| 4 | **315** | 315 | 0 |
| 5 | **45** | 45 | 90 |
| 6 | **135** | 135 | 180 |
| 7 | **315** | 270 | 315 |
| 8 | **45** | 90 | 90 |
| 9 | **90** | 135 | 135 |
| 10 | **180** | 225 | 225 |
| 11 | **0** | 0 | 0 |
| 12 | **45** | 45 | 90 |
| 13 | **90** | 90 | 135 |
| 14 | **180** | 180 | 225 |
| 15 | **0** | 0 | 0 |

In this example, the number of antenna elements is 16 and the possible phase values are 0, 45, 90, 135, 180, 225, 270 degrees (phase shifter of 45 degree).

Figure G.2 shows simulation results for the peak power density and the spatial-average power density distributions in the evaluation plane for the phase configurations in Table G.1. Note that the maximum value was found for Channel 1 (step 3).

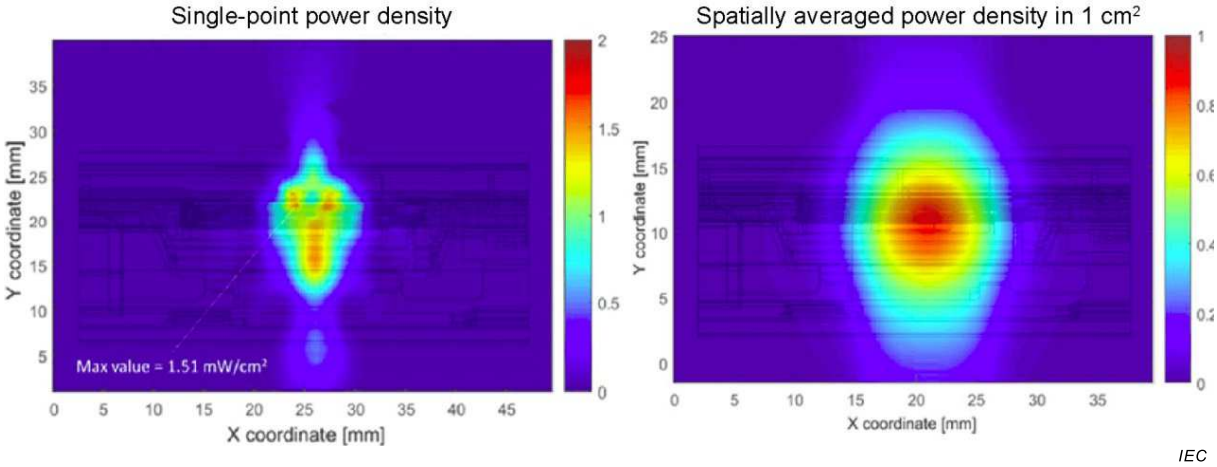


The source is determined according to the procedure described in Annex G (see also FCC ID PD918260NG).

**Figure G.2 – Local and spatial-average power densities in mW/cm$^2$**

Figure G.3 shows the changes in 1 cm$^2$ spatial-average power density at the highest exposure location with distance from the evaluation plane. Two plots are shown at 100 % and 70 % duty cycle as a function of the separation distance.

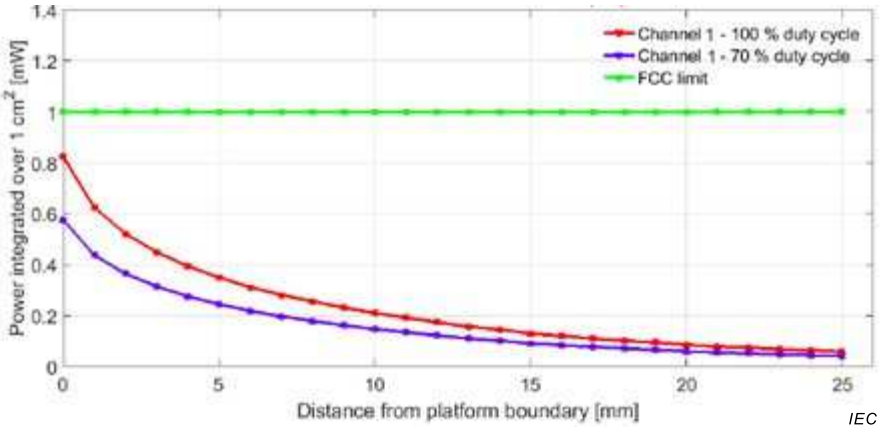


The source is FCC ID PD918260NG.

**Figure G.3 – Spatial-average power densities variation with the distance from evaluation plane**

Depending on the complexity of the antenna array, exposure conditions, availability of platform modelling details and millimetre-wave material dielectric properties, the simulation may be verified using far field measurement or near field measurement. Figure G.4 shows far-field validation of the simulation by the EIRP measurement of the device in the transition field and far field zone. Good correlation between simulation and measurement can serve to demonstrate that the near-field results provided by the simulation may be used to evaluate compliance.

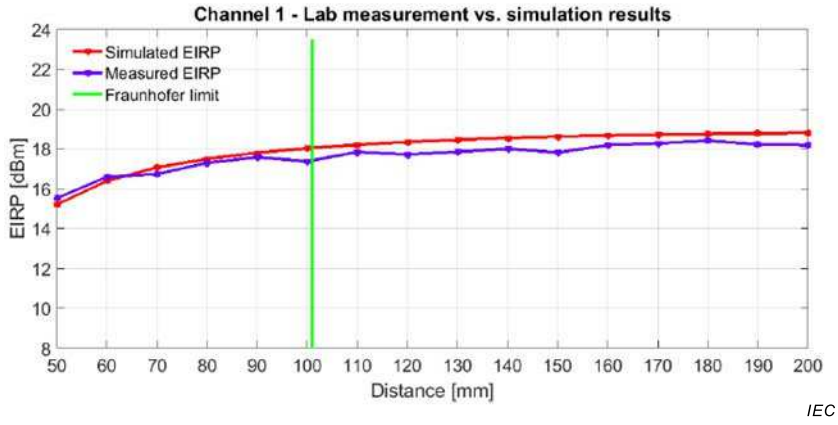


**Figure G.4 – Correlation (simulation vs. measurement)**

## G.3 Conclusion

At millimetre-wave frequencies, it is often difficult to identify certain dielectric material properties of the DUT required for numerical simulation, which can increase the simulation uncertainty. However, depending of the measurement methodology, it may not be feasible to obtain accurate power density results next to the DUT surface. Under such circumstances, simulation and measurement may be used to complement each other in order to establish compliance. Numerical techniques can be useful to assess power density levels for a comprehensive product development programme and to demonstrate compliance to RF exposure guidelines. The aforementioned numerical approach has been used successfully for certain WiGig designs to demonstrate conformance to regulatory limits and prevailing standards. As the standards for near-field millimetre-wave measurement and simulation capabilities evolve, both techniques will continue to be useful to optimize product design and supplement each other to simplify the near-field millimetre-wave RF exposure evaluation requirements.

# Annex H
(informative)

# Use cases

## H.1 General

In Annex H, results of power density measurements conducted on a mock-up device are presented. The DUT provided has a form factor typical of a mobile phone. It is characterized by an antenna array operating at about 28 GHz [24]. This is formed by several notch cuts and it is placed towards the upper edge of the device (see Figure H.1). The array antenna is printed on a 68 mm × 25 mm × 0,3 mm Rogers RO4003C™[4]; the detailed geometry of the antenna is provided in Figure H.2. The four ports are excited externally as the RF front end is not included with the mock-up. The cover of the device was realized in plastic. Figure H.3 shows the 3D radiation pattern (at 28 GHz) of the device obtained by means numerical simulations and for a uniform excitation of the four ports.

Measurements were conducted by three laboratories employing different measurement methodologies and equipment. Some of these setups involve commercial solutions available on the market while others are based on investigative and research projects.

The main purpose of this activity was to illustrate that different systems and techniques can be used when assessing power density in close proximity of a device. The assessed configurations were selected by IEC TC 106 to be representative (but not comprehensive) of the test approaches defined by this document and considering the time constraints for the project.

In order to add confidence to the measurement results, data obtained by means of numerical simulations are also presented. These, however, should not be considered as an absolute reference for the ‘true’ values as based only on an approximated modelling of the device. The Rogers RO4003 substrate on which the antenna is printed was modelled with a relative permittivity of 3,55 and loss tangent of 0,0027. The plastic box on which the antenna and the chassis are placed has a dimension of 144 mm × 72 mm × 9,8 mm and thickness of 1 mm. It is characterized by a relative permittivity of 3 and a loss tangent of 0,01.

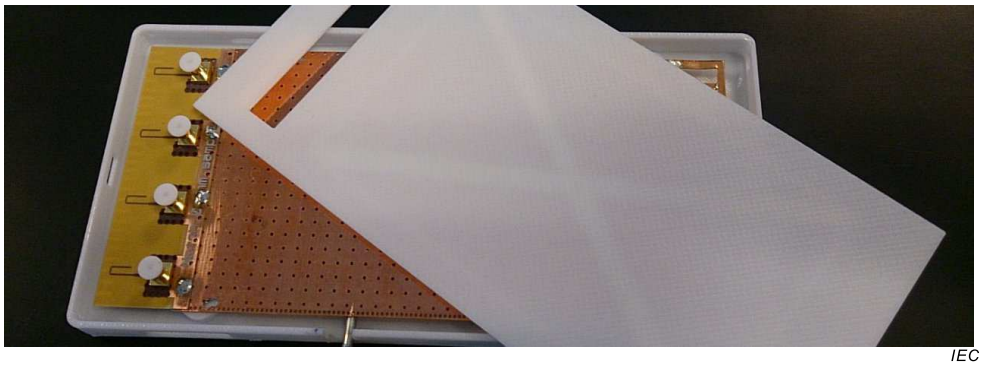

IEC

[SOURCE: Sony Mobile]

**Figure H.1 – Picture of the mock-up used for power density measurements**

4 RO4003C is the trade name of a product supplied by Rogers Corporation. This information is given for the convenience of users of this document and does not constitute an endorsement by IEC of the product named. Equivalent products may be used if they can be shown to lead to the same results.

*Dimensions in millimetres*

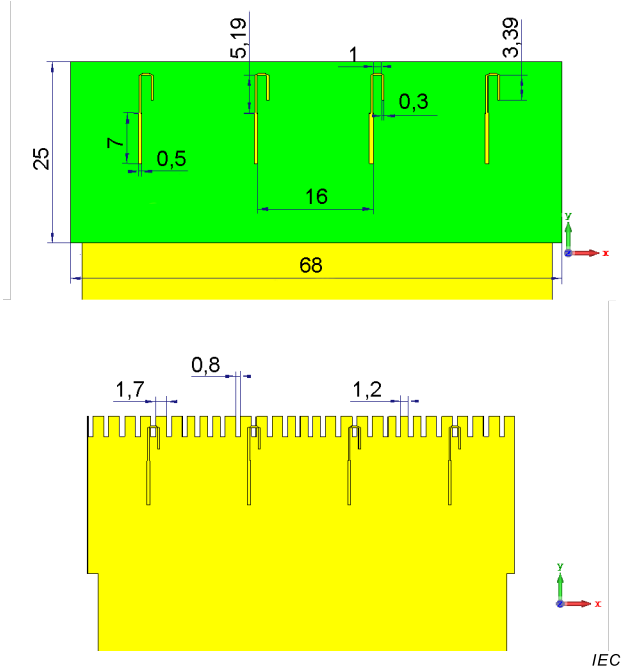


**Figure H.2 – Antenna geometry**

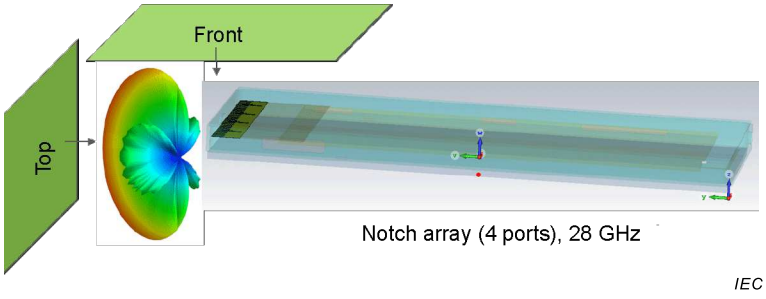


'Top' and 'Front' represent the evaluation surfaces where power density was evaluated.

**Figure H.3 – Picture of the mock-up numerical model**

## H.2 Configurations

The adopted measurement protocol is as follows.

- The test frequencies selected were: 27,5 GHz, 27,925 GHz and 28,35 GHz according to the criteria specified in 6.2.5 assuming an operating bandwidth of 27,5 GHz to 28,35 GHz (even though the antenna bandwidth was larger).
- The evaluation surfaces were chosen to be flat and parallel to the 'top edge' and to the 'front face' of the device (see Figures H.1 and H.3). The (planar) evaluation surfaces were chosen independently (at least in part) from what is specified in 6.2.5. This was necessary to reduce the measurement time and to allow different laboratories to take part in this activity within the given time frame. The selected evaluation surfaces would correspond to the flat phantom configuration in Alternative 1 of 6.2.5 . Such evaluation surfaces are also consistent with Alternative 2, as the maximum spatial-average power density was found in one of such planes.

- Results are presented for a separation distance from the device to the evaluation plane of 5 mm. At the single frequency of 27,925 GHz, power density is also provided at 10 mm and 20 mm.
- The antenna was excited through a CW signal and the spatial-average power density was determined according to Formula (2). Circular averaging areas of 1 $cm^2$, 4 $cm^2$ and 20 $cm^2$ were selected.
- The power density values are provided for an input power of 5 mW (RMS) to each antenna port.
- The precoding weights defining the possible phase and amplitude excitations for each antenna port (codebook) of the mock-up are described in Table H.1.

**Table H.1 – Phase shift values for the mockup antenna ports.**

| | $w_1$ | $w_2$ | $w_3$ | $w_4$ | $w_5$ |
|---|---|---|---|---|---|
| Port 1 | 1 | 1 | 1 | 1 | 1 |
| Port 2 | 1 | $e^{-i\frac{1}{2}\pi}$ | $e^{-i\frac{\sqrt{3}}{2}\pi}$ | $e^{i\frac{1}{2}\pi}$ | $e^{i\frac{\sqrt{3}}{2}\pi}$ |
| Port 3 | 1 | $e^{-i\pi}$ | $e^{-i\sqrt{3}\pi}$ | $e^{i\pi}$ | $e^{i\sqrt{3}\pi}$ |
| Port 4 | 1 | $e^{-i\frac{3}{2}\pi}$ | $e^{-i\frac{3\sqrt{3}}{2}\pi}$ | $e^{i\frac{3}{2}\pi}$ | $e^{i\frac{3\sqrt{3}}{2}\pi}$ |

## H.3 Results obtained at Laboratory 1

### H.3.1 General

The measurements of the mock-up provided (DUT) were performed in a temperature controlled anechoic chamber, using an automated positioning system and a miniaturized probe as described below; the amplitude of the E-field components is measured and the phase is retrieved similarly to what is described in F.4.3. In H.3.2 to H.3.8, the methodology, setup for the mock-up measurements and results are presented.

### H.3.2 Miniaturized probe

The probe is based on the pseudo-vector probe design, which not only measures the field magnitude but also derives its polarization ellipse. This probe concept also has the advantage that the sensor angle errors or distortions of the field by the substrate can be largely nullified by calibration. This is particularly important as, at these very high frequencies, field distortions by the substrate are dependent on the wavelength. The design entails two small 0,8 mm dipole sensors mechanically protected by high-density foam, printed on both sides of a 0,9 mm wide and 0,12 mm thick glass substrate. The body of the probe is specifically constructed to minimize distortion by the scattered fields.

The probe consists of two sensors with different angles ($\gamma_1$ and $\gamma_2$) arranged in the same plane in the probe axis. Three or more measurements of the two sensors are taken for different probe rotational angles to derive the amplitude and polarization information. These probes are the most flexible and accurate probes currently available for measuring field amplitude.

### H.3.3 Scans

The scan involves the measurement of two planes spaced $\lambda/4$, with three different probe rotations for each plane. The grid steps are optimized by the software based on the test frequency and the size of the device under test (DUT). The location of the lowest measurement plane is defined by the distance of first measurement layer from DUT defined by the user, in this case the planes of interest: 5 mm, 10 mm and 20 mm.

For the numerical description of an arbitrarily oriented ellipse in three-dimensional space, five parameters are needed (Figure H.4): the semi-major axis ($\vec{a}$), the semi-minor axis ($\vec{b}$), two angles describing the orientation of the normal vector of the ellipse ($\phi$, $\theta$), and one angle describing the tilt of the semi-major axis ($\psi$). For the two extreme cases, i.e. circular and linear polarizations, three parameters only ($\vec{a}$, $\phi$ and $\theta$) are sufficient for the description of the incident field.

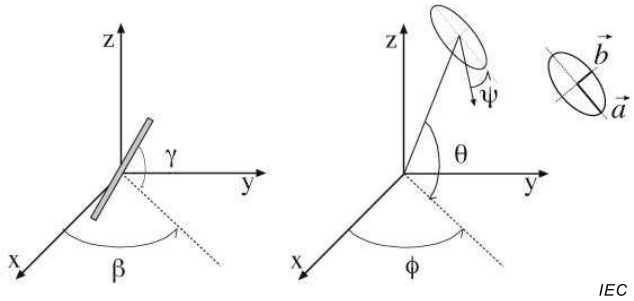


**Figure H.4 – Illustration of the angles used for the numerical description of the sensor and the orientation of an ellipse in 3-D space**

For the reconstruction of the ellipse parameters from measured data, the problem can be reformulated as a nonlinear search problem. The semi-major and semi-minor axes of an elliptical field can be expressed as functions of the three angles ($\phi$, $\theta$ and $\psi$). The parameters can be uniquely determined towards minimizing the error based on least-squares for the given set of angles and the measured data. In this way, the number of free parameters is reduced from five to three, which means that at least three sensor readings are necessary to gain sufficient information for the reconstruction of the ellipse parameters. However, to suppress the noise and increase the reconstruction accuracy, it is desirable to have an overdetermined system of equations. The solution to use a probe consisting of two sensors angled by $\gamma_1$ and $\gamma_2$ toward the probe axis and to perform measurements at three angular positions of the probe, i.e. at $\beta_1$, $\beta_2$, and $\beta_3$, results in over determinations of two. If there is a need for more information or increased accuracy, more rotation angles can be added.

The reconstruction of the ellipse parameters can be separated into linear and non-linear parts that are best solved by the Givens algorithm combined with a downhill simplex algorithm. To minimize the mutual coupling, sensor angles are set with a 90° shift ($\gamma_1$ = $\gamma_2$ + 90°), and, to simplify, the first rotation angle of the probe ($\beta_1$) can be set to 0°. Mode details can be found in [25].

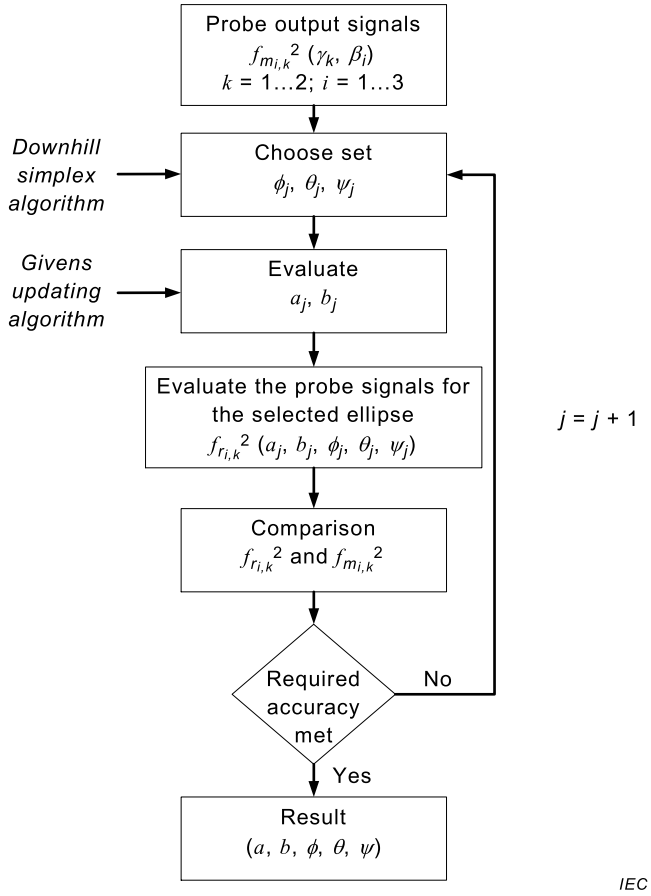


**Figure H.5 – Numerical algorithm for reconstructing the ellipse parameters**

### H.3.4 Total field and power density reconstruction

Computation of the power density in general requires knowledge of the electric (E-) and magnetic (H-) field amplitudes and phases in the plane of incidence. Reconstruction of these quantities from pseudo-vector E-field measurements is feasible, as they are constrained by Maxwell's equations. A reconstruction approach based on the Gerchberg–Saxton algorithm [26][27] has been developed, which benefits from the availability of the E-field polarization ellipse information obtained with the probe. This reconstruction algorithm, together with the ability of the probe to measure extremely close to the source without perturbing the field, permits reconstruction of the E- and H-fields, as well as of the power density, on measurement planes located as near as $\lambda/5$ away. A flow-chart of the algorithm used for reconstruction is presented in Figure H.5.

### H.3.5 Power density averaging

The average of the reconstructed power density has been evaluated over a circular area in each measurement plane. The area of the circle is defined by the user; for this study the area was defined as 1 $cm^2$, 4 $cm^2$ and 20 $cm^2$. Note that the average is only evaluated for grid points where the averaging circle is completely filled with values; for points at the edge where the averaging circle is only partly filled with values, the averaged power density is set to zero.

### H.3.6 Measuring setup

Each plane of interest was measured using the probe described above. The DUT positioning was achieved using as a reference a high-density foam.

The RF chain to feeding the DUT consisted of the following elements and is shown in Figure H.6:

- signal generator – set to one half of the target frequency with power of +5,6 dBm;
- cables and adapters;
- Ka band multiplier – 2× frequency multiplier mounted on cooling grid, input power nominal +5 dBm.

The power at the end of the chain was measured by using a thermal power sensor for the three frequencies of interest. The measured power was performed once the frequency multiplier reached a stable operation temperature. Table H.2 shows the measured power. The semi-rigid 200 mm coaxial cable and connectors used to feed the antenna ports introduced additional losses reported as 1 dB for the three frequencies. The extra losses were taken into account in order to normalize all the results to 5 mW at the input port of each antenna.

**Table H.2 – Measured power at the end of the adapter 2,4 mm to 3,5 mm and input power at the antenna port after considering extra losses introduced by the semi-rigid 200 mm coaxial cable and connectors**

| Frequency [GHz] | Measured power (dBm) | Measured power (mW) | $P_{in}$ at each port (dBm) | $P_{in}$ at each port (mW) |
|---|---|---|---|---|
| 27,500 | 19,81 | 95,72 | 18,81 | 76,03 |
| 27,925 | 19,87 | 97,05 | 18,87 | 77,09 |
| 28,350 | 19,94 | 98,63 | 18,94 | 78,34 |


[SOURCE: IT'IS Foundation]

**Figure H.6 – Measuring setup used at Laboratory 1**

Before starting the measurements, the probe was aligned using a laser beam and the DUT was taught. In this way, the zero distance reference was fixed. It is worth noting that, because the cover of the mock-up is not permanently glued, a few microns of difference can be found between each corner of the mock-up plane. Tables H.2 and H.3 show also the cases measured. Each case implies four sets of measurements, one for each port. The measured planes (5 mm, 10 mm and 20 mm) were always parallel to the system phantom (horizontal), with the probe vertically oriented. For the TOP orientation, the DUT was vertically held by using a plastic holder. For the FRONT orientation, the DUT was horizontally positioned parallel to the high-density foam support, only secured by tape. Special care was taken when changing the connected port to avoid moving the DUT. The DUT FRONT and TOP measurement configurations, as well as the convention used to number the ports, is shown in Figure H.7.


(a) FRONT orientation


(b) TOP orientation

**Figure H.7 – DUT while measuring showing the numbering for the ports**

### H.3.7 Simulated results

In order to have a reference, the CAD model was simulated using the finite-difference time-domain (FDTD) solver. However, as already explained in Clause H.1, this should not be considered as an absolute reference, as the numerical values are based only on an approximated modelling of the device, without considering fabrication tolerances and other relevant aspects.

### H.3.8 Measured results

For the different measured configurations (namely orientation, frequency and distance from DUT), the planar evaluation surfaces were chosen independently, without compromising the quality of the results. This was necessary to reduce the measurement time. All the evaluated planes are square. Table H.3 shows the dimension of one side of the scanned plane for each configuration. The values were optimized according to the field decay. For TOP orientation of the central frequency at 5 mm from the DUT, a larger scan was performed.

Figure H.8 shows the power density distribution in the top configuration in a plane located 5 mm from the DUT, at 27,925 GHz. The diagrams are shown for the four ports. As a reference, simulations are also presented. Each graph is in dB, normalized to the maximum value of the simulation and using a 100 mm × 100 mm window. Similarly, Figure H.9 shows the power density for the FRONT distribution.

Figure H.10 shows the averaged power density as a function of distance for port 1, at 27,925 GHz, for both TOP and FRONT orientations. The results are presented in a plane 5 mm from the DUT using circular averaging areas of 4 $cm^2$. As in the case of the field distributions, the graphs show also numerical results obtained from the simplified model of the device.

Figure H.11 shows the results for the averaged power density as a function of the averaging area for port 1, in TOP and FRONT orientations. The results are presented at the three frequencies of interest: 27,500 GHz, 27,925 GHz and 28,350 GHz, in a plane 5 mm from the DUT.

**Table H.3 – Edge length of the scanned planes for the different configurations**

| Distance (mm) | 27,500 GHz | | 27,925 GHz | | 28,350 GHz | |
|---|---|---|---|---|---|---|
| | TOP | FRONT | TOP | FRONT | TOP | FRONT |
| 5 | 84,5 | 62,7 | 110,1 | 61,8 | 82,0 | 60,9 |
| 10 | [a] | [a] | 83,3 | 61,8 | [a] | [a] |
| 20 | [a] | [a] | 83,3 | 61,8 | [a] | [a] |

[a] These configurations were excluded.

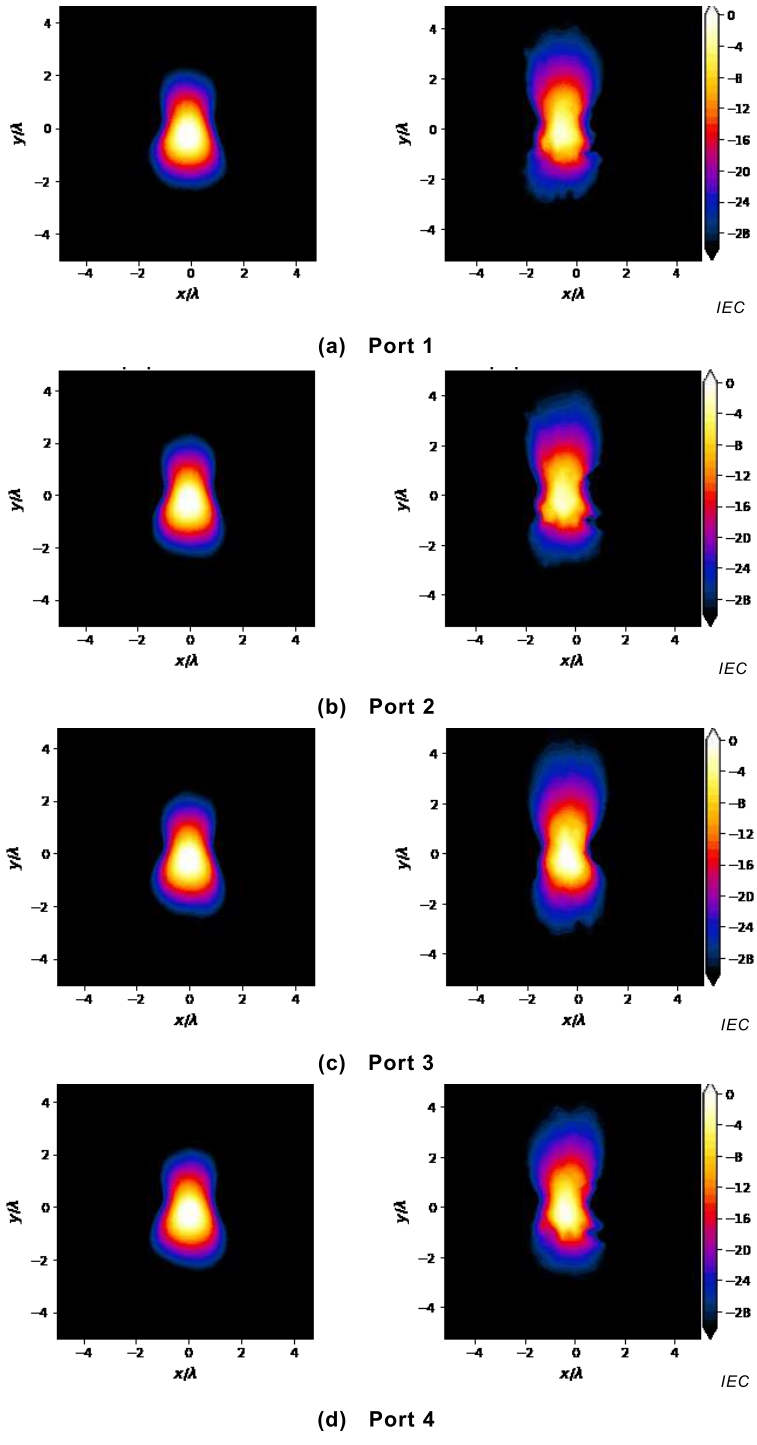


**Figure H.8 – Simulated (left) and measured (right) power density distribution for the TOP configuration**

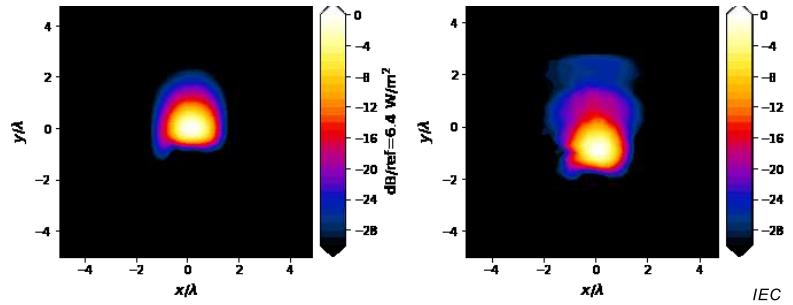


(a) Port 1

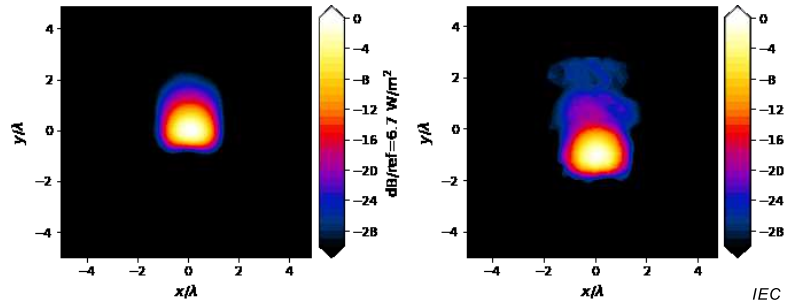


(b) Port 2

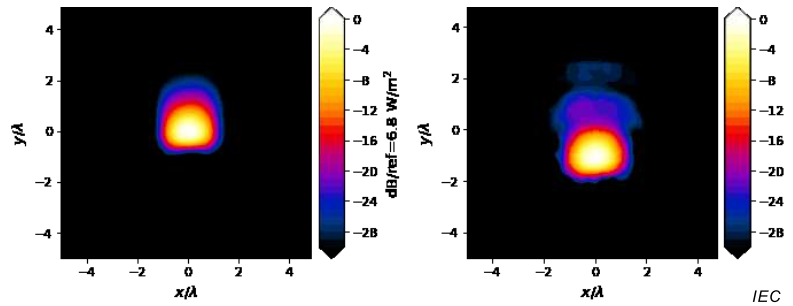


(c) Port 3

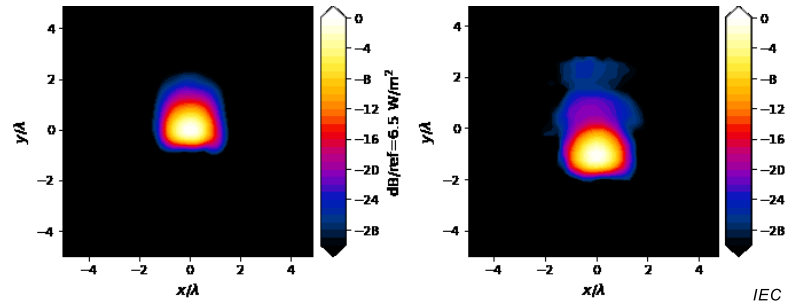


(d) Port 4

**Figure H.9 – Simulated (left) and measured (right) power density distribution for the FRONT configuration**

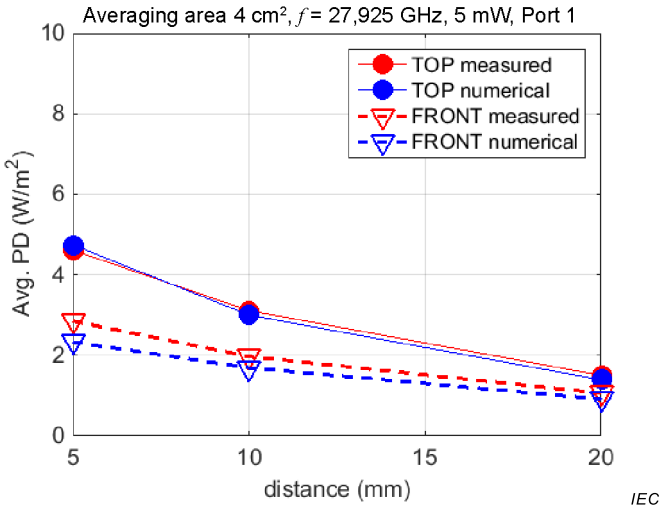


**Figure H.10 – Averaged power density as a function of distance for port 1, at 27,925 GHz, for TOP and FRONT configurations averaged over an area of 4 cm$^2$**

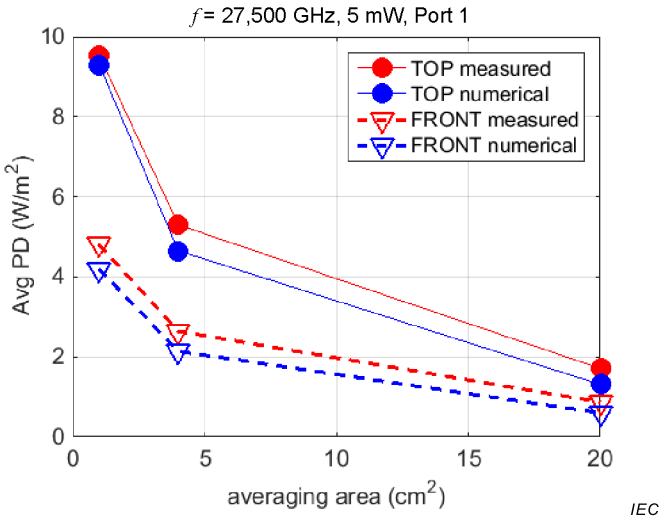


**(a) $f$ = 27,500 GHz**

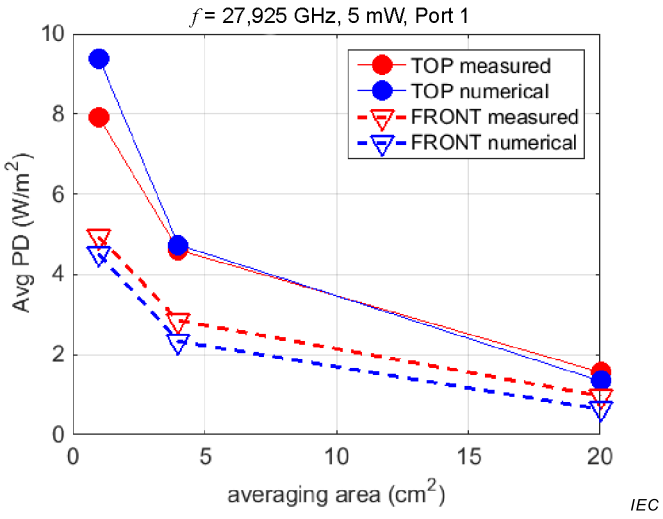


**(b) $f$ = 27,925 GHz**

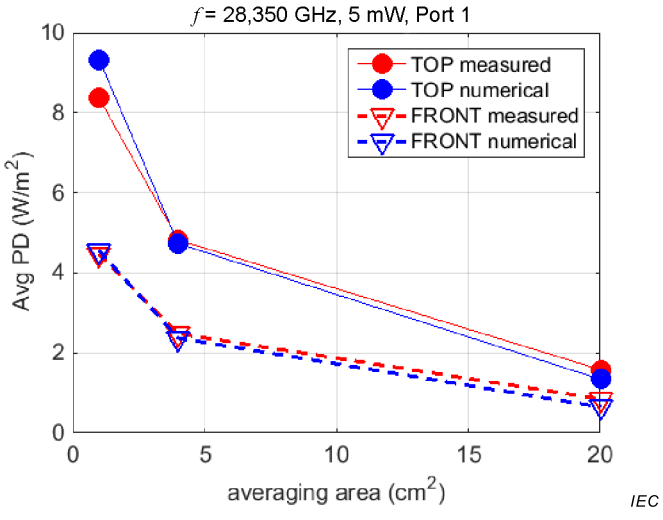


**(c) $f$ = 28,350 GHz**

**Figure H.11 – Averaged power density as a function of averaging area for port 1 at different frequencies**

By superimposing the independently measured fields with the appropriate phase shift, the total distribution for each configuration defined in Table H.1 was computed. The relative phases between the antenna elements were normalized to the location of PD maximum of each measured element for combining the field. From the five phase combinations, the largest averaged PD over a circular 4 $cm^2$ (corresponding to the configuration $w_1$ of Table H.1, i.e. zero phase-shift between ports of the array) of the TOP orientation was obtained. The measured power density was 7,6 $W/m^2$. The simulated value for the same configuration was 8,1 $W/m^2$. Figure H.12 shows the measured power density distribution.

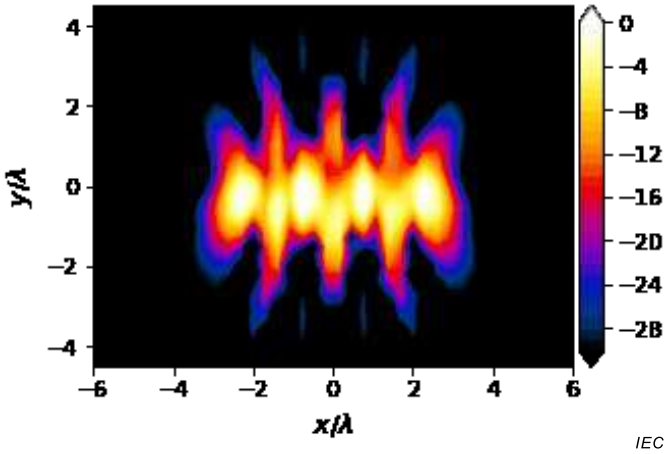


**Figure H.12 – Distribution of the power density corresponding to the array with zero phase-shift between elements (configuration $w_1$ of Table H.1)**

## H.4 Results obtained at Laboratory 2

### H.4.1 General

The measurement methodology is based on the solution of an inverse source problem similar to that described in Clause F.3. Both amplitude and phase of the E-field are measured on the measurement surface by means of a waveguide probe. In H.4.2 to H.4.4, the measurement setup and results are presented.

### H.4.2 Measurement setup

The setup used for the measurement was mounted on an optical table and the planes were measured using a custom-made waveguide probe (Figure H.13). The positioning and alignment of the DUT was performed using several positioners and further verified using cross lasers. The scan plane was realized using two positioners combined with aluminium breadboards. The points in the scan plane were sampled on an 8 mm × 8 mm grid.

The transmitting DUT was connected through cables and adapters to a vector network analyzer (VNA) with the power of −10 dBm. The receiving probe had a similar chain and was connected to a second port of the same VNA.

IEC

[SOURCE: Lund University]

**Figure H.13 –Mock-up with antenna port number 2 connected to the VNA (left) and the open waveguide probe and alignment system (right)**

The power was calibrated, with the cables included, using a thermal power sensor over the frequency interval 26 GHz to 30 GHz when a stable operation temperature was reached.

The measurements consisted of several scan planes of varying sources in order to calibrate the system. Absorbers were positioned to cover any metallic surfaces in the near surrounding. All DUT were carefully aligned with the positioners. The connection with the VNA was established using IEEE 488 (GPIB) connection and controlled using scripts. The different distances between the Sony mockup and the probe scan plane (measurement plane) used were within the 2 cm to 10 cm range and were realized using said positioners.

The mock-up was mounted using absorbers and plastic holders to avoid any unwanted interference. The mock-up was secured firmly and special care was taken when changing the active port to not change the position and further impact alignment. Several distances between the mock-up and probe were measured. For the data presented in H.4.3, the distance between the probe scan plane and the mock-up was about 6 cm.

### H.4.3 Data processing

By means of reconstruction algorithm the measured E-field was used to determine power density according to the following procedure:

– time gating to suppress reflections from far away objects [28];
– probe compensation to remove effects of the receiving open waveguide antenna (probe);
– reconstruction of equivalent currents ($\mathbf{J}$ or $\mathbf{J}$ and $\mathbf{M}$) on the surface of the device (DUT);
  - The observed (measured) E-field, $E$ = N$J$, where the matrix, N, is calculated from the E-field integral representation [29].
  - The current density is estimated using a pseudo inverse based on a singular value decomposition [30].
– calculation of the E-field and H-field from the estimated current;
– calculation of the normal component (with respect to the observation plane) of the time average Poynting vector from the E-field and H-field.

### H.4.4 Numerical simulations and comparison with measurements

The mock-up was simulated using a commercial solver making use of the multilevel fast multipole method (MLFMM). The model of the mock-up is the same as described in Clause H.2 and adopted mesh size was smaller than 1/12 wavelength. The simulated results were normalized to an input power of 5 mW for each port.

Figure H.14 shows the power density distribution in the TOP configuration in a plane located 5 mm from the DUT, at 27,925 GHz. The diagrams are shown for the four ports. As a

reference, simulations are also presented. Each graph is in dB, normalized to the maximum value using a 150 mm × 150 mm window and a 40 dB range. Similarly, Figure H.15 shows the power density for the FRONT distribution.

Figure H.16 shows the averaged power density as a function of distance for port 1, at 27,925 GHz, for both TOP and FRONT orientations. The results are presented in a plane 5 mm from the DUT using circular averaging areas of 4 $cm^2$. As in the case of the field distributions, the graphs show also numerical results obtained from the simplified model of the device.

Figure H.17 shows the results for the averaged power density as a function of the averaging area for port 1, in TOP and FRONT orientations. The results are presented at the three frequencies of interest: 27,500 GHz, 27,925 GHz $cm^2$ and 28,350 GHz, in a plane 5 mm from the DUT.

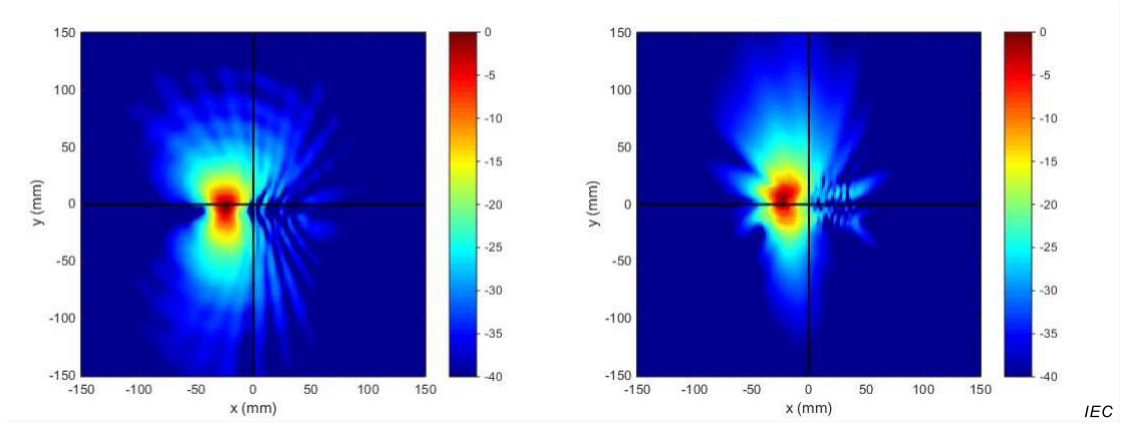


(a) Port 1

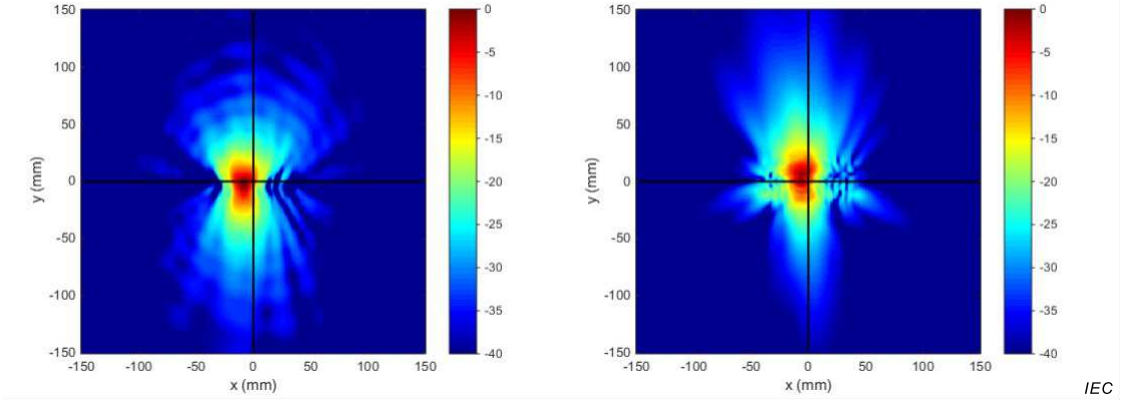


(b) Port 2

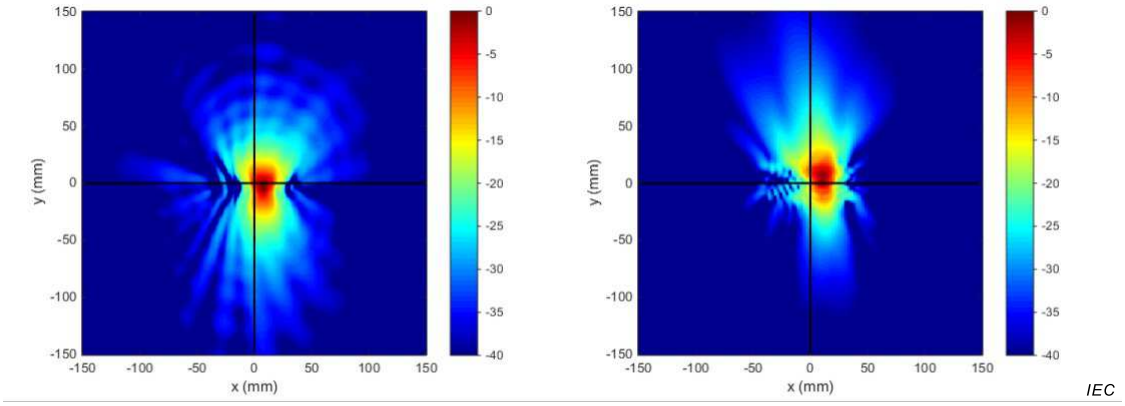


(c) Port 3

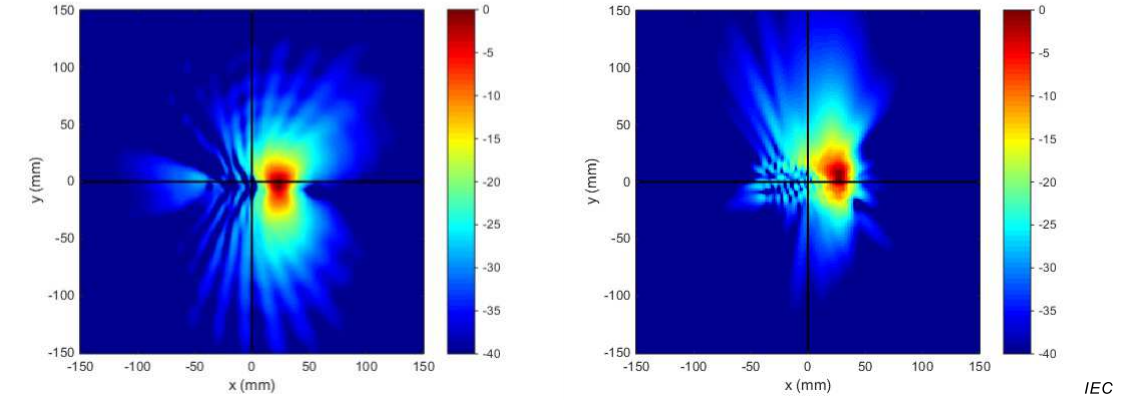


(d) Port 4

**Figure H.14 – Simulated (left) and measured (right) power density distribution for the TOP configuration over a 15 cm × 15 cm plane**

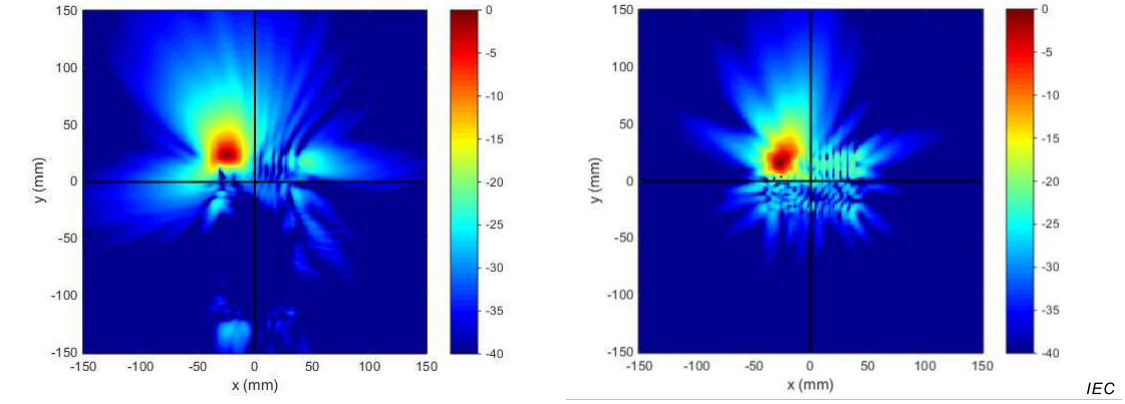


(a) Port 1

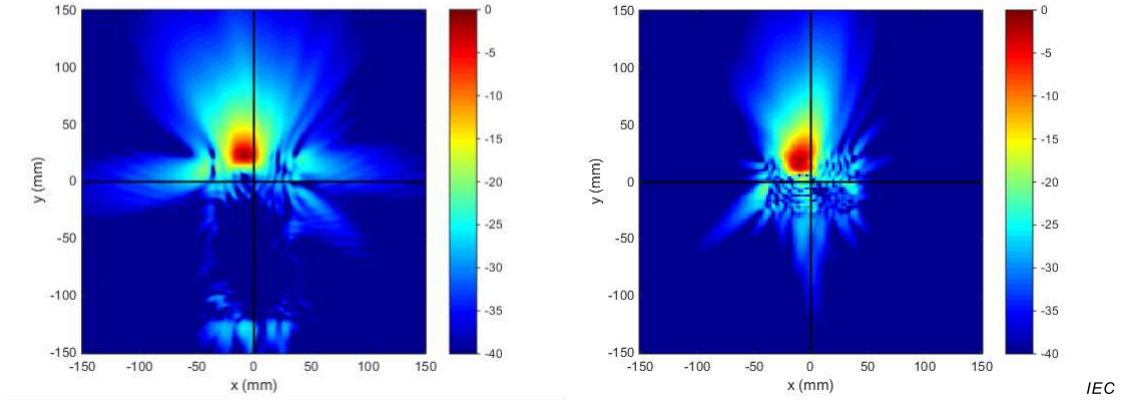


(b) Port 2

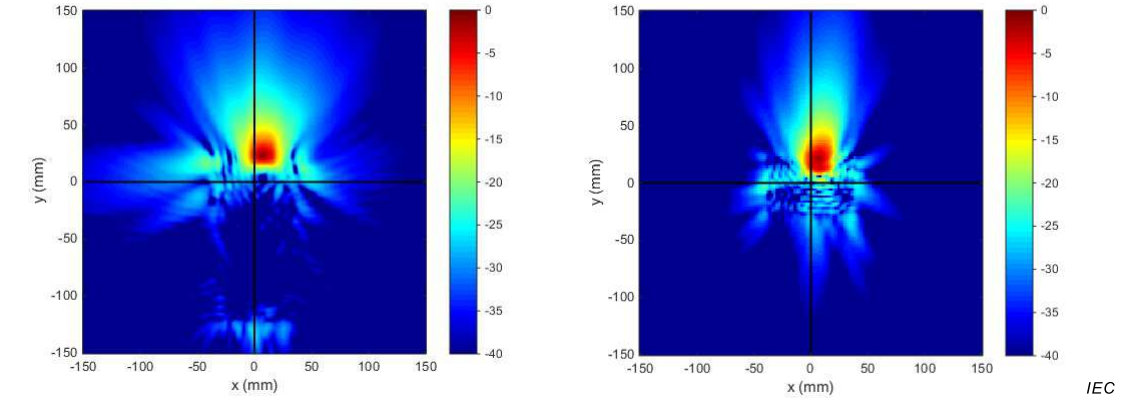


(c) Port 3

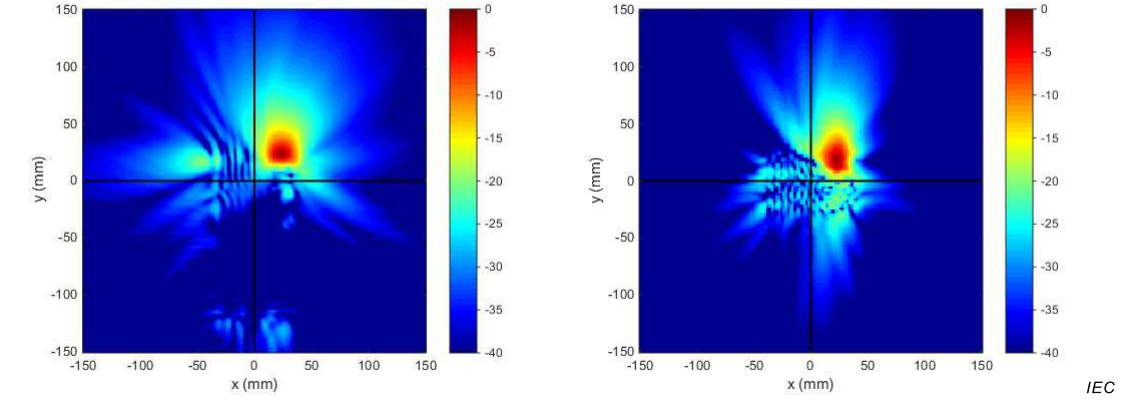


(d) Port 4

**Figure H.15 – Simulated (left) and measured (right) power density distribution for the FRONT configuration over a 15 cm × 15 cm plane**

The simulated efficiency was used to normalize the measured results to 5 mW transmitted to the antenna ports. The Poynting vector based on measurements (solid curves) and simulations (dashed curves) are depicted in Figures H.16 and H.17.

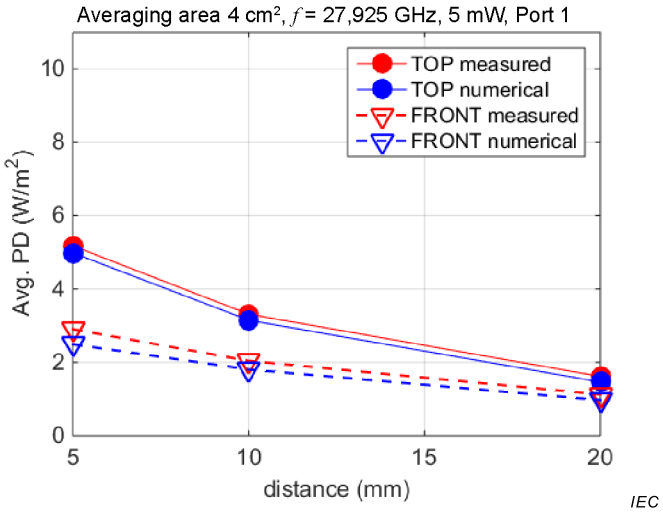


**Figure H.16 – Averaged power density as a function of distance for port 1, at 27,925 GHz, for TOP and FRONT configurations averaged over an area of 4 cm$^2$**

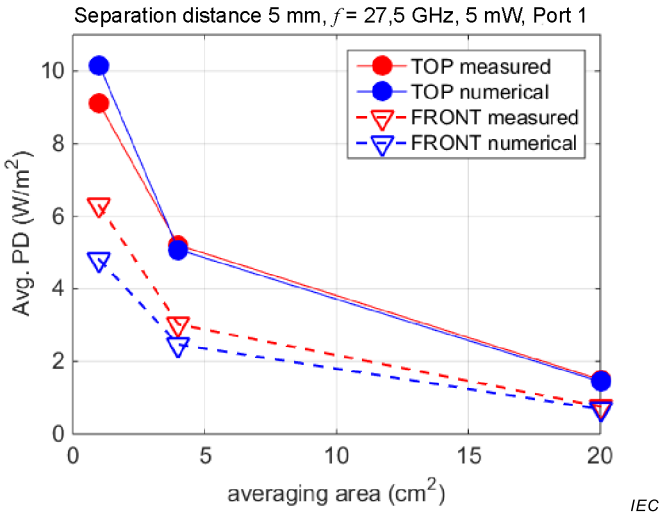


**(a) $f$ = 27,500 GHz**

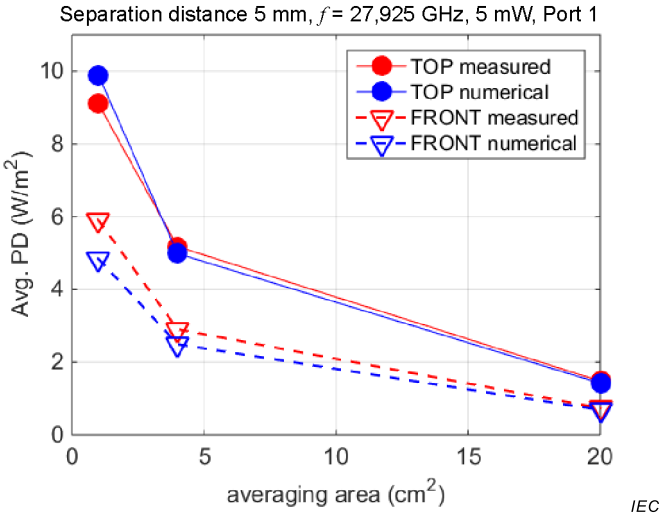


**(b) $f$ = 27,925 GHz**

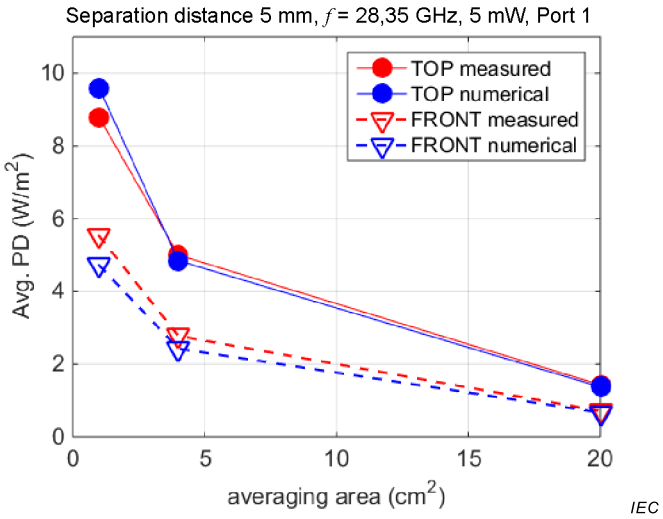


**(c) $f$ = 28,350 GHz**

**Figure H.17 – Averaged power density as a function of averaging area for port 1 at different frequencies**

The 4 $cm^2$ combined averaged power density over a circle including the contributions for the four ports was evaluated in post-processing step using the precoding weights listed in Table H.1 and based on the individual measurements of each port. At 27,925 GHz, its maximum on the top evaluation surface, for a distance of 5 mm and an accepted power of 20 mW (5 mW per port), was found to be 7,8 $W/m^2$ based on measurements and 8,3 $W/m^2$ with simulations. Figure H.18 shows the corresponding distribution obtained with measurements.

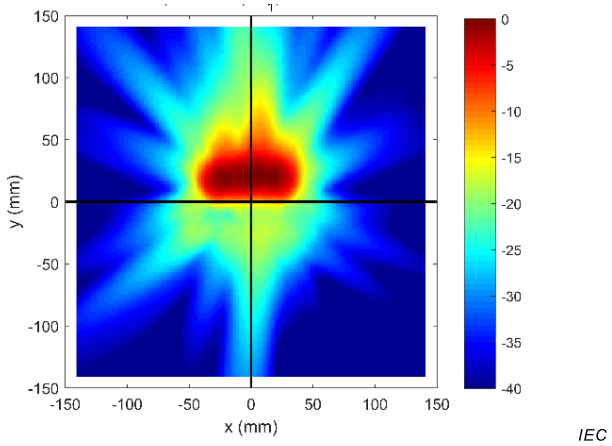


**Figure H.18 – Distribution of the power density corresponding to the array with zero phase-shift between elements (configuration $w_1$ of Table H.1)**

## H.5 Measurements at Laboratory 3

### H.5.1 General

Measurements of the mock-up are ongoing with a two-probe method where both E-field and H-field components are measured. The measurement setup and procedure are described in H.5.2 and H.5.3. The used technique doesn't make use of reconstruction algorithm as both E- and H-fields are directly measured on the evaluation surface.

### H.5.2 Measurement setup

The measurement setup is shown in Figure H.19.

The E and H antenna probes being used are a low Q broad band antenna type which utilize a developed sensor arrangement which allows for high sensitivity and directivity detection of measured fields. Probes have been characterized and assessed for sensitivity in air from 9 kHz up to 67 GHz based on the specific experimental measurement need and frequency band of analysis. Characterization is based on numerical modelling and physical quantification of the probe design where values of the probe output have been derived through simulations and experimental analysis. Probe input and output characteristics are calibrated and a simplified method for validation is provided as an end user verification check for the frequency band of interest.

A metrological method for probe characterization has been derived following a three-step calibration procedure which includes:

– Three-antenna spherical calibration method:
  - gain;
  - directivity.
– Electrical parameters:
  - $S_{11}$ return loss;
  - $S_{11}$ impedance.

– Close near-field loss using microstrip line method:
  - coupling loss factor.

### H.5.3 Scans

The scans are conducted according to the following steps:

1) Measure the electric and magnetic field amplitude on the evaluation surface. The spatial resolution depends on the signal wavelength and the distance between evaluation plane and DUT surface.

   At each point of a measurement, $E$ and $H$ probes should be rotated 360 degrees to determine the radial orientation of field vectors with a radial resolution of 15 degrees.

2) Measure the electric and magnetic field at a distance of $\lambda/2$ further from the evaluation surface to verify the signal direction. The measurement plane should be big enough to cover the possible spatial drift of the power density.

3) To determine the spatial-average power density on the evaluation surface, use Formula (H.1):

$$S_{\text{av}} = \frac{1}{2A}\int E \cdot H \cdot \sin\theta \sin^{-1}\psi \mathrm{d}A, \tag{H.1}$$

where $\theta$ is phase shift between $E$ and $H$, $A$ is the averaging surface area, and $\psi$ is the angle of signal propagation relative to the normal to the measurement surface.

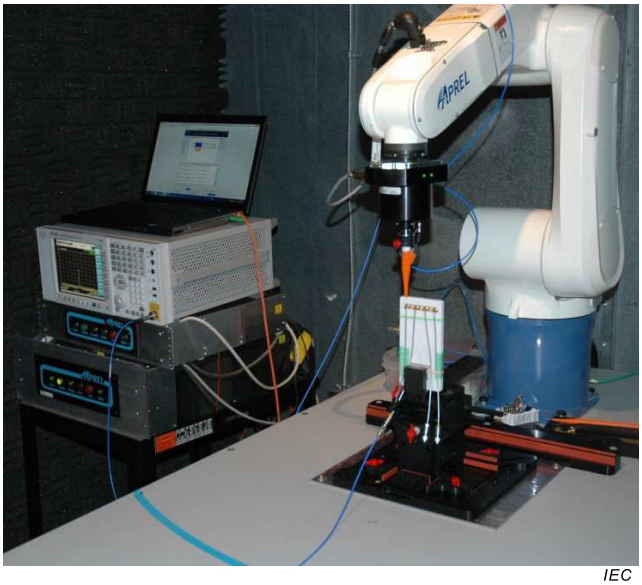


IEC

**(a) 'TOP' orientation**

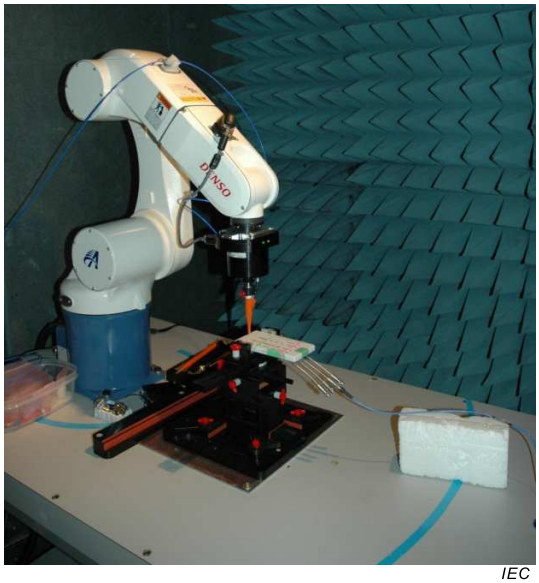


IEC

**(b) 'FRONT' orientation**

[SOURCE: Aprel Laboratories]

**Figure H.19 – Measurement setup**

# Bibliography

[1] IEEE Std C95.1-2005, *IEEE Standard for Safety levels with Respect to Human Exposure to Radio Frequency Electromagnetic Fields, 3 kHz to 300 GHz*

[2] IEC 62479, *Assessment of the compliance of low-power electronic and electrical equipment with the basic restrictions related to human exposure to electromagnetic fields (10 MHz to 300 GHz)*

[3] CISPR 16-1-4, *Specification for radio disturbance and immunity measuring apparatus and methods – Part 1-4: Radio disturbance and immunity measuring apparatus – Antennas and test sites for radiated disturbance measurements*

[4] IEEE 1720:2012, *IEEE recommended practice for near-field antenna measurements*

[5] ISO/IEC 17025, *General requirements for the competence of testing and calibration laboratories*

[6] Bansal, R., "The far-field: How far is far enough?". *Applied Microwave & Wireless,* vol. 11, no. 11, pp. 58-60, 1999

[7] Xu, B., Gustafsson, M., Shi, S., Zhao, K., Ying, Z. and He, S., "RF EMF Exposure Compliance of mmWave Array Antennas for 5G User Equipment Application," Technical Report LUTEDX/(TEAT-7248)/1-18/(2017), vol. 7248, Electromagnetic Theory Department of Electrical and Information Technology Lund University Sweden, 2017

[8] ISO/IEC Guide 98-3, *Uncertainty of measurement – Part 3: Guide to the expression of uncertainty in measurement (GUM:1995)*

[9] IEC/IEEE 62704-1:2017*, Determining the peak spatial-average specific absorption rate (SAR) in the human body from wireless communications devices, 30 MHz to 6 GHz – Part 1: General requirements for using the finite difference time-domain (FDTD) method for SAR calculations*

[10] IEC 62232, *Determination of RF field strength, power density and SAR in the vicinity of radiocommunication base stations for the purpose of evaluating human exposure*

[11] IEC 62209-2, *Human exposure to radio frequency fields from hand-held and body-mounted wireless communication devices – Human models, instrumentation, and procedures – Part 2: Procedure to determine the specific absorption rate (SAR) for wireless communication devices used in close proximity to the human body (frequency range of 30 MHz to 6 GHz)*

[12] Onishi T., Funahashi D., Iyama T., and Hirata A., "Near-field exposure assessments of power density above 6 GHz," BioEM2017, S02-2, Hangzhou, China, June 2017

[13] Sasaki K, C Jerdvisanop, Iyama T, Onishi T, and Watanabe S, "A Study on back-propagation technique for compliance assessment of power density in millimeter-wave frequency," BioEM2017, S13-2, Hangzhou, China, June 2017

[14] Harrington, R. F., *Time-harmonic electromagnetic fields*, McGraw-Hill, 1961

[15] Clemmow, P. C., *The Plane Wave Spectrum Representation of Electromagnetic Fields*, Wiley-IEEE Press, ISBN: 978-0-7803-3411-3, 1996

[16] Cozza, A., Derat, B., and Bolomey, J.-C., “Theoretical analysis of the exponential approximation for SAR assessment in a flat-phantom”, 2007 IEEE Antennas and Propagation Society International Symposium, pp. 4328-4331, 2007

[17] Colton, D. and Kress, R., *Integral Equation Methods in Scattering Theory*, Wiley-Interscience Publication, New York., 1983

[18] Colton, D. and Kress, R., *Inverse Acoustic and Electromagnetic Scattering Theory*, Third Edition, Springer, 1998

[19] Hansen, P. C., *Discrete Inverse Problems: Insight and Algorithms*, Society for Industrial and Applied Mathematics, 2010

[20] Cappellin, C. “Antenna diagnostic for spherical near-field antenna measurements,” Ph.D. thesis, Department of Electrical Engineering, Technical University of Denmark, Lyngby, Denmark, 2007

[21] Morozov, V. A., *Methods for Solving Incorrectly Posed Problems*, Springer-Verlag, 1984

[22] Neumaier, A., “Solving ill-conditioned and singular linear systems: A tutorial on regularization,” *SIAM Review*, 40, 636-666, 1988

[23] Fiddy, M. A. and Shahid, U., “Legacies of the Gerchberg–Saxton algorithm”, *Ultramicroscopy*, 134, pp. 48-54, 2013

[24] Zhinong Ying, “Novel notch antenna array with corrugation slots for mm wave 5G terminal,” European Patent (EP), Status: Pending , Earliest Priority Date: 06 Nov 2014 , Filing Date: 01 May 2015 , Application Number: 15724377.5

[25] Pokovic, K., Schmid, T., Frohlich, J. and Kuster, N., “Novel probes and evaluation procedures to assess field magnitude and polarization,” *IEEE Transactions on Electromagnetic Compatibility*, 42(2), 240-244, 2000

[26] Gerchberg, R. W. and Saxton, W. O., “A practical algorithm for the determination of phase from image and diffraction plane pictures,” *Optik* 35(2), 237-246, 1972

[27] Anderson, A. P. and Sali, S., “New possibilities for phaseless microwave diagnostics. Part 1: Error reduction techniques,” *IEE Proceedings H – Microwaves, Antennas and Propagation*, 132(5), 291-298, 1985

[28] Rao, S. M., ed., *Time domain electromagnetics*, Academic Press, 1999

[29] Kristensson, G., *Scattering of electromagnetic waves by obstacles*, The Institution of Engineering and Technology, 2016

[30] Hansen, P. C., *Discrete inverse problems: insight and algorithms*, Society for Industrial and Applied Mathematics, 2010

_____

INTERNATIONAL
ELECTROTECHNICAL
COMMISSION

3, rue de Varembé
PO Box 131
CH-1211 Geneva 20
Switzerland

Tel:  + 41 22 919 02 11
Fax: + 41 22 919 03 00
info@iec.ch
www.iec.ch